The Contour Deformation Method in Momentum Space and Effective Interactions for Weakly Bound Nuclei

(Preliminary title)

Gaute Hagen

Thesis submitted in partial fulfillment of the requirements
for degree Doctor Scientiarum

Department of Physics and Technology
University of Bergen
March 11, 2005

ISBN 82-497-0101-1
Bergen, Norway 2002 (fra halvor moll-nilsen)

Acknowledgements

I would like to express gratitude to my supervisors Jan S. Vaagen and Morten Hjorth-Jensen for stimulating discussions and guidance during my phd work. Im especially thankful towards Morten Hjorth-Jensen for giving me thorough training in computational techniques, and arranging an exceptional good work enviroment for me during my many stays at the Physics Department at the University of Oslo.

Also, I would like to thank Centre of Mathematics for Applications (CMA) at the Univeristy of Oslo for letting me stay there for four months in the final completing stages of my phd.

I would also like to thank Boris V. Danilin Sergei Ershov and my good friend Maxim Kartamyshev for stimulating discussions during my phd.

Im also very grateful towards my girlfriend Hanne Gril Thomassen, who has been a great support to me in the last five years.

Finally I would like to thank all my friends for giving me support and stimulating discussions over the last years.

Contents

Chapter 1

Introduction

The complexity of the nuclear many-body problem has made nuclear physics a field driven by discoveries of outstanding phenomena. Tanihata's discovery in 1985 [1] of vastly spatially extended nuclei (^{6,8}He; ^{11}Li; ^{11}Be) at the neutron dripline, triggered an interest in the study of weakly bound and resonance phenomena in few-body systems. With access to secondary exotic nuclear beams, the edges of the nuclear landscape itself are being explored, *i.e.* the very limits of nuclear existence. At these limits, the so-called neutron (proton) *driplines*, additional neutrons(protons) literally drip out of the nucleus. Nuclei far from stability allow us to amplify and isolate particular aspects of the nuclear interaction and dynamics. Using what we learn from these nuclei we can then return to the nuclei of the world around us and understand them far better than ever before. Progress in nuclear structure is made at the various levels where one attempts to understand nuclear phenomena; (i) Experimental data and phenomenology, (ii) 'Local models' (effective models with few emergent degrees of freedom), (iii) 'Global nuclear models', (iv) Ab initio NN-interaction based procedures, (v) QCD. There is an overall effort to explain higher levels in terms of lower ones, but a more reductionist "deductive approach" is likely to have as precursor an approach which tries to isolate and understand the characteristic degrees of freedom.

1.1 Few-body aspects of dripline nuclei.

Nuclei along the dripline with an extreme dilute neutron skin have been labeled *halo nuclei*. Understanding the mechanisms underlying the formation of such nuclei has been a theoretical challenge, especially two-neutron Borromean[1] halos such as ^{6}He and ^{11}Li. The Borromean nuclei display extreme clusterization into an ordinary core nucleus and veil of halo nucleons – forming exceptionally dilute neutron matter. This clusterization has motivated few-body approaches such as the hyperspherical harmonic method and momen-

[1]The three Borromean rings, the heraldic symbol of the Italian Borromeo family, are interlocked in such a way that if any of them were removed, the other two would also fall apart. The three interwined Borromean rings are now widely used as the logo of the halo field.

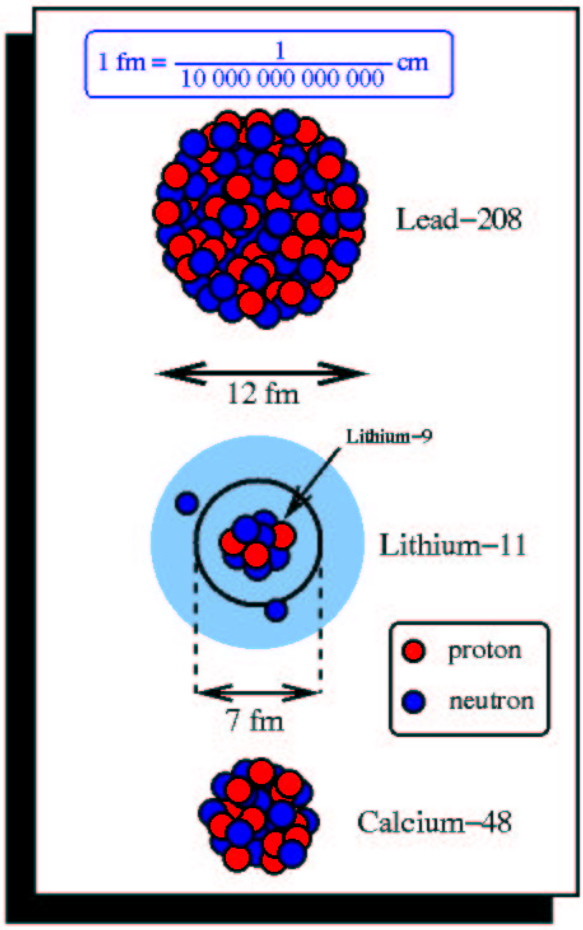

Figure 1.1: The matter size of ^{11}Li is compared to that of ^{48}Ca and ^{208}Pb

tum space Faddeev equations, to these nuclei [2]. Borromean nuclei such as ^{6}He and ^{11}Li has been especially suitable for few-body models, they are characterized by pairwise constituents with no bound states but modelled as a three-body system they achieve binding. The extreme size of these dilute neutron excessive nuclei is mainly caused by the outermost neutrons being very loosely bound or even unbound, causing a large tail in their wave functions. Figure 1.1 shows the spatial extension of the Borromean nuclei ^{11}Li in comparison with the nuclei ^{48}Ca and ^{208}Pb. The spatial extension is huge, the rms matter radius of ^{11}Li is as large as that of ^{48}Ca, and the radius of the halo neutrons is as large as for the outermost neutrons in ^{208}Pb. To understand theoretically this abnormal feature of dripline nuclei has been a challenge over the years.

Borromean nuclei along the dripline have the property of being bound in their ground state. The ground-state properties of the Borromean nuclei ^{6}He has been well understood in terms of few-body modelling [2]. The α core of ^{6}He is stable and well bound, and it may be frozen in its ground state. The relevant degrees of freedom are then described by

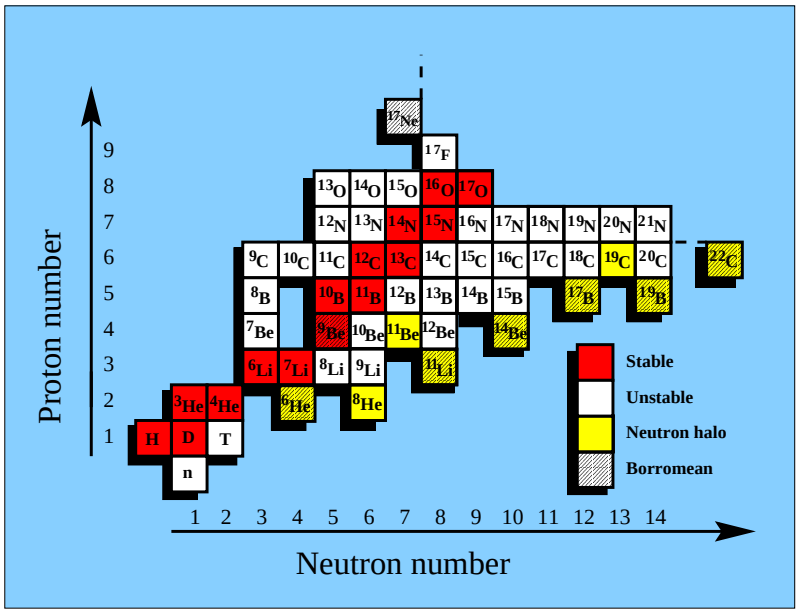

Figure 1.2: The nuclear chart exhibits the stability of Borromean nuclei among different isotope chains

the two halo neutrons relative to the core. In three-body models of halo nuclei such as ^{6}He, Pauli blocking is needed to remove components of the halo wave function that would disappear under full antisymmetrization. This, and also other aspects of the composite nature of the clusters make the challenge somewhat different from that of three-nucleon systems.

However, most nuclei along the dripline exhibit an unstable character, in that their ground state is embedded in the continuum, in the form of a resonance. The hadronic stability of Borromean nuclei is mainly due to strong pairing effects between the outermost neutrons. Figure 1.2 gives the hadronic stability of various isotope chains, and it is seen that while ^{5}He is unbound ^{6}He is bound, ^{7}He is unbound but ^{8}He is again bound. A recent review [3] looks at all the dripline nuclei. Dripline physics, which involves nuclei with one or a few weakly bound states, is physics of threshold phenomena where structure and reaction theory merge. Hence the development of methods for dealing with resonance and other continuum phenomena in such nuclei is of great importance.

1.2 Resonances in quantum mechanical few-body systems.

The characteristic feauture of exotic states embedded in the continuum is that they only exist for a limited time, before they fall apart into their decay products. Such states are labeled quasi-stationary or resonant states. In a two-body picture, they may understood

as states trapped inside the centrifugal barrier for limited time, before they tunnel through the barrier and decay. Such resonant structures are often called *shape resonances*, see figure (1.3). Considering the time dependent wave function, which satisfies the Schrödinger

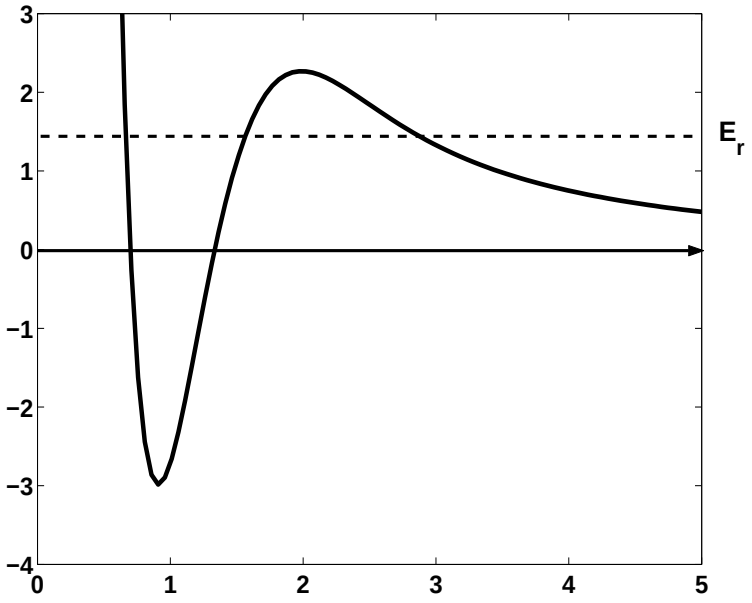

Figure 1.3: Confining potential in which a resonant state at real energy E_R is formed.

equation for a complex energy $z = E_R - i\Gamma/2$,

$$\Psi(\mathbf{r}, t) = \Phi(\mathbf{r}) exp(-i\frac{z}{\hbar}t),$$

it is seen that the probability density at a point $\mathbf{r}$,

$$|\Psi(\mathbf{r}, t)|^2 = |\Phi(\mathbf{r})|^2 exp(-i\frac{\Gamma}{\hbar}t),$$

decreases exponentially with time only for $\Gamma > 0$. As already pointed out by Gamow in 1928 in his work on radioactive decay [4], this wave function is the only one appropriate for description of resonances or quasi-stationary states. Resonances are observed in experiments as enhancements in the cross section when plotted as a function of energy. In the case of isolated resonances, where the distance in energy between the resonances exceeds their widths, and the resonaces are far from decay thresholds, the total cross section over the resonance peak may be parametrised by the Breit-Wigner formula [5],

$$\sigma \propto \frac{\frac{1}{4}\Gamma^2}{(E - E_R)^2 + \frac{1}{4}\Gamma^2}$$

A detailed analysis of such data often reveals that this enhancement is due to one specific partial wave. To that extent, resonances have a definite set of quantum numbers just like

bound states, the only differences being the fact that these states have a definite lifetime and thus correspond to complex energy eigenstates. Standard quantum mechanics is formulated for Hermitian operators. This raises the question of how a Hermitian Hamiltonian could give rise to a complex eigenvalue and whether such states should be included in our Hilbert space?

How to actually solve for single particle resonances has been a separate study in many different areas of quantum physics over the years. The specialization trend within all disciplines of applied quantum physics makes it almost impossible to understand questions and problems raised within the different branches of quantum physics, on the other hand a methodological unification has taken place in many areas. The theory of resonances is such an example. The theory underlying the formation and decay of long lived states in molecules, atoms, nuclei, and condensed matter is from a quantum mechanical viewpoint methodologically basically the same. By acknowledging this, it is possible to obtain new perspectives in various fields by adopting methods originally developed in different fields of physics A variety of methods has been developed for understanding the basic mechanisms of formation of resonant states and processes taking place in the continuum. They are described in text books such as [6, 7, 8, 9]. All the methods have in common that they originate from standard scattering theory, and are based on the method of analytical continuation. The relevant equations are analytically continued from the physical energy sheet through the unitarity cuts onto the second energy sheet of the complex energy plane, where resonances may be located.

One of the more popular methods during the last decades has been the complex scaling method, originally formulated by Aguilar, Balslev and Combes in the early 70's [10, 11], and developed to examine the spectrum of the Green's function on the second energy sheet. Later this method has been adapted in other fields such as atomic and molecular fields to the study of resonances by complex scaling. In the context of complex coordinate scaling applied to quantum chemistry, Moiseyev [12, 13, 14] developed a generalized complex variational principle for resonant states. During the last decade the complex coordinate method has also been applied in nuclear physics, as interest in loosely bound nuclear halo systems has grown, see for example [15, 16, 17, 18] for an application to the resonant states of Borromean halo nuclei.

More recently a method based on exact differential equations for functions closely related to the Jost functions has been developed [19, 20]. The method exploits the idea of complex rotation of the coordinates, but differs from the traditionally used complex scaling methods using expansions and variational principles. The Jost function at a complex energy is obtained directly from exact equations, and resonances are associated with zeros of the Jost function on the second energy sheet.

Another popular approach is method based on analytic continuation in the coupling constant (ACCC) [7, 21]. The ACCC method uses analytic continuation in the coupling strength of the potential instead of the usual continuation in energy. All these methods are usually formulated in coordinate represenation.

One of the disadvantages of the coordinate space approach is that the boundary conditions have to be built into the equations, and convergence may be slow if the basis does not

mirror the physical outgoing boundary conditions well. Instead, it is possible to represent the Schrödinger equation in momentum representation, invoking the Fourier transform. One of the most obvious advantages of this, is that the boundary conditions for bound and resonant states are automatically built into the transformed integral equations. Diagonalizing, using a plane wave basis is very accurate [22], since the convergence is only governed by the number of integration points.

As shown by Afnan [23] a rotation of the integration contour in the lower half complex k-plane is equivalent to the complex coordinate rotation method, and in this respect the coordinate and momentum space versions are complementary. It should be mentioned that the contour deformation method (CDM) formulated *in momentum space* is not new in nuclear physics. It was studied and applied in the 1960's and 1970's, see for example [24, 25, 26, 27], especially in the field of three-body systems. Most of these references applied a *contour rotation* in momentum space. By restricting oneself to a rotated contour certain limitations and restrictions however appear in the equations, determined by the analytical structure of the integral kernels and potentials. In [27] a more sophisticated choice of contour, based on rotation and translation, was applied to the three-nucleon momentum space Faddeev equation for a separable Yamaguchi interaction. This choice of contour made it possible to avoid the logarithmic singularities of the Faddeev kernel and hence allowed for a continuation in energy to the non-physical energy sheet. The method has recently been revived to study anti-bound and resonant states in subatomic physics [22], where a general contour was considered.

The question now arises, whether resonant states can be made part of a complete set of states, appropriate for eigenfunction expansions. In the late 60's Berggren proved that for a finite range potential, a finite set of bound and resonant states together with a set of non-resonant continuum states form a complete set [28] of bi-orthogonal functions.

$$\mathbf{1} = \sum_n |\psi_{nl}\rangle\langle\psi_{nl}| + \int_{L^+} dk k^2 |\psi_l(k)\rangle\langle\psi_l(k)|, \tag{1.1}$$

This representation has later become known as the *Berggren basis*. The non-resonant continuum integral is defined along a contour in the in the fourth quadrant of the complex k-plane, and the discrete sum is over both bound and resonant states.

In this representation the usual inner-product is no longer Hermitian. The resonant states are not normalizable in the usual sense, as they oscillate and diverge exponentially along the real axis. As first shown by Zel'dovich [9], the inner product of a resonant state together with its complex conjugate, may be given a definite value by some reguarlization procedure. Expanding the scattering and reaction amplitudes in this basis, makes it possible to separate the resonance behaviour from the smooth non-resonant background in the scattering amplitudes. This is motivated by the fact that the most interesting phenomena taking place in the continuum are the resonance phenomena.

1.3 Modern *Ab initio* approaches to nuclear structure.

In physics one often attacks a specific problem within a reductionist way of thinking. That is, the phenomena of the whole system should be described in terms of the theories and laws of the parts of the system.

In nuclear physics one would ideally like to start from nucleon degrees of freedom. The dominant philosophy within the nuclear theory community is that the nucleus (at low energies) as a whole may be fully described in terms of the the interactions between these constituents. Building up the nucleus from these basic constituents and their mutual interactions, the quantum mechanical description of the many-body system however becomes extremely complex and hard to tackle as the number of nucleons increases.

In the history of nuclear structure the shell model has been very successful in describing properties of nuclei near the valley of stability. The traditional shell model has usually been formulated in a harmonic oscillator representation, this is based on the assumption that the single particle motion within the nucleus is well described by harmonic oscillator orbitals. This is certainly true for well bound nuclei where the tail of the single particle wave functions fall of rapidly. The harmonic oscillator wave functions are also favourable as they are given in terms of well known mathematical functions. However, the possibly most attractive aspect is that the Hamiltonian describing the motion of two particles in a harmonic oscillator potential may be written in separable form in both relative and center-of-mass coordinates and shell model coordinates. This is extremely favourable since the effective interaction between the nucleons are given in relative coordinates.

The shell model approaches to nuclear structure are usually not truely reductionistic. For heavier nuclei the number of degrees of freedom becomes too large to handle with modern computers. Therefore it has been customary to define an inert core of the nucleus which sets up a mean-field in which the valence nucleons move. Thus the nucleus ^{18}O may be modelled with two valence nucleons moving in the $s-d$ shell with respect to the closed shell nucleus ^{16}O acting as an inert core. As the number of valence particles grows the number of nucleon configurations within a valence space becomes larger and larger, making it diffucult to handle numerically. Nevertheless, in the last decade one has experienced an extreme development of computational power, making it possible to extend the shell model into regions previously inaccessible.

The growth of computational power has also sparkled a belief in *ab initio* calculations of nuclei, taking into account all degrees of freedom. The most ambitious of these 'reductionist' attempts are Green's Function Monte Carlo (GFMC) calculations [29, 30, 31, 32, 33, 34, 35], extending previous variational Monte Carlo (VMC). According to the authors these are the first microscopic calculations that directly produce nuclear shell structure from realistic interactions that fit NN scattering data. Another line of approach are the large-basis no-core shell-model (NCSM) calculations of Barrett's group [36, 37, 38, 39], where the shell model is combined with microscopic effective interactions derived from modern nucleon-nucleon potentials.

The exponential growth of the configuration space as the number of active particles increases makes it extremely difficult to reach into the range of medium size nuclei, within these *ab intio* formalisms. The cost of matrix diagonalization increases as the third power of the number of basis states, and the memory required to store the Hamiltonian matrix increases as the square of the number of basis states. The practitioners have, however, already had success with their pioneering attempts. So far converged results for nuclei with up to $A = 12$ active particles have been reported. Further, GFMC and NCSM calculations for A=6 do produce an alpha-like core object, and two alpha-particles for ^{8}Be, both promising features.

Another *ab initio* approach which recently has proved promising in the medium size region of the nuclear chart, is the Coupled-Cluster method. The Coupled-Cluster method originated in nuclear physics in the 60's [40, 41], but has since that time only appeared sporadic within nuclear physics. On the other hand Coupled-Cluster theory has been extensively used, and with great success, in quantum chemistry over the years [42, 43]. Basically the Coupled-Cluster method is based on an exponential ansatz for describing correlations within a nucleus.

$$\Psi_{CC} = exp(\hat{T})\Psi_0, \;\; \hat{T} = \hat{T}_1 + \hat{T}_2 + \hat{T}_3 + ...,$$

where $\hat{T}_n$ are linear combinations of all n-type excitations. Including only single and double excitations (CCSD), the computational cost scales as $N^7$where N is the size of the system. Instead of direct matrix diagonalization, a non-linear set of equations is solved iteratively. Very recently [44, 45, 46], converged Coupled-Cluster results for the ground- and first excited state of ^{16}O have been reported, using modern nucleon-nucleon interactions derived from effective field-theory.

1.4 Exotic many-body states embedded in a continuum.

All of the above mentioned many-body approaches have been formulated using a harmonic oscillator basis describing single particle motion. Adopting a harmonic oscillator picture, one assumes from the very start that the interacting nucleons are isolated from an external environment of positive scattering states. The tremendous success of the multi-configurational shell model over the second part of the last century, in describing properties of nuclei where continuum aspects are more or less absent, has given little focus on mechanisms involved in the formation and decay of nuclei far away from the valley of *beta*-stability. However, approacing the drip-lines new aspects and properties of nuclei emerge, such as the instability of decay, enormous size of halo nuclei and the melt down of shell structures and new shell closures.

To bridge the gap between reaction and structure theory, microscopical shell model calculations using a Berggren representation for the single particle states were proposed some years ago [47, 48]. The proximity of the scattering continuum in weakly bound and

unbound nuclei, implies that these nuclei cannot be properly described without taking into account the coupling between discrete states and the positive energy continuum. In other words, a proper description of loosely bound nuclei should take into account the coupling of the internal with the external environment, which has been totally neglected in classic shell model approaches. The coupling of the 'external' continuum of positive energy states, with the 'internal' nuclear states has for a long time been basic ingredient in nuclear reaction theory. Feshbach was the first to formulate a unified description of direct and compound nuclear reactions within the projection operator method [49, 50]. He showed that the coupling of the internal with the external environments could give rise to compound nuclear states, such as multi-channel resonances. As he was the first to formulate a general theory of such states, they became known as Feshbach resonances. Also in atomic physics Feshbach resonances are of great importance. In the early 60's, at the same time of Feshbach's work, Fano [51] discussed how the mixing of a configuration belonging to a discrete spectrum with configurations belonging to a continuous spectrum gives rise to the phenomena of *autoionization*, which is considered a multi-channel resonance or in other words a Feshbach resonance.

Entering the realm of weakly bound nuclei, it becomes evident that the standard separation of nuclear structure and nuclear reaction methods has to be abdoned. A merging of the two fields, where many-body methods from the structure community are united with reaction theory, where the importance of the continuum has been studied over several years, seems to be a fruitful way of approach. Treating the continuum aspects properly within existing many-body theories, is however much more difficult than when dealing with well bound nuclei. Existing many-body structure approaches have to be reformulated and developed further since the harmonic oscillator representation has to be abdoned. All the nice mathematical properties of the harmonic oscillator basis are non-existent in all other single particle representations, e.g. the Woods-Saxon basis.

Having determined a single particle basis consisting of bound, resonant and non-resonant continuum states, it is natural to again focus on the application of this basis in nuclear structure calculations of weakly bound and/or unbound nuclei. Ideally one would like an *ab intio* description of these nuclei, taking into account all relevant degrees of freedom. In the hyperspherical description of three-body Borromean and halo nuclei, the problem of treating core excitations and the anti-symmetrization between core and valence nucleons has not fully been solved. Treating such nuclei microscopically, a reformulation of the shell model using a single particle basis of bound, resonant and scattering states may appear to be the most straightforward method. The recently developed Shell Model Embedded in the Continuum (SMEC), see e.g. Refs. [52, 53, 54, 55], offers such a possibility. SMEC is closely related to the Feshbach projection operator technique. In SMEC the bound,resonant and scattering states are treated on equal footing, by introducing two subspaces and taking their coupling into account. However, most SMEC calculations have not taken into account coupling with decay channels containing more than one nucleon.

Restricting the theory to only one-nucleon decay channels, limits the applicability of SMEC along the drip-lines. Borromean nuclei for which the $A$and $A-2$ nuclei are particle stable, while the nuclei $A-1$ are not, requires a theoretical description which

takes into account decay channels involving all valence nucleons. That is, all many body configurations involving bound and scattering states should be considered. The newly developed Gamow shell model is devoted to such an approach, see for example Refs. [56, 57, 58, 48, 59, 60, 61, 62, 63, 22]. The Gamow shell model starts with the Berggren representation (1.1) for single particle states. A complete many-body Berggren basis may then be constructed from the discretized single-particle Berggren orbitals

$$\sum_n |\Psi_n\rangle\langle\tilde{\Psi}_n| = 1,$$

where the many body Slater determinants $|\Psi_n\rangle$are constructed from the discrete bound, resonant and non-resonant continuum orbitals. This is in full analogy with the standard shell model using a harmonic oscillator basis. When the exact multi-particle resonance wave function is expanded in a complete set of Slater determinants consisting of discretized single particle Berggren orbitals, an interpretation of these exotic multi-particle structures in terms of single particle resonances becomes possible.

Intuitively one would expect that the Slater determinant built from single-particle resonances only, would be the major component in the fully correlated many body wave function. This is certainly true if the residual nucleon-nucleon interaction is weak compared with the mean-field in which the valence particles move. More interesting is the opposite case, where the residual interaction is strong. In this case it is not obvious that the pure pole configurations are the most important. However, the Gamow shell model may provide an answer to the question of how exotic structures, such as multi-particle resonances, embedded in the continuum are formed. The Gamow shell model is a promising many-body approach in the study of unstable nuclei along the drip-lines. And it is in the unifying spirit of scientific development, in that it reconciles the reaction and the structure part of the community. The Gamow shell model is in its early stages, and so there exist a vast area of applications and mayor theoretical and computational challenges to be dealt with. One of the first challenges and problems encountered in the Gamow shell model, was the *identification problem*, and first addressed in [48, 59]. The physical multi-particle resonances will in many cases be embedded in a dense distribution of continuum states, depending on the contour on which the continuum states are defined. Refs. [48, 59] related this *identification problem* to the problem of choosing a contour in the complex k-plane which in the case of several valence particles selects the physical interesting states from the dense continuum background. They found that in the two-particle case, choosing a *square-well* contour makes an identification of physical states based on inspection of the zeroth order energy surface possible. This solution is only applicable in the two-particle case, already in the tree-particle case the physical states get mixed in with the continuum states. In Refs. [57, 60, 61] the problem of identifying multi-particle resonances was approached from a different angle. The proposed algorithm is a two step procedure. In the first step a diagonalization within the pole space, where all particles are in resonant single particle orbitals, is performed. Secondly a diagonalization within the complete configuration space is done. Under the assumption of weak coupling of the pole configurations with the configurations where at least one particle moves in a continuum orbital, the physical states

may be picked out unambiguously from the states obtained after a full diagonalization, using the criterion of largest overlap with the pole space. The weak coupling limit may not always be a valid assumption, as pointed out in Ref.[63] for the case of ^{11}Li the two-particle resonances may have a larger continuum component as compared to the pole component, depending on the strength of the residual nucleon-nucleon interaction. Presently one may conclude that the *identification problem* has not been solved generally, and developing an algorithm which picks out physical states unambiguously from the dense continuum background is still an open problem.

Another challenge for the Gamow shell model is the *dimensionality problem*. As the number of active particles moving in a valence space increases, the number of Slater determinants in the many-body Berggren basis increases dramatically. This explosion of many-body configurations is even more severe than in the standard shell model approach where only bound states appear. In the Gamow shell model one has for each partial wave a finite number of non-resonant continuum states which are absent in the standard shell model. In solving this problem, one has to take advantage of effective operator and perturbation method techniques typically used and developed for large scale shell model calculations using harmonic oscillator bases.

With further progress in computational power one may hope that *ab intio* calculations of light and medium size nuclei within the Berggren representation may become possible in the near future. Coupled-Cluster techniques has proven to be a promising method for microscopical calculations of medium size nuclei such as ^{16}O, a promising way of approach would be to generalize the Coupled-Cluster method to complex interactions, and at the first stage see how resonant structures are formed in light nuclei starting from an *ab initio* approach. Another interesting application would be to see how single particle resonances are formed starting from a realistic nucleon-nucleon interaction. In conclusion, one may say that nuclear physicists are living in exciting times.

1.5 Outline of Thesis.

This thesis combines results which are published in international journals with results which appear only in this thesis. The main purpose of this thesis, may nevertheless be summarized in the two published papers *The contour deformation method in momentum space, applied to subatomic physics* and *Effective Interaction Techniques for the Gamow Shell Model*. However, since these papers deal with topics which may be less familiar to the audience, this thesis aims at giving a more detailed and thorough discussion of the formalisms and theories underlying this work. The outline of the thesis is the following.

Chapter 2 gives a detailed discussion of the scattering functions and Jost functions starting with the coordinate representation of the Schrödinger equation. The most general distribution of poles of the scattering matrix is discussed, together with their physical interpretations. Chapter 2 also dicusses some typical regularization procedures for matrix elements involving resonant states. An outline of the proof of the general Berggren completeness which includes bound, anti-bound and resonant states is given, and a discus-

sion of the physical interpretation of expectation values of observable operators involving resonant states.

Chapter 3 starts with the momentum representation of the Schrödinger equation (Section 3.1), and discusses how the Schrödinger equation may be analytically continued to the second energy sheet using the Contour Deformation Method (CDM) (Section 3.2). A complete set of single particle states, involving all kinds of poles, is obtained. Chapter 3 contains several applications which are not included in the published papers. Section 3.3 gives an application of the CDM to the problem of solving for resonances in a deformed field is given Section 3.4 gives an application of CDM to resonances and bound states in complex absorbtive and emitting potentials. Section 3.6.1 gives an application of CDM to the solution of pair instabilities of the CD-Bonn interaciton in a infinite nuclear medium, and discusses how poles on the second energy sheet may be interpreted as resonance like states.

Chapter 4 discusses the application of a single-particle basis constructed by CDM may serve as a starting point for Gamow-Shell-Model studies. Section 4.3 gives a formal derivation of the Lee-Suzuki similarity transformation method for complex interactions, and shows how a complex symmetric interaction may be obtained by a second similarity transformation. Section 4.4 discusses the use of Many-Body perturbation theory in Gamow-Shell-Model calculations. A derivation of the standard Rayleig-Schrödinger perturbation expansion for a single model space state is given for the case of complex interactions. It is shown that the standard single-reference perturbation theory does not give satisfactory results when treating many-body resonance perturbatively. The Multi-Reference-Perturbation-Theory-Method (MRPTM) is subsequently derived. This theory differs from standard perturbation theory, in that it is a one-state-at-a-time perturbation theory. Finally, Section 4.5 gives an effective interaction scheme for the Gamow-Shell-Model which combines the Lee-Suzuki similarity transformation method with the one-state-at-a-time MRPTM.

Chapter 5 gives a short introduction to the article *The contour deformation method in momentum space, applied to subatomic physics.*

Chapter 6 gives a short introduction to the article *Effective Interaction Techniques for the Gamow Shell Model.*

In Chapter 7 conclusions of the present work, and future perspectives are given.

Chapter 2

General theory of resonances and the Berggren completeness.

2.1 Physical interpretation of scattering matrix poles.

Resonance phenomena are associated with processes taking place in the continuum. Any quantum mechanical system may be experimentally found to be either in a bound stationary state or in a scattering state located in the positive continuum. Resonance states with definite lifetime are never directly observed, but instead the scattering states into which they decay are observed. It is therefore natural to start with the radial Schrödinger equation, for a spherically symmetric potential $V(r)$,

$$\left(-\frac{d^2}{dr^2} + v(r) + \frac{l(l+1)}{r^2} - k^2\right) u_l(k,r) = 0 \tag{2.1}$$

here $v(r) = 2\mu V(r)/\hbar^2$ and the energy is related to the wavenumber by $k^2 = 2\mu E/\hbar^2$, where μ is the reduced mass of the system. There are four different types of physical states associated with this Schrödinger equation, bound, anti-bound, resonant and scattering states, differing in the boundary conditions imposed on the wave functions at large distances.

In the following an overview of the properties of the regular and irregular solutions of the Schrödinger equation, and their relation to the physical scattering wave function is given. For a more detailed review the reader is referred to the text books of Newton [6] or Sitenko [8] on scattering theory.

Next we assume that the central potential is less singular near the origin than r^{-2} and vanishes faster than r at infinity, that is,

$$\lim_{r\to 0} r^2 V(r) = 0, \quad \lim_{r\to\infty} rV(r) = 0. \tag{2.2}$$

From the theory of ordinary second order differential equations the condition that the potential $V(r)$ has a "weaker" singularity than r^{-2} at the origin, means that the point

$r = 0$ is a *regular singular point.* It is customary to label those solutions of equation (2.1) which vanish $r = 0$ *regular* and those which do not *irregular* solutions. The regular $\phi_l(k, r)$ and irregular solutions $f_l(k, r)$ to equation (2.1), are uniquely defined by the boundary conditions,

$$\lim_{r\to 0}(2l+1)!!r^{-l-1}\phi_l(k,r) = 1,$$
$$\lim_{r\to\infty}\exp(ikr)f_l(k,r) = i^l. \tag{2.3}$$

The irregular solutions $f_l(k, r)$ are called the Jost solutions, and from the boundary condition it follows that they have the asymptotic form

$$f_l(k,r) \to \exp(-ikr), \;\; r\to\infty \tag{2.4}$$

The Jost solutions $f_l(k, r)$ and $f_l(-k, r)$ are linearly independent solutions of equation (2.1). This follows from the fact that the Wronskian of $f_l(k, r)$ and $f_l(-k, r)$ is non-vanishing,

$$W\left[f_l(k,r), f_l(-k,r)\right] = 2ik, \tag{2.5}$$

which is easily shown using the asymptotic forms of the Jost solutions as $r \to \infty$. Since $f_l(k, r)$ and $f_l(-k, r)$ are linearly independent solutions, the regular solutions $\phi_l(k, r)$ may be expressed as a linear combination of the Jost solutions. The coefficients of $f_l(k, r)$ and $f_l(-k, r)$ are determined from the boundary conditions imposed on the regular solutions $\phi_l(k, r)$ at $r = 0$, and it follows that

$$\phi_l(k,r) = \frac{1}{2}ik^{-l-1}\left[f_l(-k)f_l(k,r) - (-1)^l f_l(k)f_l(-k,r)\right]. \tag{2.6}$$

Here the Jost functions $f_l(k) = f_l(k, r = 0)$ and $f_l(-k) = f_l(-k, r = 0)$ have been introduced, and they are given by the Wronskian

$$f_l(k) = k^l W\left[f_l(k,r), \phi_l(k,r)\right], \tag{2.7}$$

which follows directly from equation (2.6). It can be shown [6, 8] that the regular function $\phi_l(k, r)$ is an entire function in the complex k-plane, while the irregular Jost solution $f_l(k, r)$ is an analytic function in the lower half complex k-plane. From the boundary conditions in equation (2.3) it follows for complex k that the regular and irregular solutions satisfy the following conditions,

$$\phi_l(k,r) = \phi_l^*(k^*,r), \;\; f_l(k,r) = f_l^*(-k^*,r). \tag{2.8}$$

Further the regular solutions satisfy

$$\phi_l(k,r) = \phi_l(-k,r), \tag{2.9}$$

since the $\phi_l(k, r)$ is an everywhere regular function of k^2.

The physical scattering solutions $u_l(k,r)$of equation (2.1)are given for a mixed set of boundary conditions, regularity at $r = 0$ and the asymptotic behaviour of scattering wave functions as $r \to \infty$ [6], i.e.

$$u_l(k,r) \underset{r\to\infty}{\longrightarrow} \sqrt{\frac{1}{2\pi}} i \left\{ e^{-ikr} - (-1)^l S_l(k) e^{ikr} \right\} \tag{2.10}$$

Here $S_l(k)$ is the partial wave scattering matrix element, which determines the phase shift of the outgoing wave at inifinity. Since all physical solutions are regular at the origin, they differ from the regular solutions $\phi_l(k,r)$ only by a normalization constant. However, different asymptotic behaviours of the regular solutions are specified at specific points on the complex k-plane. The proper boundary conditions for physical states are only given at certain points in the complex k-plane. If the regular solution $\phi_l(k,r)$ is known in the entire complex k-plane, all physical states is in principle known. From equation (2.6) it follows that the asymptotic form of the regular solutions is given by

$$\phi_l(k,r) \underset{r\to\infty}{\longrightarrow} \frac{1}{2} i k^{-l-1} f_l(-k) \left\{ e^{-ikr} - (-1)^l \frac{f_l(k)}{f_l(-k)} e^{ikr} \right\}. \tag{2.11}$$

Comparing with equation (2.10) it is easily seen that the partial wave S-matrix element, $S_l(k)$, is given in terms of the Jost functions

$$S_l(k) = \frac{f_l(k)}{f_l(-k)}. \tag{2.12}$$

Comparing the asymptotics of the physical wave function with the asymptotics of the regular solution $\phi_l(k,r)$, the physical scattering function may be written in terms of the regular solution $\phi_l(k,r)$ and the Jost function $f_l(k)$,

$$u_l(k,r) = \sqrt{\frac{2}{\pi}} \frac{k^{l+1} \phi_l(k,r)}{f_l(-k)}, \tag{2.13}$$

which is delta-function normalized.

Knowing all analytic properties of the Jost functions, all analytic properties of $S_l(k)$ follow directly. From the definition of $S_l(k)$ given in equation (2.12) follows that

$$S_l(-k) = S_l^{-1}(k), \tag{2.14}$$

and from the symmetry property of the Jost functions given in equation (2.8) follows that

$$S_l^*(k^*) = S_l^{-1}(k), \tag{2.15}$$

where the latter property coincides with the unitarity condition for the scattering matrix for real values of k. Further, these properties establish a one-to-one correspondence between values of the scattering matrix in different quadrants of complex k-plane. Say that we know the value of scattering matrix at a point in the fourth quadrant of the complex k-plane,

$S_l(k) = S$. Then it follows immediately from equation (2.14) that $S_l(-k) = S^{-1}$, and from equation (2.15) $S_l(-k^*) = S^*$. Using again the symmetry relation in equation (2.14) it finally follows $S_l(k^*) = S_l^{-1}(-k^*) = S^{-1}$. This shows that knowing the values of $S_l(k)$ in one quadrant of the complex k-plane, the scattering matrix is automatically known in the whole complex k-plane.

The scattering wave function and the $S-$ matrix element $S_l(k)$ have poles at the same location in the complex k-plane, given by the zeroes $k = k_n$ of the Jost function $f_l(-k) = 0$. Due to the symmetry of the Jost functions given in equation (2.8), for each pole $k = k_n$ there is in addition a pole located at $k = -k_n^*$. Furthermore the symmetry property in equation (2.14) of $S_l(k)$ implies that for each pole $k = k_n$ of $S_l(k)$, it has a zero at $k = -k_n$. The poles in the complex k-plane are divided into four categories depending on their location in the k-plane, and are often labeled by the letters $a - d$. Consider first the case where $S_l(k)$ has a zero for $k = -i\kappa$ for real $\kappa > 0$. Then both the regular solutions $\phi_l(k, r)$ and the physical wave functions $u_l(k, r)$ are square integrable functions since they fall off exponentially as $\exp(-\kappa r)$. Furthermore the corresponding energy is real and negative $E = -\hbar\kappa^2/2\mu$ corresponding to a bound state of the system. It can be shown that in the upper half-plane the scattering matrix $S_l(k)$ can have poles only on the imaginary axis [8]. These poles correspond to the boundary conditions of bound states at infinity, i.e. belonging to the L^2functional space, with exponentially decaying tails, and are labeled b. In the lower half-plane the it can be shown that the poles can be positioned anywhere.

Poles located in the fourth quadrant of the complex k-plane are associated with resonant states with outgoing boundary conditions at infinity, often called *decaying* resonances, labeled d. To see that they correspond to outgoing asymptotics consider the regular function in equation (2.6) at a pole of the scattering matrix,

$$\phi_l(k_n, r) = \underset{r\to\infty}{\longrightarrow} \frac{-1}{2}(-1)^l i k^{-l-1} f_l(k_n) e^{ik_n r} \tag{2.16}$$

A pole $k = k_n = k_1 - ik_2$ in the fourth quadrant of the complex k-plane gives the specific asymptotics

$$\phi_l(k_n, r) \to e^{ik_1 r} e^{k_2 r}$$

where $k_1, k_2 > 0$. This shows that the decay resonances correspond to outgoing asymptotics, furthermore they are not square integrable in the normal sense since they are exponentially increasing and oscillating functions. The energy of the decay states is written in the form

$$E_n = \mathcal{E} - i\frac{\Gamma}{2\mu} = \frac{\hbar^2}{2\mu}\left((k_1^2 - k_2^2) - i2k_1k_2\right). \tag{2.17}$$

where the pole in the complex $k-$ plane is written $k_n = k_1 - ik_2$, where $k_1, k_2 > 0$. *Proper* physical resonances are often defined as poles where $k_1 > k_2$, where it is seen that the real part of the energy given in equation (2.17) is positive. For poles where $k_2 > k_1$ the real part becomes negative and they are often called *unphysical* poles. The most interesting resonances physically, are the resonances which show up as sharp peaks

in the cross sections, and this occurs for $\Gamma \ll \mathcal{E}$. For resonance poles where the width Γ is large, the resonance contribution to the cross section tends to get smeared out within the continuum background.

For each pole located in the fourth quadrant there is a pole in the third quadrant symmetrically situated about the imaginary k- axis, these poles corresponds to resonant states with incoming boundary conditions at infinity, often called *capture* resonances, labeled c. That they are incoming waves is seen from equation (2.16),

$$\phi_l(k_n, r) \to e^{-ik_1 r} e^{k_2 r}, \;\; k_1 > 0, \; k_2 > 0,$$

Poles located on the imaginary axis in the lower half-plane correspond to anti-bound states, labeled a, often called virtual states. These states increases exponentially at large distances, contrary to the bound states, and are clearly not normalizable,

$$\phi_l(k_n, r) \to e^{\kappa r}, \;\; \kappa > 0.$$

Figure 2.1 sums up the most general distribution of poles of the scattering matrix and the corresponding zeros.

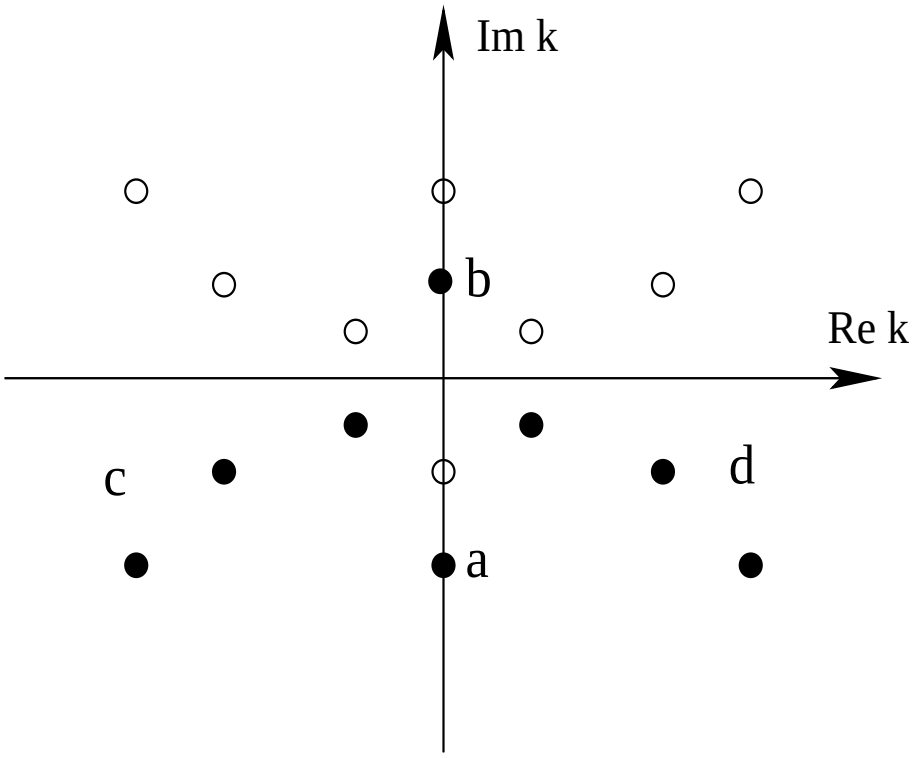

Figure 2.1: Distribution of $S-$ matrix poles (filled circles) and corresponding zeroes (open circles) in the complex $k-$plane. $a =$ anti-bound, $b =$ bound, $c =$ capture and $d =$ decay.

2.2 Regularizing divergent integrals of states on the second energy sheet.

The radial wave function $u_l(k,r)$ of a decay resonant state, with $k = k_n$ located in the fourth quadrant of the complex $k-$plane, satisfies the radial Schrödinger equation (2.1). The decay resonances are regular at the origin, $u_l(k,0) = 0$, and have purely outgoing waves, $u_l(k,r) \to O_l(k,r)$, at infinity as boundary conditions. If the potential has a finite range, in the sense that it vanishes identically beyond some finite distance $r = a$. The outgoing solutions $O_l(kr)$ are given in terms of spherical Riccati-Hankel functions $h_l^{(+)}(kr)$. In the case of long-range potentials, such as the Coulomb potential, the asymptotic form of the wave functions are given by the more complicated Coulomb functions.

From the requirement that the wave functions and their derivatives should be continuous at the boundary of the potential $r = a$, follows that the logarithmic derivative should be continuous, giving the condition

$$u_l(k,a)O'_l(k,a) - u'_l(k,a)O_l(k,a) = 0. \tag{2.18}$$

For each pole $k = k_n$ in the fourth quadrant there is a pole $k = \tilde{k}_n = -k_n^*$ in the third quadrant associated with a capture resonance. The capture states, $u_l(\tilde{k}_n, r)$, are solutions of the complex conjugated version of the radial Schrödinger equation (2.1), with regularity at the origin and with purely incoming waves at infinity, $I_l(k,r)$. Where $I_l(kr)$ is given in terms of spherical Riccati-Hankel functions $h_l^{(-)}(kr)$. The corresponding boundary conditions for the capture states becomes,

$$u_l(\tilde{k},a)I'_l(\tilde{k},a) - u'_l(\tilde{k},a)I_l(\tilde{k},a) = 0. \tag{2.19}$$

In the following we define the the decay and capture states by

$$u_{nl}(r) \equiv u_l(k_n,r), \;\; \tilde{u}_{nl}(r) \equiv u_l(\tilde{k}_n,r) \tag{2.20}$$

The capture and decay resonances are related through

$$\tilde{u}_{nl}(r) = u^*_{nl}(r), \;\; \text{i.e.} \;\; \tilde{u}^*_{nl}(r) = u_l(r) \tag{2.21}$$

Normalization of the decay resonances through the usual Euclidean inner product,

$$\langle u_{nl}|u_{nl}\rangle = \int_0^\infty dr\, u^*_{nl}(r)u_{nl}(r) = \int_0^\infty \tilde{u}_{nl}(r)u_{nl}(r) \tag{2.22}$$

is not possible in the upper limit, since the integrand diverges exponentially as

$$\tilde{u}_{nl}(r)u_{nl}(r) \underset{r\to\infty}{\longrightarrow} e^{2k_2 r} \tag{2.23}$$

for $k_n = k_1 - ik_2$ and $k_1, k_2 > 0$. On the other hand, the fact the decay and capture resonances come in conjugate pairs, may suggest that they form a *bi-orthogonal* set of functions, and that the normalization integral,

$$\langle \tilde{u}_{nl}|u_{nl}\rangle = \int_0^\infty \tilde{u}^*_{nl}(r)u_{nl}(r) = \int_0^\infty u^2_{nl}(r), \tag{2.24}$$

may exist, and be given a definite value. The integrand of this integral still increases exponentially but oscillates as

$$\tilde{u}^*_{nl}(r)u_{nl}(r) \underset{r\to\infty}{\longrightarrow} e^{2ir(k_1-ik_2)}. \tag{2.25}$$

The hope is that the oscillations at large distances will cancel each other, such that

$$0 < |\langle \tilde{u}_l(k)|u_l(k)\rangle| < \infty \tag{2.26}$$

2.2.1 Regularization by $e^{-\epsilon r^2}$.

From the theory of divergent integrals and series, see e.g. Ref. [64], many integrals which are divergent in the conventional sense, may be regularized by some regularization procedure. Zel'dovich [9] proposed the following integration procedure for regularizing integrals involving resonant states, which have an exponentially oscillating divergent tail along the real r-axis.

$$I = \lim_{\epsilon\to 0}\int_0^\infty dr\; e^{-\epsilon r^2}u^2_{nl}(r) \tag{2.27}$$

From the asymptotic behaviour of the resonant states in equation (2.25), it is natural to study the integral

$$I_n(k) = \lim_{\epsilon\to 0} I_n(k,\epsilon) = \lim_{\epsilon\to 0}\int_0^\infty dr\; e^{-\epsilon r^2}r^n e^{\kappa r}, \tag{2.28}$$

where $n = 0, 1$ and $\kappa = ik$. For a positive and finite value ϵ the regularizing factor $e^{-\epsilon r^2}$ decreases more rapidly than the exponential function $e^{\kappa r}$ increases for an arbitrary exponent κ, and the integral $I_n(k,\epsilon)$ converges. It is convienient to introduce a variable change in $I_0(k,\epsilon)$

$$t = r\sqrt{\epsilon},\;\; x = \frac{\kappa}{2\sqrt{\epsilon}} \tag{2.29}$$

which gives

$$I_0(k,\epsilon) = \frac{1}{\sqrt{\epsilon}}e^{x^2}\int_{-x}^\infty dt\; e^{-t^2} = \sqrt{\frac{\pi}{\epsilon}}e^{x^2}\left[1 - 2\mathrm{Erfc}(x)\right] \tag{2.30}$$

where

$$\mathrm{Erfc}(x) = \frac{2}{\sqrt{\pi}}\int_x^\infty dt\; e^{-t^2}. \tag{2.31}$$

is the complementary error function [65]. As $\epsilon \to 0$ then $x \to \infty$, and using the asymptotic expansion of the error function [65], the integral $I_0(k,\epsilon)$ may be written as

$$\begin{aligned} I_0(k,\epsilon) &= \sqrt{\frac{\pi}{\epsilon}}e^{x^2} - \frac{1}{2x\sqrt{\epsilon}}\left(1 - \frac{1}{2x^2} + \frac{3}{4x^4} - ...\right) \\ &= \sqrt{\frac{\pi}{\epsilon}}e^{-\frac{k^2}{4\epsilon}} + \frac{i}{k} - \frac{2\epsilon}{k^3} + O(\epsilon^2). \end{aligned} \tag{2.32}$$

The integral $I_1(k,\epsilon)$ is calculated using the relation,

$$I_1(k,\epsilon) = \frac{\partial}{\partial\kappa} I_0(k,\epsilon) = \frac{1}{2\epsilon}\left(\kappa I_0(k,\epsilon) + 1\right), \tag{2.33}$$

Inserting the asymptotic expansion for $I_0(k,\epsilon)$ in equation (2.32), gives for the $I_1(k,\epsilon)$ integral,

$$I_1(k,\epsilon) = -\sqrt{\frac{\pi}{4\epsilon^3}} ike^{-\frac{k^2}{4\epsilon}} - \frac{1}{k^2} + O(\epsilon). \tag{2.34}$$

Dealing with regularization of integrals involving *proper* resonances, in which the real part of the resonance energy is positive, the restriction $|\mathrm{Re}\, k| > |\mathrm{Im}\, k|$ follows, and consequently $\mathrm{Re}\, k^2 > 0$.In this case the relation

$$\lim_{\epsilon\to 0} \epsilon^p e^{-\frac{k^2}{4\epsilon}} = 0, \tag{2.35}$$

is valid for any real p, and may be used to obtain the following finite expressions for the integrals $I_0(k)$ and $I_1(k)$,

$$I_0(k) = \frac{i}{k}, \;\; I_1(k) = -\frac{1}{k^2}. \tag{2.36}$$

2.2.2 Regularization by complex scaling.

The regularization factor $e^{-\epsilon r^2}$ is not unique, and there exists a variety of other regularization procedures, all yielding the same unique finite result for the integrals $I_1(k)$ and $I_2(k)$. One such regularization procedure, more tractable from a numerical standpoint, is based on complex rotation in the complex r-plane, first discussed in Ref. [66]. Consider the zero contour integrals

$$\int_C dz\, e^{ikz} = 0, \;\; \int_C dz\, z e^{ikz} = 0, \tag{2.37}$$

where the contour $C = C_1 + C_2 + C_3$ is defined by a rotation angle θ in the complex r-plane as shown in figure 2.2. For $R \to \infty$ the integral along the arc C_2 vanishes and by the Cauchy Riemann integral theorem it follows

$$\tilde{I}_0(k) = \int_0^\infty dr\, e^{ikr} = e^{i\theta} \int_0^\infty dr\, e^{ikr(\cos\theta + i\sin\theta)} \tag{2.38}$$

$$\tilde{I}_1(k) = \int_0^\infty dr\, re^{ikr} = e^{2i\theta} \int_0^\infty dr\, re^{ikr(\cos\theta + i\sin\theta)}. \tag{2.39}$$

$$\tag{2.40}$$

For $k = k_1 - ik_2$ and $k_1, k_2 > 0$ these integrals converge for a rotation angle $\theta > \mathrm{atan}(k_2/k_1)$, and it is easily shown that they take the finite values

$$\tilde{I}_0(k) = I_0(k) = \frac{i}{k}, \tag{2.41}$$

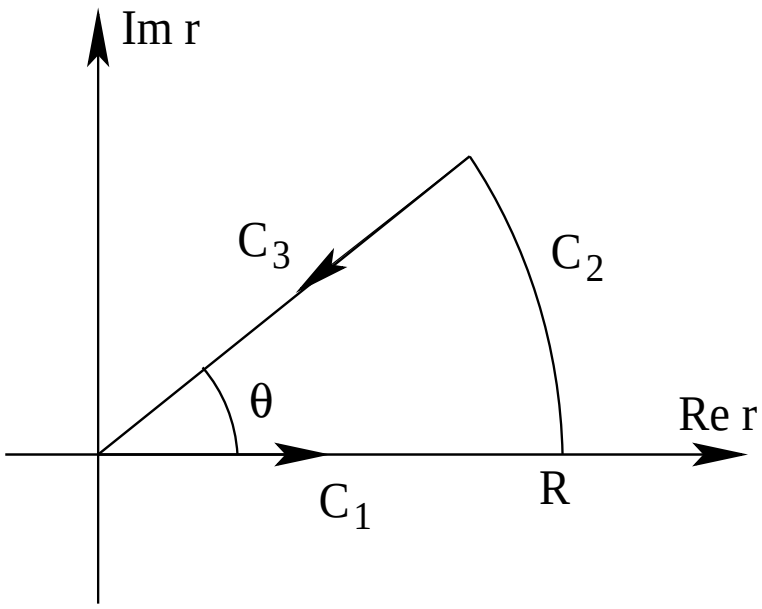

Figure 2.2: Integration contour in the complex$r$-plane used for regularization of integrals involving resonant states.

In the same way it is easily shown that the integral $\tilde{I}_2(k)$ takes the finite value

$$\tilde{I}_1(k) = I_1(k) = -\frac{1}{k^2}, \tag{2.42}$$

illustrating that different regularization procedures of divergent integrals must yield the same unique finite value, if it exists.

From the above analysis it is found that the innerproduct given in equation (2.27) of a d - and the corresponding conjugate c resonant state may be given a finite value, i.e. it is possible to normalize these states. It remains to examine whether resonant states at different energies, i.e. $k_1 \neq k_2$, form a *bi-orthogonal* set. Starting with the Schrödinger equation for two different resonant states $u_{n_1 l}(r)$ and $u_{n_2 l}(r)$ and multiplying the left with $u_{n_2 l}(r)$ and $u_{n_1 l}(r)$ respectively, one obtains by subtracting the two equations,

$$\frac{d}{dr}\left[u_{n_2 l}(r)u'_{n_1 l}(r) - u'_{n_2 l}(r)u_{n_1 l}(r)\right] = \left(k_2^2 - k_1^2\right)\tilde{u}^*_{n_2 l}(r)u_{n_1 l}(r). \tag{2.43}$$

Multipying from the left with $\int_0^\infty dr\, e^{-\epsilon r^2}$, one obtains the following expression by partial integration,

$$\begin{aligned}\int_0^\infty dr\, e^{-\epsilon r^2}\frac{d}{dr}\left[u_{n_2 l}(r)u'_{n_1 l}(r) - u'_{n_2 l}(r)u_{n_1 l}(r)\right] = \\ 2\epsilon\int_0^\infty dr\, r e^{-\epsilon r^2}\left[u_{n_2 l}(r)u'_{n_1 l}(r) - u'_{n_2 l}(r)u_{n_1 l}(r)\right] \\ = \left(k_2^2 - k_1^2\right)\int_0^\infty dr\, e^{-\epsilon r^2}\tilde{u}^*_{n_2 l}(r)u_{n_1 l}(r),\end{aligned} \tag{2.44}$$

where the boundary condition $u_{nl}(r=0)=0$ has been used. From the asymptotic form of the integrand $re^{-\epsilon r^2}e^{i(k_1+k_2)r}$ it is seen that the integrals in equation (2.44) are comparable with the finite result for the integral $I_1(k,\epsilon)$ as $\epsilon \to 0$. It follows that

$$\left(k_2^2-k_1^2\right)\lim_{\epsilon\to 0}\int_0^\infty dr\, e^{-\epsilon r^2}\tilde{u}^*_{n_2 l}(r)u_{n_1 l}(r)=0. \tag{2.45}$$

Defining the inner product of resonant states as this limit, we finally obtain

$$\langle \tilde{u}_{n_1 l}|u_{n_2 l}\rangle = \langle u^*_{n_1 l}|u_{n_2 l}\rangle = \delta_{n_1,n_2}, \tag{2.46}$$

which shows that the resonant states together with the bound states are orthogonal in this sense. In the case where bound states enter the inner product, there is no divergence problem since the bound states has an exponential decay as $r\to\infty$. This symmetric inner product is often called the c- product [14], which states that the resonances form a *bi-orthogonal* set. In the case where k_1 and k_2 are real, the c-product coincides with the usual Hermitian inner product.

2.3 The generalized Berggren completeness; proof and discussion

We have shown that the regular solution $\phi_l(k,r)$ with $k=k_n$ being the poles of the scattering matrix or zeros of the Jost function, can be normalized by some regularization procedure. Further it was shown that regular solutions $\phi_l(k,r)$ located at different k_n in the complex k-plane are orthogonal to each other, through the symmetric inner product given in equation (2.46). This suggests that the regular solutions at the poles of the scattering matrix, are part of a complete set of *bi-orthogonal*states, which may serve as an expansion basis when dealing with processes taking place in the continuum regime. This is the subject of this section.

We start with the standard completeness relation defined along the real k-axis,

$$\sum_{n=b} u_{ln}(r)u^*_{nl}(r')| + \frac{1}{2}\int_{-\infty}^{\infty} dk\, u_l(k,r)u^*_l(k^*,r') = \delta(r-r') \tag{2.47}$$

where the discrete sum is over the bound state poles located along the positive imaginary k-axis, and the integral is over the continuum of scattering functions located along the real k-axis. Note that on the real axis we have $u^*_l(k^*,r')=u^*_l(k,r')$. A proof of this completeness is given by Newton in Ref. [6]. Newton considered the integral

$$I(r)=\int_C dk\, k\int_0^\infty dr'\, h(r')G_l(k;r,r'), \tag{2.48}$$

where $h(r)$ is part of the L^2 functional space and $G_l(k;r,r')$ is the complete Green's function or resolvent. The integration contour C runs along the real k-axis from $-\infty$ to ∞, and

is closed by a semicircle in the upper half k-plane. The Green's function has poles at the same locations in the complex k-plane as the scattering matrix, and using Cauchy's residue theorem the various contributions to the integral in equation (2.48) is evaluated by the residues at the bound state poles along the positive imaginary k-axis. In the end it is shown that a l^2 function $h(r)$ may be expanded in a complete set of bound- and scattering wave functions given in equation(2.47). The class of square integrable functions, includes those with exponential asymptotics, $h(r) \to e^{ikr}$, $r \to \infty$, where k is in the upper half complex k-plane.

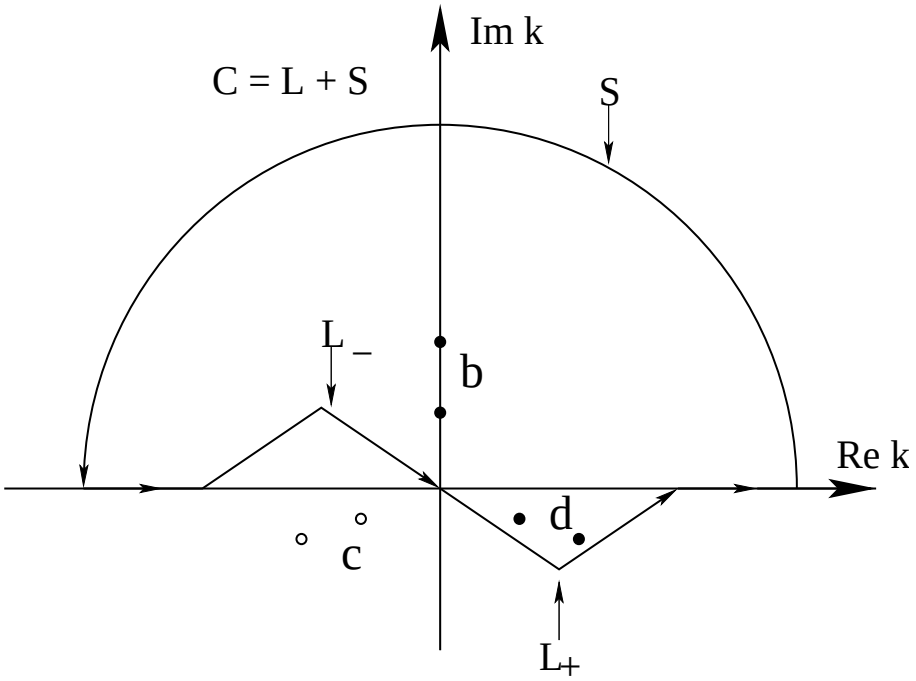

Figure 2.3: Integration contour $C = L + S$ used in deriving the Berggren completeness relation.

In Ref. [28] Berggren showed that there exist a modified completeness relation, where the resonant contributions hidden in the continuum integral were disentangled from the background of continuum states, and included in the discrete sum over bound states. The proof of Berggren, is based on the same complex analysis used by Newton, only that the integration contour C in equation (2.48) where modified to enclose not only the bound state poles, but in addition a set of *proper* resonant poles, see figure 2.3.

Later Lind [47] presented a straightforward method for deriving various completeness relations starting from the standard completeness relation given in equation (2.47). This method is based on analytic continuation of the integral over scattering functions, using the the known analytic properties of the scattering functions in the complex k-plane. As discussed in the previous section 2.1, the scattering functions have poles wherever the Green's function $G_l(k)$ or the scattering matrix elements $S_l(k)$ have poles. Deforming the integra-

tion contour defined along the real k-axis for the continuum integral in equation (2.47), one obtains by the Cauchy residue theorem

$$-\int_0^\infty dk\, u_l(k,r)\tilde{u}_l^*(k,r') + \int_{L^+} dk\, u_l(k,r)\tilde{u}_l^*(k,r') = 2\pi i \sum_{k_n\in\mathbf{C}} \operatorname*{Res}_{k=k_n} u_l(k,r)\tilde{u}_l^*(k,r'), \quad (2.49)$$

where the contour L^+ is part of the inversion symmetric contour $L = L^- + L^+$, and is the deformation of the positive real k-axis. Here $\tilde{u}_l(k,r) = u_l(k^*,r)$ are associated with scattering functions on the conjugated contour L^*, which encloses the capture resonances which are orthogonal to the decay resonances enclosed by L. Inversion symmetric contour meaning that if k is on L, then so is $-k$. The product of scattering functions $u_l(k,r)\tilde{u}_l(k,r')$ is a meromorphic function of k with poles given by the Jost functions $f_l(-k) = 0$ and $f_l^*(-k^*) = 0$. The residue is evaluated at each pole $k = k_n$ of the scattering functions, located in the region between the contour L^+ and the real positive k-axis labeled $\mathbf{C}$. In writing equation (2.49) the inversion symmetry of L and the symmetry of the integrand in the continuum integral has been exploited to give

$$\int_{L^-} dk\, u_l(k,r)\tilde{u}_l^*(k,r') = \int_{L^+} dk\, u_l(k,r)\tilde{u}_l^*(k,r') \quad (2.50)$$

In Ref. [47] the importance of choosing an inversion symmetric contour was discussed. If L is inversion symmetric, the complex continuum integral can be rewritten in terms of scattering functions, and the continuum integrals can be written using energy as the integration variable. In deriving the general Berggren completeness the residues in equation (2.49) have to be evaluated. Writing the physical wave function in terms of the regular solution and the Jost function, see Sec. 2.1 for further details, one gets

$$u_l(k,r) = \sqrt{\frac{2}{\pi}}\frac{k^{l+1}\phi_l(k,r)}{f_l(-k)}, \quad (2.51)$$

and for the conjugate wave function $\tilde{u}_l(k,r)$,

$$\tilde{u}_l(k,r) = u_l(k^*,r) = \sqrt{\frac{2}{\pi}}\frac{(k^*)^{l+1}\phi_l(k^*,r)}{f_l(-k^*)} = \left(\sqrt{\frac{2}{\pi}}\frac{k^{l+1}\phi_l(k,r)}{f_l(k)}\right)^*, \quad (2.52)$$

where use has been made of the symmetry properties of the regular and Jost functions given in equation (2.8). The residue in equation (2.49) may then be written as

$$\operatorname*{Res}_{k=k_n} u_l(k,r)\tilde{u}_l^*(k,r') = \operatorname*{Res}_{k=k_n} \frac{2}{\pi}\frac{k^{2l+2}\phi_l(k,r)\phi_l(k,r')}{f_l(k)f_l(-k)}, \quad (2.53)$$

Making use of the property $\mathrm{Res}_{z=z_0} h(z)/g(z) = h(z_0)/g'(z_0)$ where $h(z)$ and $g(z)$ are analytic functions at $z = z_0$, it is seen that following derivative has to be evaluated,

$$\frac{d}{dk}f_l(k)f_l(-k)\bigg|_{k=k_n} = f_l(k_n)\left.\frac{d}{dk}f_l(-k)\right|_{k=k_n}, \quad (2.54)$$

here the fact the Jost function $f_l(-k) = 0$ for $k = k_n$ has been used. The problem of determining the residue in equation (2.49) has now been reduced to the problem of determining the derivative of the Jost function at the resonance pole $k = k_n$. In Ref. [47] the derivative of the Jost function where proven to be

$$\frac{d}{dk} f_l(-k)\Big|_{k=k_n} = i4k_n^{2l+2} Reg \int_0^\infty dr r^2 \phi_l^2(k_n, r) = i4k_n^{2l+2} N^2, \tag{2.55}$$

where N is the norm of the regularized resonances wave functions appearing in the integral. The sum over residues in equation (2.49) now becomes,

$$\begin{aligned} 2\pi i \sum_{k_n \in \mathbf{C}} \operatorname*{Res}_{k=k_n} u_l(k,r)\tilde{u}_l^*(k,r') &= 4i \sum_{k_n \in \mathbf{C}} \frac{k^{2l+2}\phi_l(k_n,r)\phi_l(k_n,r')}{\frac{d}{dk} f_l(k) f_l(-k)\big|_{k=k_n}} \\ &= \sum_{k_n \in \mathbf{C}} \frac{\phi_l(k_n,r)\phi_l(k_n,r')}{N^2} = \sum_{k_n \in \mathbf{C}} u_{nl}(r)\tilde{u}_{nl}^*(r'), \end{aligned} \tag{2.56}$$

inserting this into equation (2.49), one gets the following expression for the integral over scattering functions along the real k-axis (positive energy states),

$$\int_0^\infty dk\, u_l(k,r)\tilde{u}_l^*(k,r') = \sum_{k_n \in \mathbf{C}} u_{nl}(r)\tilde{u}_{nl}^*(r') + \int_{L^+} dk\, u_l(k,r)\tilde{u}_l^*(k,r'), \tag{2.57}$$

where it is explicitly seen that the resonant contributions hidden in the the continuum integral along the real k-axis has been disentangled. In Ref. [47] it was shown for finite range potentials that the continuum integral along the contour L^+ produces a smooth background, but is in most cases non-neglible. Switching to abstract vector notation, it has been shown that for a general inversion symmetric contour L, see figure 2.4, the generalized Berggren completeness becomes,

$$\mathbf{1} = \sum_{n=a,b,c,d} |u_{nl}\rangle\langle\tilde{u}_{nl}| + \int_{L^+} dk\, |u_l(k)\rangle\langle\tilde{u}_l(k)|. \tag{2.58}$$

The discrete sum includes all types of poles of the scattering matrix, i.e. anti-bound (a), bound (b), capture resonant (c) and decay resonant (d) states. This completeness can be used to expand all functions with exponential asymptotics, e^{ikr}, $r \to \infty$ where k is located within the closed contour $C = L + S$. Keeping only the discrete part of the completeness relation (2.58), one ends up with the pole-approximation. As shown in figure 2.4 a typical inversion symmetric contour cannot separate all poles from the continuum integral. In this particular case the red circles gives the poles which are not included in the discrete sum, while the black circles give the poles which are included in the sum. It is important to emphasize that completeness defined either along the real k-axis or along a distorted contour L in the complex k-plane are equivalent in the sense,

$$\begin{aligned} \mathbf{1} &= \sum_{n=a,b,c,d} |u_{nl}\rangle\langle\tilde{u}_{nl}| + \int_{L^+} dk\, |u_l(k)\rangle\langle\tilde{u}_l(k)| \\ &= \sum_{n=b} |u_{nl}\rangle\langle\tilde{u}_{nl}| + \int_0^\infty dk\, |u_l(k)\rangle\langle\tilde{u}_l(k)| \end{aligned} \tag{2.59}$$

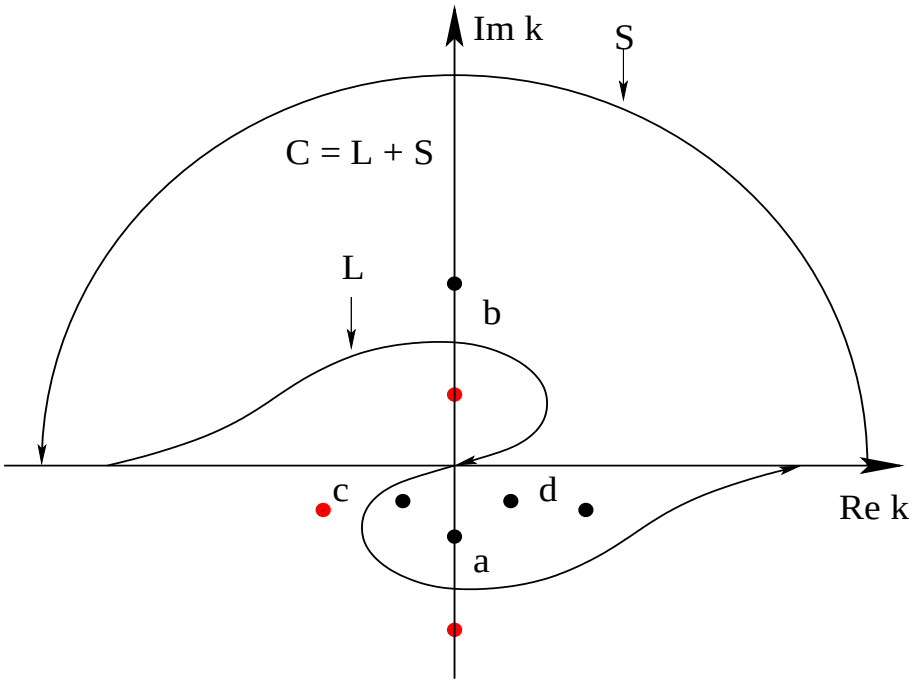

Figure 2.4: General inversion symmetric contour $C = L+S$ used in deriving the generalized Berggren completeness relation. The black circles represents the poles which are included in the discrete sum, while the red circles are poles which are embedded in the continuum integral along the contour L^+.

the difference being that for a completeness defined along the real k-axis all the interesting processes taking place in the continuum are hidden as peaks within the continuum integral, while for a completeness defined along L the most interesting phenomena, i.e. the resonant contributions, are extracted out of the continuum integral and can be studied separately.

2.4 Interpretation of complex observables

Turning to the interpretation of expectation values of observable operators involving resonant states, it is natural to ask what physical meaning one should assign to such expectation values. The resonant states are complex, yielding complex expectation values of the Hamiltonian H and any other Hermitian observable operator A. If resonant states are to be seen as excited states in which a particular system can undergo transition from and to, and such transitions are expected to be seen experimentally, a physical interpretation of the real and imaginary parts of $\langle A \rangle$ is necessary. This question was first raised by Berggren [28] and later by Gyarmati et. al. [67], where it was conjectured that the physical meaning of an expectation value $\langle A \rangle$ when the system is in a resonant state is given by the real part,

$$\langle A \rangle = \mathrm{Re}\langle \tilde{u}_{nl}|A|u_{nl}\rangle \tag{2.60}$$

A theoretical justification of this conjecture was given by Berggren in Ref. [68], where it was shown starting from scattering theory, that the real part of the complex cross section for populating a resonance is equal to the energy integral of the in-elastic continuum cross section across the resonance peak. The imaginary part of the cross section where identified with the strength of the resonance-background interference. In Ref. [69] this conclusion where generalized to hold for any observable operator A involving resonant states. To throw some light on this interpretation, consider the matrix element of an operator A with a scattering function defined on the real energy axis,

$$\langle \tilde{u}_l(k)|A|u_l(k)\rangle = \mathrm{Re}\langle \tilde{u}_l(k)|A|u_l(k)\rangle. \tag{2.61}$$

Suppose now that the Jost function $f_l(-k)$ has a zero located close to the real k-axis, which is associated with a narrow resonance. Since the scattering wave functions have poles wherever the Jost functions have zeroes, see equation (2.13) of section 2.1, the matrix element 2.61 will display a sharp peak when it is plotted as a function of energy, and the energy traverses the real part of the resonance energy. The momentum (energy)-integrated matrix elemenent is,

$$\int_0^{k_{\max}} dk\, \langle \tilde{u}_l(k)|A|u_l(k)\rangle =$$

$$\int_C dk\, \langle \tilde{u}_l(k)|A|u_l(k)\rangle - 2\pi i \operatorname*{Res}_{k=k_n} \langle \tilde{u}_l(k)|A|u_l(k)\rangle, \tag{2.62}$$

where C is a contour in the fourth quadrant of the complex k-plane enclosing the pole at $k = k_n$, and joining the real axis at$k = 0$ and $k = k_{\max}$, see figure 2.4. The residue in

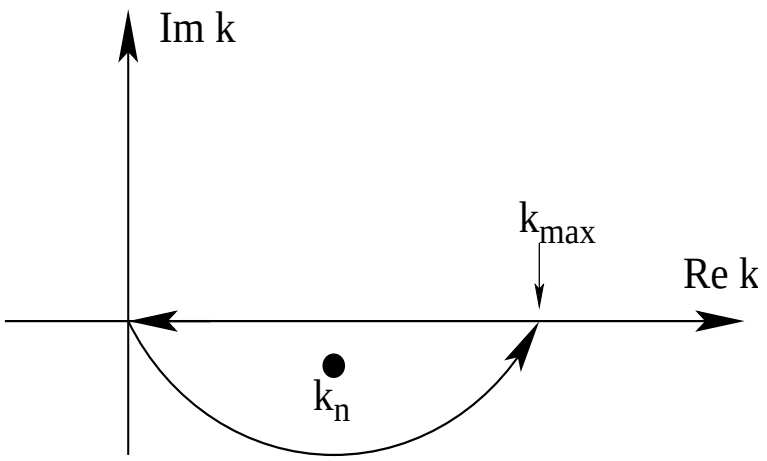

Figure 2.5: Integration contour used in evaluating the pure resonance contribution to the energy-integrated expectation value.

equation (2.62) is given by equation (2.53) from the previous section, and consequently,

$$\begin{aligned}
&\int_0^{k_{\max}} dk\, \langle \tilde{u}_l(k,r)|A|u_l(k,r)\rangle = \\
&\int_C dk\, \langle \tilde{u}_l(k,r)|A|u_l(k,r)\rangle + \langle \tilde{u}_{nl}|A|u_{nl}\rangle = \\
&\mathrm{Re}\int_C dk\, \langle \tilde{u}_l(k)|A|u_l(k)\rangle + \mathrm{Re}\langle \tilde{u}_{nl}|A|u_{nl}\rangle .
\end{aligned} \tag{2.63}$$

Since the expectation value is by definition real, the imaginary parts of the contour integral of the scattering functions and the imaginary part of the matrix element involving the resonance at $k = k_n$ must cancel, in this way it is illustrated that the imaginary part of $\langle \tilde{u}_{nl}|A|u_{nl}\rangle$ may be interpreted as an interference effect with the continuum background.

Assuming now that equation (2.60) is a reasonable physical interpretation of the formal expectation value $\langle \tilde{u}_{nl}|A|u_{nl}\rangle$, what meaning should one assign the imaginary part? Let us start with the usual definition of the average deviation, or indeterminacy, of an operator A which is assumed to commute with the Hamiltonian H,

$$(\Delta A)^2 = \langle A^2 - \langle A\rangle^2\rangle = \langle A^2\rangle - \langle A\rangle^2 \tag{2.64}$$

Using the definition of $\langle A\rangle$ in equation (2.60), it is easily found that

$$\langle A^2\rangle = \mathrm{Re}\langle \tilde{u}_{nl}|A^2|u_{nl}\rangle = \left[\mathrm{Re}\langle \tilde{u}_{nl}|A|u_{nl}\rangle\right]^2 - \left[\mathrm{Im}\langle \tilde{u}_{nl}|A|u_{nl}\rangle\right]^2 \tag{2.65}$$

and

$$\langle A\rangle^2 = \left[\mathrm{Re}\langle \tilde{u}_{nl}|A|u_{nl}\rangle\right]^2 . \tag{2.66}$$

Inserting this into equation (2.64) yields,

$$(\Delta A)^2 = \langle A^2 - \langle A\rangle^2\rangle = -\left[\mathrm{Im}\langle \tilde{u}_{nl}|A|u_{nl}\rangle\right]^2 . \tag{2.67}$$

Thus is is then formally shown that the imaginary part of the expectation value of an operator A in a resonant state, gives the uncertainty or indetermiacy of the measured result. This may also be understood from physical grounds. Resonant states have definite lifetimes, i.e. they decay in time. The lifetime of the resonant state is determined by the propability of tunneling through the potential barrier, in which the resonance is formed. The probability of decay is proportional to the imaginary part of the resonance pole or in other words the resonance width Γ. Let the operator A be the Hamiltonian of the system, $A = H$, then equation (2.67)becomes,

$$(\Delta H)^2 = \langle H^2 - \langle H\rangle^2\rangle = -\frac{\Gamma^2}{4}, \tag{2.68}$$

where it is explicitly seen that by the defintion of $\langle H\rangle$, the width Γ determines the uncertainty in energy measurements.

Chapter 3

Contour deformation method (CDM) in momentum space; theory and applications

3.1 The momentum space Schrödinger equation.

The Schrödinger equation in abstract vector representation is

$$(T+V)\,|\psi_n\rangle = E_n|\psi_n\rangle \tag{3.1}$$

Here T is the kinetic energy operator and V is the potential operator. The eigenstates form a complete orthonormal set according to

$$\mathbf{1} = \sum_n |\psi_n\rangle\langle\psi_n|, \;\; \langle\psi_n|\psi_{n'}\rangle = \delta_{n,n'}$$

The most commonly used representations of equation 3.1 are the coordinate and the momentum space representations. They define the completeness relations

$$\mathbf{1} = \int d\mathbf{r}\,|\mathbf{r}\rangle\langle\mathbf{r}|, \;\; \langle\mathbf{r}|\mathbf{r}'\rangle = \delta(\mathbf{r}-\mathbf{r}') \tag{3.2}$$

$$\mathbf{1} = \int d\mathbf{k}\,|\mathbf{k}\rangle\langle\mathbf{k}|, \;\; \langle\mathbf{k}|\mathbf{k}'\rangle = \delta(\mathbf{k}-\mathbf{k}') \tag{3.3}$$

Here the basis states in both **r**- and **k**-space are dirac-delta function normalized. From this it follows that the plane-wave states are given by, [1]

$$\langle\mathbf{r}|\mathbf{k}\rangle = \left(\frac{1}{2\pi}\right)^{3/2} \exp\left(i\mathbf{k}\cdot\mathbf{r}\right) \tag{3.4}$$

[1] Some authors define the plane wave by $\langle\mathbf{r}|\mathbf{k}\rangle = \exp\left(i\mathbf{k}\cdot\mathbf{r}\right)$, in which case $\langle\mathbf{k}|\mathbf{k}'\rangle = (2\pi)^3\,\delta(\mathbf{k}-\mathbf{k}')$ and each $\int d\mathbf{k}$ is replaced by $(1/2\pi)^{3/2}\int d\mathbf{k}$.

which is a transformation function defining the mapping from the abstract $|\mathbf{k}\rangle$ to the abstract $|\mathbf{r}\rangle$ space. That the $\mathbf{r}$-space basis states are delta-function normalized follows from

$$\delta(\mathbf{r}-\mathbf{r}') = \langle \mathbf{r}|\mathbf{r}'\rangle = \langle \mathbf{r}|\mathbf{1}|\mathbf{r}'\rangle = \int \mathrm{d}\mathbf{k}\langle \mathbf{r}|\mathbf{k}\rangle\langle \mathbf{k}|\mathbf{r}'\rangle = \left(\frac{1}{2\pi}\right)^3 \int \mathrm{d}\mathbf{k} e^{i\mathbf{k}(\mathbf{r}-\mathbf{r}')} \tag{3.5}$$

and the same for the momentum space basis states,

$$\delta(\mathbf{k}-\mathbf{k}') = \langle \mathbf{k}|\mathbf{k}'\rangle = \langle \mathbf{k}|\mathbf{1}|\mathbf{k}'\rangle = \int \mathrm{d}\mathbf{r}\langle \mathbf{k}|\mathbf{r}\rangle\langle \mathbf{r}|\mathbf{k}'\rangle = \left(\frac{1}{2\pi}\right)^3 \int \mathrm{d}\mathbf{r} e^{i\mathbf{r}(\mathbf{k}-\mathbf{k}')} \tag{3.6}$$

Projecting equation 3.1 on momentum states[2], the momentum space Schrödinger equation is obtained,

$$\frac{\hbar^2}{2\mu}k^2\psi_n(\mathbf{k}) + \int d\mathbf{k}'\, V(\mathbf{k},\mathbf{k}')\psi_n(\mathbf{k}') = E_n\psi_n(\mathbf{k}) \tag{3.7}$$

Here the notation $\psi_n(\mathbf{k}) = \langle \mathbf{k}|\psi_n\rangle$ and $\langle \mathbf{k}|V|\mathbf{k}'\rangle = V(\mathbf{k},\mathbf{k}')$ has been introduced. The potential in momentum space is given by a double Fourier-transform of the potential in coordinate space, i.e.

$$V(\mathbf{k},\mathbf{k}') = \left(\frac{1}{2\pi}\right)^3 \int \mathrm{d}\mathbf{r} \int \mathrm{d}\mathbf{r}'\, e^{-i\mathbf{k}\mathbf{r}} V(\mathbf{r},\mathbf{r}') e^{i\mathbf{k}'\mathbf{r}'} \tag{3.8}$$

Here it is assumed that the potential interaction does not contain any spin dependence. Instead of a differential equation in coordinate space, the Schrödinger equation becomes an integral equation in momentum space. This has many tractable features. Firstly, most realistic nucleon-nucleon interactions derived from field-theory are given explicitly in momentum space. Secondly, the boundary conditions imposed on the differential equation in coordinate space are automatically built into the integral equation. And last, but not least, integral equations are easy to numerically implement, and convergence is obtained by just increasing the number of integration points. Instead of solving the three-dimensional integral equation given in equation (3.7), an infinite set of 1-dimensional equations can be obtained by invoking a partial wave expansion. The wave function $\psi_n(\mathbf{k})$ can be expanded in a complete set of spherical harmonics, i.e.

$$\psi_n(\mathbf{k}) = \sum_{lm} \psi_{nlm}(k) Y_{lm}(\hat{k}), \;\; \psi_{nlm}(k) = \int d\hat{k} Y^*_{lm}(\hat{k})\psi_n(\mathbf{k}). \tag{3.9}$$

By inserting equation 3.9 in equation 3.7, and projecting from the left $Y_{lm}(\hat{k})$, the three-dimensional Schrödinger equation (3.7) is reduced to an infinite set of 1-dimensional angular momentum coupled integral equations,

$$\left(\frac{\hbar^2}{2\mu}k^2 - E_{nlm}\right)\psi_{nlm}(k) = -\sum_{l'm'} \int_0^\infty dk' k'^2 V_{lm,l'm'}(k,k')\psi_{nl'm'}(k') \tag{3.10}$$

[2]In the literature the momentum states are often called plane-wave states.

where the angular momentum projected potential takes the form,

$$V_{lm,l'm'}(k,k') = \int \mathrm{d}\hat{k} \int \mathrm{d}\hat{k}'\, Y^*_{lm}(\hat{k}) V(\mathbf{k},\mathbf{k}') Y_{l'm'}(\hat{k}') \tag{3.11}$$

here $\mathrm{d}\hat{k} = \mathrm{d}\theta \sin\theta\, \mathrm{d}\varphi$. In many cases the potential is given in position space, so it is convinient to establish the connection between $V_{lm,l'm'}(k,k')$ and $V_{lm,l'm'}(r,r')$. Inserting position space completeness in equation (3.11) gives

$$\begin{aligned} V_{lm,l'm'}(k,k') = \int \mathrm{d}\mathbf{r} \int \mathrm{d}\mathbf{r}' \int \mathrm{d}\hat{k} \int \mathrm{d}\hat{k}'\, Y^*_{lm}(\hat{k}) \langle \mathbf{k}|\mathbf{r}\rangle \langle \mathbf{r}|V|\mathbf{r}'\rangle \langle \mathbf{r}'|\mathbf{k}'\rangle Y_{lm}(\hat{k}') = \\ \int \mathrm{d}\mathbf{r} \int \mathrm{d}\mathbf{r}' \left\{ \int \mathrm{d}\hat{k} Y^*_{lm}(\hat{k}) \langle \mathbf{k}|\mathbf{r}\rangle \right\} \langle \mathbf{r}|V|\mathbf{r}'\rangle \left\{ \int \mathrm{d}\hat{k}'\, Y_{lm}(\hat{k}') \langle \mathbf{r}'|\mathbf{k}'\rangle \right\} \end{aligned} \tag{3.12}$$

Since the plane waves depend only on the absolute values of position and momentum, $|\mathbf{k}|$, $|\mathbf{r}|$, and the angle between them, θ_{kr}, they may be expanded in terms of bipolar harmonics of zero rank [70], i.e.

$$e^{i\mathbf{k}\cdot\mathbf{r}} = 4\pi \sum_{l=0}^{\infty} i^l j_l(kr) \left(Y_l(\hat{k}) \cdot Y_l(\hat{r}) \right) = \sum_{l=0}^{\infty} (2l+1) i^l j_l(kr) P_l(\cos\theta_{kr}) \tag{3.13}$$

Where the addition theorem for spherical harmonics has been used in order to write the expansion in terms of Legendre polynomials. The spherical Bessel functions, $j_l(z)$, are given in terms of Bessel functions of the first kind with half integer orders [71, 72],

$$j_l(z) = \sqrt{\frac{\pi}{2z}} J_{l+1/2}(z).$$

Inserting the plane-wave expansion into the brackets of equation (3.12) yields,

$$\begin{aligned} \int \mathrm{d}\hat{k} Y^*_{lm}(\hat{k}) \langle \mathbf{k}|\mathbf{r}\rangle &= \left(\frac{1}{2\pi}\right)^{3/2} 4\pi i^{-l} j_l(kr) Y^*_{lm}(\hat{r}), \\ \int \mathrm{d}\hat{k}'\, Y_{lm}(\hat{k}') \langle \mathbf{r}'|\mathbf{k}'\rangle &= \left(\frac{1}{2\pi}\right)^{3/2} 4\pi i^{l'} j_{l'}(k'r') Y_{l'm'}(\hat{r}). \end{aligned}$$

The connection between the momentum- and position space angular momentum projected potentials are then given,

$$V_{lm,l'm'}(k,k') = \frac{2}{\pi} i^{l'-l} \int_0^{\infty} dr\, r^2 \int_0^{\infty} dr'\, r'^2 j_l(kr) V_{lm,l'm'}(r,r') j_{l'}(k'r') \tag{3.14}$$

which is known as a double Fourier-Bessel transform. The position space angular momentum projected potential is given by,

$$V_{lm,l'm'}(r,r') = \int \mathrm{d}\hat{r} \int \mathrm{d}\hat{r}'\, Y^*_{lm}(\hat{r}) V(\mathbf{r},\mathbf{r}') Y_{l'm'}(\hat{r}'). \tag{3.15}$$

No assumptions of locality/non-locality and deformation of the interaction has so far been made, and the result in equation (3.14) is general. In position space the Schrödinger equation takes form of an integro-differential equation in case of a non-local interaction, in momentum space the Schrödinger equation is an ordinary integral equation of the Fredholm type, see equation (3.10). This is a further advantage of the momentum space approach as compared to the standard position space approach. If we assume that the interaction is of local character, i.e.

$$\langle \mathbf{r}|V|\mathbf{r}'\rangle = V(\mathbf{r})\delta(\mathbf{r}-\mathbf{r}') = V(\mathbf{r})\frac{\delta(r-r')}{r^2}\delta(\cos\theta-\cos\theta')\delta(\varphi-\varphi'), \tag{3.16}$$

then equation (3.15) reduces to

$$V_{lm,l'm'}(r,r') = \frac{\delta(r-r')}{r^2}\int \mathrm{d}\hat{r}\; Y^*_{lm}(\hat{r})V(\mathbf{r})Y_{l'm'}(\hat{r}), \tag{3.17}$$

and equation (3.14) reduces to

$$V_{lm,l'm'}(k,k') = \frac{2}{\pi}i^{l'-l}\int_0^\infty dr\; r^2\; j_l(kr)V_{lm,l'm'}(r)j_{l'}(k'r) \tag{3.18}$$

where

$$V_{lm,l'm'}(r) = \int \mathrm{d}\hat{r}\; Y^*_{lm}(\hat{r})V(\mathbf{r})Y_{l'm'}(\hat{r}), \tag{3.19}$$

In the case that the interaction is central, $V(\mathbf{r}) = V(r)$, then

$$V_{lm,l'm'}(r) = V(r)\int \mathrm{d}\hat{r}\; Y^*_{lm}(\hat{r})Y_{l'm'}(\hat{r}) = V(r)\delta_{l,l'}\delta_{m,m'}, \tag{3.20}$$

and

$$V_{lm,l'm'}(k,k') = \frac{2}{\pi}\int_0^\infty dr\; r^2\; j_l(kr)V(r)j_{l'}(k'r)\delta_{l,l'}\delta_{m,m'} = V_l(k,k')\delta_{l,l'}\delta_{m,m'} \tag{3.21}$$

where the momentum space representation of the interaction finally reads,

$$V_l(k,k') = \frac{2}{\pi}\int_0^\infty dr\; r^2\; j_l(kr)V(r)j_l(k'r). \tag{3.22}$$

For a local and spherical symmetric potential, the coupled momentum space Schrödinger equations given in equation (3.10) decouples in angular momentum, giving

$$\frac{\hbar^2}{2\mu}k^2\psi_{nl}(k) + \int_0^\infty dk'k'^2V_l(k,k')\psi_{nl}(k') = E_{nl}\psi_{nl}(k) \tag{3.23}$$

Where we have written $\psi_{nl}(k) = \psi_{nlm}(k)$, since the equation becomes independent of the projection m for spherical symmetric interactions. The momentum space wave functions $\psi_{nl}(k)$ defines a complete orthogonal set of functions, which spans the space of functions with a positive finite Euclidean norm (also called l^2-norm), $\sqrt{\langle\psi_n|\psi_n\rangle}$, which is a Hilbert space. The corresponding normalized wave function in coordinate space is given by the Fourier-Bessel transform

$$\phi_{nl}(r) = \sqrt{\frac{2}{\pi}}\int dk\; k^2 j_l(kr)\psi_{nl}(k) \tag{3.24}$$

3.2 Analytic continuation of momentum space Schrödinger equation by CDM

In Chapter 2 it was shown how the generalized Berggren completeness relations may be derived from the completeness relation defined on the physical energy sheet using analytic continuation techniques to reach into the non-physical energy sheet. Having obtained a generalized completeness relation, the corresponding eigenvalue problem may easily be deduced. On the other hand one may start with the eigenvalue problem for bound- and scattering scates, and investigate under which conditions the Schrödinger equation may be continued to the non-physical energy sheet where the most interesting continuum phenomena, i.e. the resonance phenomena, are located. In this section we outline a method which analytically continue the momentum space Schrödinger equation through the unitarity cut onto the second Riemann sheet of the complex energy plane, which is based on deforming the integration contour. This method is known as the *contour deformation (distortion) method* (CDM). The contour deformation method was first introduced in the study of the full off-shell scattering amplitudes in two- and three particle scattering in the early 60's, see Refs. [73, 74, 75, 25]. A rotation of the integration contour in the momentum space integral equations extended the domain over which the integral kernel is a compact (Schmidt)-operator. This has numerical advantages as the kernel is no longer singular. In 1954 Wick [76] introduced the method of contour rotation in momentum space; in transforming the equation to the imaginary axis the strong singularities of the interaction kernel where avoided. A rotation of the contour in momentum space has therefore often been referred to as Wick rotation. The contour deformation method has therefore two important applications, first the Schrødinger equation is analytically continued onto the non-physical sheet revealing resonant structures and secondly it provides a method for making the integral kernels compact enabling stable numerical solutions for the scattering amplitudes.

In the following we consider the momentum space Schrødinger equation given in equation (3.10) where the potential is assumed spherically symmetric and with no spin- or tensor components. Equation 3.23 may be rewritten as an integral equation for the bound states

$$\psi_{nl}(k) = \frac{1}{E_{nl} - k^2/2\mu} \int_0^\infty dk' k'^2 V_l(k,k') \psi_{nl}(k'). \tag{3.25}$$

For real k, k' this equation is defined on the physical energy sheet, i.e. in the upper half complex k-plane. If this equation to describe a resonant or anti bound state, it has to be anlytically continued through the branch cut along the real energy axis and onto the non-physical energy sheet, defined as the lower half complex k-plane.

The most straightforward method of analytic continuation is by use of power series. Consider a function $f(z)$ analytic in the domain D, and let f_1 and f_2 be taylor series of $f(z)$ about z_0 and z_0' on domains D_1 and D_2, respectively,

$$f_1(z) = \sum_{n=0}^{\infty} a_n (z - z_0)^n, \quad f_2(z) = \sum_{n=0}^{\infty} b_n (z - z'_0)^n$$

Both domains D_1 and D_2 are in D, and the radius of convergence is determined by distance from z_0 and z_0' to the nearest point on the boundary of analyticity region D. Further suppose that the intersection $D_1 \cap D_2$ is not empty and that $f_1 = f_2$ on $D_1 \cap D_2$. Then f_2 is called an analytic continuation f_1 of to D_2, and vice versa. This procedure may be iterated to obtain the values of $f(z)$ in the entire domain D based on its values in the subdomains $D_1, D_2, ...$

Consider now the analytic continuation of the bound state equation given in equation (3.25). In analytic continuation of integral equations we state the general rule, see for example [7, 6]:
Continuing an integral in the complex plane, the moving singularities of the integrand must not intercept the integration contour.
First of all, it is seen that the analytic properties of $\psi_{nl}(k)$ is determined by the interaction, $V_l(k,q)$ entering the integral kernel. The analytic continuation of equation (3.25) to the lower half complex energy plane is a stepwise process where overlapping domains of analyticity are created. Each step of analytic continuation of the bound state Schrödinger equation to the lower half complex energy plane involves the following three steps:

1. The analyticity domain, D_1, for the wavefunction $\psi_{nl}(k)$ is determined. The analyticity of $\psi(k)$ is given by the potential $V(k,q)$, where in the first step q is defined along the real axis.

2. Having determined the analyticity region D_1 in the lower half k-plane, the integration in q along the real axis may be distorted onto a contour L_1^+ in the lower half complex k-plane, using the Cauchy integral formula. All points on the contour L_1^+ must be contained in the analyticity domain D_1.

3. A new analyticity domain D_2 is determined for the wavefunction $\psi(k)$. The domain D_2 is again determined by the singularity structure of the potential $V(k,q)$ where q is now on the distorted contour L_1^+. If and only if the contour L_1^+ also lies in the new domain of analyticity D_2, we may choose k on L_1^+ as well. This gives a closed integral equation, and the Schrödinger equation is transformed onto the contour L_1^+.

This process of analytic continuation may be continued iteratively uncovering larger domains of interest in the complex energy plane. The contour L^+ start at $k = 0$, and is therefore by definition part of the inversion symmetric contour $L = L^- + L^+$. The analytically continued equation (3.23) on a general inversion symmetric contour then takes the form

$$\frac{\hbar^2}{2\mu}k^2\psi_{nl}(k) + \frac{2}{\pi}\int_{L^+} dk' k'^2 V_l(k,k')\psi_{nl}(k') = E_{nl}\psi_{nl}(k). \tag{3.26}$$

Here both k and k' are defined on the inversion symmetric contour L^+ in the lower half complex k-plane, giving a closed integral equation. [3] The analytically continued wave functions $\psi_{nl}(k)$ defines a complete bi-orthogonal set of functions, which spans the space

[3] See Paper I for an application of CDM to the solution of anti-bound and resonant states and scattering in the Malfliet-Tjon potential.

of functions with exponential asymptotics in the domain above the inversion symmetric contour L^+, see also Chapter 2. The wave functions are normalized according to the generalized inner product (c-product), see e.g. [14, 77]

$$\int_{L^+} dk k^2 \psi_{nl}(k)\psi_{n'l}(k) = \delta_{n,n'} \tag{3.27}$$

The corresponding normalized wave function in coordinate space is given by the Fourier-Bessel transform

$$\phi_{nl}(r) = \sqrt{\frac{2}{\pi}} \int dk\, k^2 j_l(kr)\psi_{nl}(k) \tag{3.28}$$

the orthogonality of the coordinate wave functions is easily proved using the orthogonality of the spherical Bessel functions [71],

$$\int dr\, r^2 j_l(kr) j_l(k'r) = \frac{\pi}{2} \frac{\delta(k-k')}{kk'}. \tag{3.29}$$

Equation (3.26) is analytically solvable for only a limiting class of potenials. Newton [6] proved that for all separable potentials, equation (3.26) admits solutions in closed forms. In most practical applications the solutions have to be approximated numerically. This is for example the case for the Woods-Saxon potential which is widely used in nuclear physics. In solving equation 3.26 numerically, one chooses a set of N grid points in $k-$space by some quadrature rule, e.g. Gauss-Legendre. The integral is then discretized by $\int dk \to \sum_{i=1}^{N} w_i$. On the chosen grid, equation 3.26 takes the form

$$\frac{\hbar^2}{2\mu} k_i^2 \psi_{nl}(k_i) + \sum_j^N w_j k_j^2 V_l(k_i, k_j)\psi_{nl}(k_j) = E_{nl}\psi_{nl}(k_i) \tag{3.30}$$

this equation represents a non-symmetric eigenvalue problem which is easily solved numerically. As most diagonalization routines are optimized for specific classes of matrices, it would be preferable to obtain a symmetric matrix, in the complex case the computational cost is drastically reduced if the matrix to be diagonalized can be made symmetric, see e.g. [78, 79, 80]. Equation 3.30 is easily made symmetric by multiplying through with $\sqrt{w_i}k_i$. Defining $\psi_{nl}(i) \equiv \sqrt{w_i}k_i\psi_{nl}(k_i)$, one gets the symmetric eigenvalue problem,

$$\frac{\hbar^2}{2\mu} k_i^2 \psi_{nl}(i) + \sum_j^N \sqrt{w_i w_j} k_i k_j V_l(k_i, k_j)\psi_{nl}(j) = E_{nl}\psi_{nl}(i) \tag{3.31}$$

The norm integral in equation (3.27) becomes the discrete sum

$$\delta_{n,n'} = \sum_{i=1}^{N} \psi_{nl}(i)\psi_{n'l}(i) = \sum_{i=1}^{N} w_i k_i^2 \psi_{nl}(k_i)\psi_{n'l}(k_i), \tag{3.32}$$

and the discretized completeness relation then takes the form

$$\mathbf{1} = \sum_{n}^{N} |\psi_{nl}\rangle\langle\psi_{nl}^{*}| = \sum_{n}^{N}\sum_{i=1}^{N} \psi_{nl}(i)\psi_{nl}(i) \tag{3.33}$$

Changing from a continuous to a discrete plane-wave basis, it becomes transparent that the coordinate wave function is an expansion in a basis of spherical-Bessel functions

$$\phi_{nl}(r) = \sqrt{\frac{2}{\pi}} \sum_{i=1}^{N} \sqrt{w_i} k_i j_l(k_i r) \psi_{nl}(i) \tag{3.34}$$

where $\psi_{nl}(i)$ are the expansion coefficients. Defining the functions

$$f_l(k_i r) = \sqrt{\frac{2}{\pi}} \sqrt{w_i} k_i j_l(k_i r) \tag{3.35}$$

and using the discrete representation of the Dirac-delta function

$$\delta(k - k') \to \frac{\delta_{k_i,k_j}}{\sqrt{w_i w_j}} \tag{3.36}$$

we get the expansion

$$\phi_{nl}(r) = \sum_{i=1}^{N} \psi_{nl}(i) f_l(k_i r) \tag{3.37}$$

where it is easily seen that the functions $f_l(k_i r)$ are orthogonal for different k_i and normalized

$$\int dr\, r^2 f_l(k_i r) f_l(k_j r) = \delta_{k_i,k_j} \tag{3.38}$$

where δ_{k_i,k_j} is the Kronecker delta. The eigenfunctions satisfy the general Berggren completeness relation discussed in the previous sections, and constitute a *bi-orthogonal* set and are normalized according to the general c-product. Collecting the results from the discussion on the Berggren completeness relation in the previous section, and on the analytic continuation of the momentum space Schrödinger equaiton by CDM, the choice of contour in the complex k-plane must therefore be based on the following.

- The contour must be *inversion symmetric.*
- The contour must be located in overlapping domains of analyticity, see step (iii) above, and the wavefunction must admit analytic continuation onto the contour L^{+}.
- The choice of contour must be based on an *a posteriori* knowledge of poles in each partial wave of the scattering matrix.

In figure 3.2 a plot of the $l = 1$trajectory of the imaginary part of the bound and antibound state poles in the complex k-plane as a function of interaction strength ν_A is given, for the Malfliet-Tjon potential. In figure 3.2 a plot of how the $l = 1$ bound state in the Malfliet-Tjon potential approaches the scattering threshold and develop into decay resonant states for decreasing interaction strength ν_A is shown.

See Paper I for further details on the potential parameters.

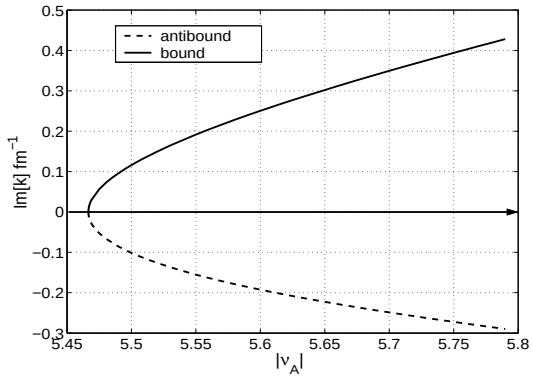

Figure 3.1: Plot of the bound and antibound state pole trajectory for the $l = 1$ component of Malfliet-Tjon interaction. The location of the poles along the imaginary k-axis is plotted as a function of interaction strength ν_A.

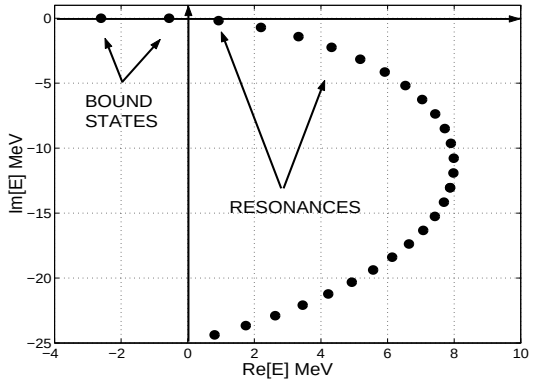

Figure 3.2: Plot of pole trajectory in the complex energy plane for the $l = 1$ partial wave solution of the Malfliet-Tjon interaction for ν_A varied from -5.6 to -2.9 in steps of 0.1.

3.3 Single particle resonances in a deformed field

In this section we will consider formation of resonances in an axially deformed field. The study of resonances in deformed fields has so far only been considered on rare occuations. In Ref. [81] energy levels and conditions for bound states to become resonances and resonances to become bound states were investigated for an axially deformed Woods-Saxon potentialm, by solving the the radial Schrödinger for coupled channels with outgoing asymptotics. However, the coupled channels method used in Ref. [81] does not easily generalize to the non-resonant continuum. This implies that a complete Berggren basis in a deformed field is difficult to obtain, and all evaluated observables will become complex quantities unless the non-resonant continuum is taken properly into account. In Ref. [82] a different approach were considered. Their aim was to propose a method to obtain scattering wave functions in the vicinity of a multi-channel resonance on the real axis. Then calculate the phase shifts, and investigate whether a resonance condition is met. Further this method allows for evaluation of observables where the continuum is properly taken into account, and they become real quantities. Here we propose an alternative method, starting with the momentum space Schrödinger equation given in equation (3.7). The obvious advantage of this, is that the boundary conditions are automatically built into the integral equations, further we will show that a single particle Berggren basis taken into account all non-resonant continuum states is possible to obtain within this approach.

We consider an axially deformed Gaussian potential with no spin and tensor components. In spherical coordinates it is given as

$$V(r,\theta) = V_0 \exp\left(-r^2(\alpha\cos^2\theta + \beta\sin^2\theta)\right) \tag{3.39}$$

or in cartesian coordinates,

$$V(x,y,z) = V_0 \exp\left(-\beta(x^2+y^2)\right)\exp(-\alpha z^2) \tag{3.40}$$

here V_0 is the strength of the potential and α and β are shape parameters. In the case $\alpha = \beta$ the potential is just a spherical Gaussian potential. In the case $\alpha > \beta$the potential field is stretched out in the x,y-plane, and defines an *oblate*shape. In the case $\alpha < \beta$ the potential field is stretched out in along the z-axis, and defines a *prolate* shape. Defining a deformation parameter δ in the following way,

$$\delta = 1 - \frac{\alpha}{\beta}, \tag{3.41}$$

equation (3.39) can be written in the form,

$$V(r,\theta;\ \beta,\delta) = V_0 \exp(-\beta r^2)\exp(\beta\delta r^2\cos^2\theta) = V(r;\ \beta)D(r,\theta;\ \beta,\delta) \tag{3.42}$$

Here $V(r;\ \beta)$ is a spherically symmetric formfactor and $D(r,\theta;\ \beta,\delta)$ a deformation formfactor. We require that the volume of the central potential, with the shape parameter $\alpha_0 = \alpha = \beta$, is equal to the volume of the axially deformed potential. This gives implies

that the shape parameters of the non-central and central Gaussian potential satisfy the following relation,

$$\alpha\beta^2 = \alpha_0^3 \tag{3.43}$$

In figure 3.3 a plot of the isocurves $V(r,\theta) = 0.5$ are shown in the x,z-plane for the deformation parameters $\delta = \pm 0.5$. $\delta = 0.5$ gives the shape parameters for the deformed potential $\alpha = 2^{-2/3}$ and $\beta = 2^{1/3}$, and $\delta = 0.5$ gives the parameters $\alpha = (3/2)^{2/3}$ and $\beta = (2/3)^{1/3}$. Here potential parameters $\alpha_0 = 1$ and $V_0 = 1$ are used. It is seen that $\delta = 0.5$ corresponds to an *oblate* shape, where the field is stretched out in the x,y-plane. For $\delta = -0.5$ the potential takes a *prolate* shape, where the field is stretched out along the symmetry axis (z-axis). In order to assess the shape structure in more detail, it is

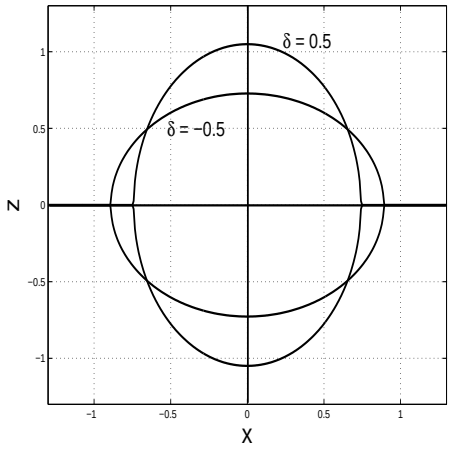

Figure 3.3: Plot of isocurves $V(r,\theta) = 0.5$ of the deformed potential for deformation $\delta = \pm 0.5$ with potential strength $V_0 = 1$ in the x,z-plane. For the spherically symmetric potential a shape parameter $\alpha_0 = 1$ were chosen.

instructive to study the multipole components of the potential. An axially symmetric potential may be expanded in terms of Legendre polynomials, i.e.

$$V(r,\theta) = \sum_\lambda V_\lambda(r) P_\lambda(\cos\theta) \tag{3.44}$$

the multipole components are then given by the integrals

$$V_\lambda(r) = \frac{(2\lambda+1)}{2} V_0 \exp(-\beta r^2) \int_{-1}^{1} dx \, \exp(\beta\delta r^2 x^2) P_\lambda(x) \tag{3.45}$$

Here it is explicitly seen that only *even* multipoles give non-vanishing contributions, since the Legendre polynomials have the property

$$P_\lambda(-x) = (-1)^\lambda P_\lambda(x),$$

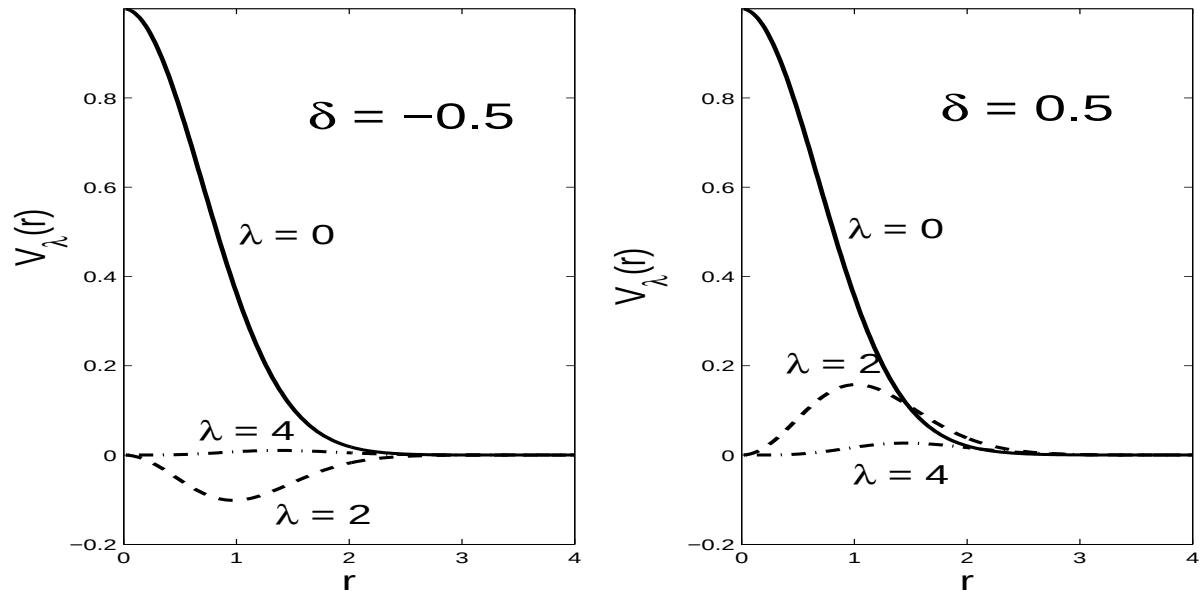

Figure 3.4: Plot of $\lambda = 0, 2, 4$ multipoles of the Gaussian potential with deformation parameters $\delta = 0.5$ (right plot) and $\delta = -0.5$ (left plot) and $\alpha_0 = 1$

and the potential is an even function in x. Figure 3.4 gives a plot of the $\lambda = 0, 2, 4$ multipoles of the Gaussian potential with deformation parameters $\delta = \pm 0.5$. It is seen that the radial monopole distribution is more or less identical for $\delta = 0.5$ and $\delta = -0.5$. From the volume conservation imposed on the deformed potential, it follows that the volume of the monopole part of the potential is independent of the deformation parameter δ. This is easy to show, since $P_\lambda(\cos\theta) = Y_{\lambda 0}(\theta, \varphi)$ and using the well known property of the spherical harmonics (see e.g. [83]),

$$\int d\hat{r} Y_{lm}(\hat{r}) = \sqrt{4\pi}\delta_{l,0}\delta_{m,0} \tag{3.46}$$

from which it follows directly,

$$\int dV\, V(\mathbf{r}) = \int_0^\infty dr\, r^2 V_{\lambda=0}(r) \tag{3.47}$$

Further it is seen that the deformed Gaussian potential is nearly a pure quadrupole deformation, since the $\lambda = 4$ multipole is almost vanishing in both cases. This may be understood from considering the exponent of the deformed formfactor in equation (3.42), which can be rewrittin in terms of the $Y_{20}(\hat{r})$ spherical harmonic.

Having discussed the shape and multipoles of the deformed Gaussian potential, we now turn to the acually solution of the Schrödinger equation for this potential. We wish to solve the momentum space Schrödinger equation given in equation (3.7). The Fourier

transformation of the deformed Gaussian potential in equation (3.40) is,

$$\begin{aligned} V(q_x,q_y,q_z) &= \frac{V_0}{(2\pi)^3}\int dx\,dy\,dz\ \exp\left(i(q_x x+q_y y+q_z z)\right)\exp\left(-\beta(x^2+y^2)-\alpha z^2\right) \\ &= \frac{V_0}{8\pi^{3/2}\beta\alpha^{1/2}}\exp\left(-\frac{1}{4\beta}(q_x^2+q_y^2)\right)\exp\left(-\frac{1}{4\alpha}q_z^2\right) \end{aligned} \tag{3.48}$$

here $q_i = k_i - k_i'$, $i = x,y,z$. In terms of spherical coordinates k,θ,φ the potential takes the form,

$$\begin{aligned} V(\mathbf{k},\mathbf{k}') &= \frac{V_0}{8\pi^{3/2}\beta\alpha^{1/2}}\exp\left(-\frac{1}{4\beta}(k^2\sin^2\theta+k'^2\sin^2\theta')-\frac{1}{4\alpha}(k^2\cos^2\theta-k'^2\cos^2\theta')^2\right) \\ &\times \exp\left(-\frac{1}{4\beta}kk'\sin\theta\sin\theta'\cos\left(\varphi-\varphi'\right)\right) \end{aligned} \tag{3.49}$$

due to axial symmetry the dependence of the potential on the azimuthal angles φ,φ' is only the difference $\omega = \varphi - \varphi'$. The potential may therefore be expanded in a complete set of harmonics, i.e.

$$V(\mathbf{k},\mathbf{k}') = \sum_{\mu=-\infty}^{\infty} V_\mu(\tilde{k},\tilde{k}')\exp(i\mu\omega), \tag{3.50}$$

here $\tilde{k} = k,\theta$. The harmonics $\exp(i\mu\omega)$ obey the orthogonality relation

$$\int_{-\pi}^{\pi} d\omega\ \exp(-i\mu\omega)\exp(i\mu'\omega) = 2\pi\delta_{\mu,\mu'} \tag{3.51}$$

the μ'th harmonic of the potential is therefore given by the integral

$$V_\mu(\tilde{k},\tilde{k}') = \frac{1}{2\pi}\int_{-\pi}^{\pi} d\omega\ \exp(-i\mu\omega)V(\mathbf{k},\mathbf{k}') \tag{3.52}$$

From equation (3.49) it is seen, that for the integral over ω, we have to consider the following integral,

$$I_\mu(y) = \frac{1}{2\pi}\int_{-\pi}^{\pi} d\omega\ \exp(-i\mu\omega)\exp(y\cos\omega) = \frac{1}{\pi}\int_0^{\pi} d\omega\ \cos(\mu\omega)\exp(y\cos\omega) \tag{3.53}$$

where we have introduced the variable

$$y = \frac{1}{2\beta}kk'\sin\theta\sin\theta'.$$

The integral in equation (3.53) is just the definition of the modified Bessel function of the 1'st kind (see e.g. [72]). The μ'th harmonic of the potential is analytic form given by,

$$\begin{aligned} V_\mu(\tilde{k},\tilde{k}') &= \frac{V_0}{8\pi^{3/2}\beta\alpha^{1/2}}\times \\ \exp\left(-\frac{1}{4\beta}(k^2\sin^2\theta-k'^2\sin^2\theta')^2-\frac{1}{4\alpha}(k^2\cos^2\theta-k'^2\cos^2\theta')^2\right)&\exp(-y)I_\mu(y) \end{aligned} \tag{3.54}$$

Inserting the expansion of the potential given in equation (3.50) into the momentum space Schrödinger equation (3.7) and projecting the equation on the harmoncis $\exp(i\mu\omega)$, the three-dimensional integral equation has been reduced to an infinite set of two-dimensional integral equations. The μ'th integral equation is easily solved as a matrix diagonalization problem with dimension $N_r \times N_\theta$. Where N_r is the number of integration points for the radial integral and N_θ is the number of integration points for the angle integral. The Schrödinger equation can be further reduced to a coupled set of one-dimensional integral equation by projecting on spherical harmonics (see equation (3.10)). The angular momentum projected potential in equation (3.49) then takes the form,

$$\begin{aligned} V_{lm,l'm'}(k,k') &= \int \mathrm{d}\hat{k} \int \mathrm{d}\hat{k}'\, Y^*_{lm}(\hat{k}) \left\{ \sum_{\mu=-\infty}^{\infty} V_\mu(\tilde{k},\tilde{k}') \exp(i\mu\omega) \right\} Y_{l'm'}(\hat{k}') \\ &= 2\pi \int_0^\pi d\theta\, \sin\theta \int_0^\pi d\theta'\, \sin\theta' \bar{P}_{lm}(\cos\theta) V_m(\tilde{k},\tilde{k}') \bar{P}_{l'm}(\cos\theta')\, \delta_{m,m'} \end{aligned} \tag{3.55}$$

where $\bar{P}_{lm}(x)$ are the normalized associated Legendre polynomials,

$$\bar{P}_{lm}(x) = \left\{ \frac{2l+1(l-m)!}{2(l+m)!} \right\}^{1/2} P_{lm}(x). \tag{3.56}$$

We wish to study the formation of resonances in the deformed Gaussian potential by the contour deformation method. The 1-dimensional coupled integral equation are then analytically continued from the physical to the non-physical energy sheet by distorting the integration contour. Choosing a suitable inversion symmetric contour L^+, discussed in the previous section, we end up with the analytically continued coupled integral equations for the axially deformed Gaussian potential,

$$\left(\frac{\hbar^2}{2\mu} k^2 - E_{nlm} \right) \psi_{nlm}(k) = -\sum_{l'} \int_{L^+} dk' k'^2 V_{lm,l'm}(k,k') \psi_{nl'm}(k') \tag{3.57}$$

As a case study we consider a Gaussian potential which in the spherically symmetric case reproduce the $J^\pi = 3/2^-_1$ resonance in ^{5}He. The $J^\pi = 3/2^-_1$ resonance, to be associated with the single-particle orbit $p_{3/2}$, is experimentally known to have a width of $\Gamma \approx 0.60$ MeV. Using the following parameters for the sperically symmetric Gaussian given in equation (3.39),

$$V_0 = -53.5\mathrm{MeV}, \;\; \alpha_0 = 0.188\mathrm{fm}^{-2} \tag{3.58}$$

the Gaussian potential supports a bound state for the $l^\pi = 0^+$ channel with energy $E = -14.9044$MeV, and a resonance for the $l^\pi = 1^-$ channel with energy $E = 0.7268 - 0.3096i$MeV. Here the nucleon spin $s = 1/2$is neglected since the energy levels are degenerate for $j = l \pm 1/2$, which follows from the spin independence of the Gaussian potential. Table 3.1 gives the convergence of the $m^\pi = 0^+$ ground state for deformation parameters $\delta = \pm 0.9$. It is seen that the deformation $\delta = 0.9$ affects the bound state the most, and the ground state becomes much more less bound $E = -12.1$MeV, for the prolate deformation.

	$\delta = 0.9$		$\delta = -0.9$	
$l_{\max}$	Re[E]	Im[E]	Re[E]	Im[E]
0	-10.5843	0.	-14.4816	0.
2	-11.9041	0.	-14.6533	0.
4	-12.0741	0.	-14.6551	0.
6	-12.0953	0.	-14.6551	0.
8	-12.0979	0.	-14.6551	0.
10	-12.0983	0.	-14.6551	0.

Table 3.1: Convergence of groundstate, $m^\pi = 0^+$, for deformation parameters $\delta = \pm 0.9$ as the number of partial waves increases. In the spherically symmetric case $\delta = 0$ the $l^\pi = 0^+$ Gaussian potential supports a bound state at energy $E = -14.9044$MeV.

On the other hand, the oblate deformation $\delta = -0.9$ has little effect on the ground state energy $E = -14.7$MeV. This may be understood by considering the monopole term of the potential, which is the main component in the multipole expansion in equation (3.44). In figure 3.5 a plot of the monopole part of the Gaussian potential with deformation parameters $\delta = \pm 0.9$ is given, together with a plot of the spherically symmetric potential. It is seen that the monopole term for the $\delta = -0.9$potential is more or less identical to the spherically symmetric potential (slightly less attractive), on the other hand the monopole term for the $\delta = 0.9$ potential is less attractive for small radii, but more attractive at large distances. From this one may conclude that the ground state of the $\delta = -0.9$ potential will be more bound than for the $\delta = 0.9$ potential, since the ground state is deeply bound and the wave function will be mainly located in the interior part of the potential.

The resonant orbit $l^\pi = 1^-$ in the spherically symmetric potential is split into two non-degenerate orbits ($m^\pi = 0^-$ and $m^\pi = 1^-$) in the case of an axially symmetric deformation. This is a characteristic of axially deformed potentials. Table 3.2 gives the convergence of the $m^\pi = 0^-$ and $m^\pi = 1^-$ excited negative parity states in the Gaussian potential for deformation parameters $\delta = \pm 0.5$. In all cases a satisfactory convergence is obtained with $l_{\max} = 5$.For the states with angular momentum projection along the z-axis ($m = 0$), it is seen that for $\delta = 0.5$, (prolate deformation), the $l^\pi = 1^-$ state has become a bound state with energy $E = -0.680$MeV. For zero angular momentum projection, the particle moves in an orbit making $\theta = 0$ degrees with the z-axis. So in the case of a prolate deformation, where the field is stretched out along the z-axis, a particle moving in this orbit will "feel" the field more strongly than compared with the spherically symmetric field, and it will become more bound. This explains also why the particle with $m = 0$ becomes more unbound in the case of the oblate deformation $\delta = -0.5$, see Columns 6 and 7 of table 3.2.

For the $m = 1$ case the opposite takes place. In the case of $\delta = 0.5$ the particle becomes more unbound, while in the of $\delta = -0.5$ the particle becomes more bound. By considering the dipole ($l = 1$) term of the wave function, the particle moves in an orbit making $\theta = \pi/4$degrees with the z-axis. From this it may be understood that particle gains

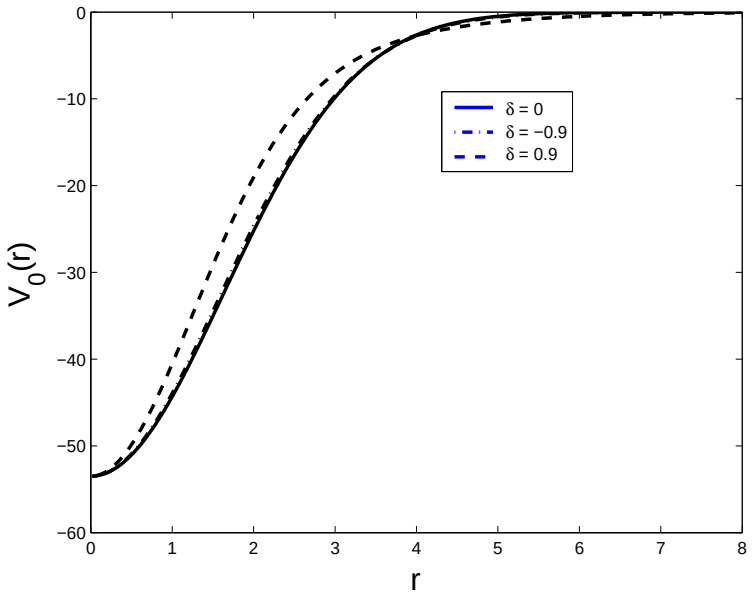

Figure 3.5: Plot of the monopole part of the Gaussian potential with deformation parameters $\delta = 0$ and $\delta = \pm 0.9$.

	$\delta = 0.5$				$\delta = -0.5$			
	$m^\pi = 0^-$		$m^\pi = 1^-$		$m^\pi = 0^-$		$m^\pi = 1^-$	
$l_{\max}$	Re[E]	Im[E]	Re[E]	Im[E]	Re[E]	Im[E]	Re[E]	Im[E]
1	-0.5282	0.	1.4865	-1.0177	1.5402	-1.0701	0.3815	-0.1139
3	-0.6772	0.	1.4419	-0.9631	1.5170	-1.0404	0.3602	-0.1042
5	-0.6802	0.	1.4410	-0.9621	1.5168	-1.0402	0.3601	-0.1041
7	-0.6803	0.	1.4410	-0.9620	1.5168	-1.0402	0.3601	-0.1041
9	-0.6803	0.	1.4410	-0.9620	1.5168	-1.0402	0.3601	-0.1041

Table 3.2: Convergence of the $m^\pi = 0^-$ and $m^\pi = 1^-$ states, for deformation parameters $\delta = \pm 0.5$ with increasing number of partial waves. In the spherically symmetric case ($\delta = 0$) the $l^\pi = 1^-$ Gaussian potential supports a resonance state at energy $E = 0.7268 - 0.3096i$MeV.

	$\delta = 0.5$				$\delta = -0.5$			
	$m^\pi = 0^-$		$m^\pi = 1^-$		$m^\pi = 0^-$		$m^\pi = 1^-$	
l	Re$[\psi_l^2]$	Im$[\psi_l^2]$	Re$[\psi_l^2]$	Im$[\psi_l^2]$	Re$[\psi_l^2]$	Im$[\psi_l^2]$	Re$[\psi_l^2]$	Im$[\psi_l^2]$
1	0.9947	0.	0.9982	2.31E-03	0.9992	1.1E-03	0.9993	3.E-04
3	5.7E-03	0.	1.8E-03	-2.3E-03	8.E-04	-1.1E-03	7.E-04	-3.E-04
5	5.E-05	0.	2.E-05	-2.E-05	3.E-06	-3.E-06	2.E-06	-9.E-07
7	6.E-07	0.	3.E-07	-2.E-07	2.E-08	-1.E-08	9.E-09	-4.E-09
9	8.E-09	0.	4.E-09	-3.E-09	9.E-11	-7.E-11	4.E-11	-2.E-11

Table 3.3: Convergence of the $m^\pi = 0^-$ and $m^\pi = 1^-$ states, for deformation parameters $\delta = \pm 0.5$ with increasing number of partial waves. In the spherically symmetric case ($\delta = 0$) the $l^\pi = 1^-$ Gaussian potential supports a resonance state at energy $E = 0.7268 - 0.3096i$MeV.

more binding in the case of an oblate deformation $\delta = -0.5$ and becomes more unphysical in the opposite case $\delta = 0.5$ (see columns 4,5,8 and 9 of table 3.2).

In table 3.3 the squared amplitudes of the wave functions are given for each partial wave l. It is seen that in all cases that the squared amplitudes for the $l = 1$ component of the total wave function, is nearly equal to the norm of the total wave function, while all other partial wave amplitudes are vanishing. In this sense one may say that the orbital angular momentum is approximatetly a "good" quantum number.

In figure (3.6) a plot of the bound state energy of the $m^\pi 0 = 0^+$ state are given for the deformation parameter δ taking values between $-0.9$and 0.9. It is seen that the position of the bound state varies much more strongly for a prolate deformation ($\delta > 0$), than for an oblate deformation.

In figure (3.7) a plot of the real and imaginary parts of the $m^\pi = 0^-$ state are given for the deformation parameter δ taking values between $-0.9$and 0.9. Here it is seen that resonance in the $\delta = 0$ becomes a bound state for $\delta > 0.3$. For $\delta < 0$ the resonance becomes more unphysical with δ.

In figure (3.8) a plot of the real and imaginary parts of the $m^\pi = 1^-$ state are given for the deformation parameter δ taking values between $-0.9$and 0.9. Here the resonance state never becomes a bound state for $\delta \in (-0.9, 0.9)$. For $\delta \in (-0.9, 0.2)$ the resonance display a weak variation from the $\delta = 0$ resonance. On the other hand, as $\delta \to 0.9$ the imaginary part of the energy dives into the lower half complex energy plane, and the resonance state becomes strongly unphysical.

In figure (3.9) a combined plot of the real and imaginary parts of the $m^\pi = 0^-$ and $m^\pi = 1^-$states are given for the deformation parameter δ taking values between $-0.9$and 0.9. Here the splitting of the $l^\pi = 1^-$ resonant level with respect to the angular momentum projection m is clearly seen.

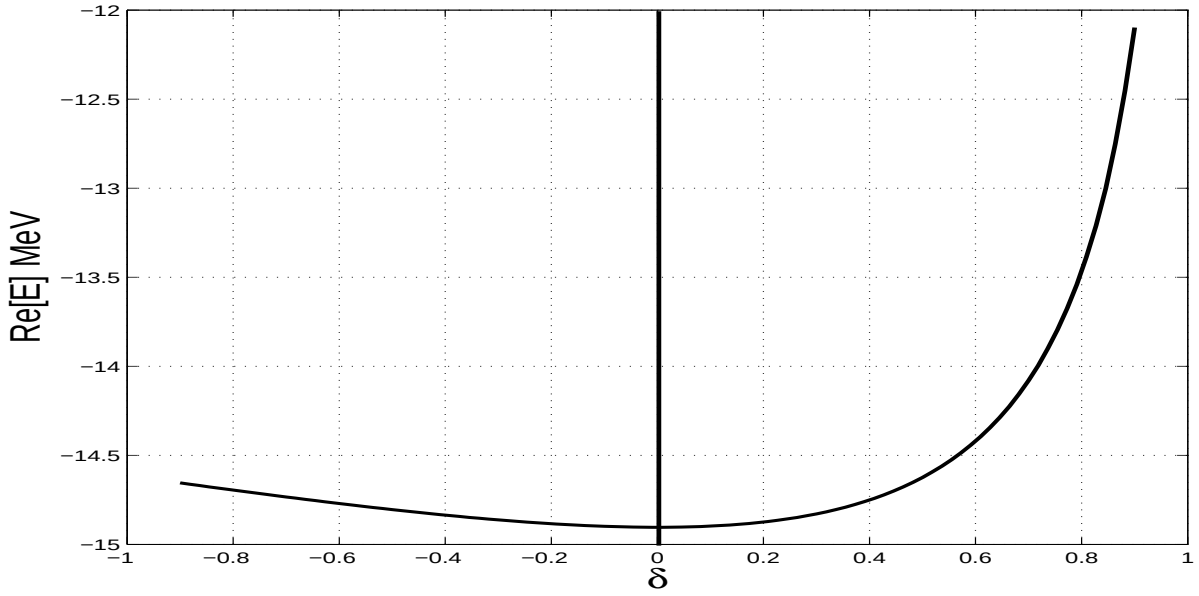

Figure 3.6: Bound state trajectory for the $m^{\pi} = 0^{+}$ state in the deformed Gaussian potential. Energy is plotted as function of deformation parameter δ.

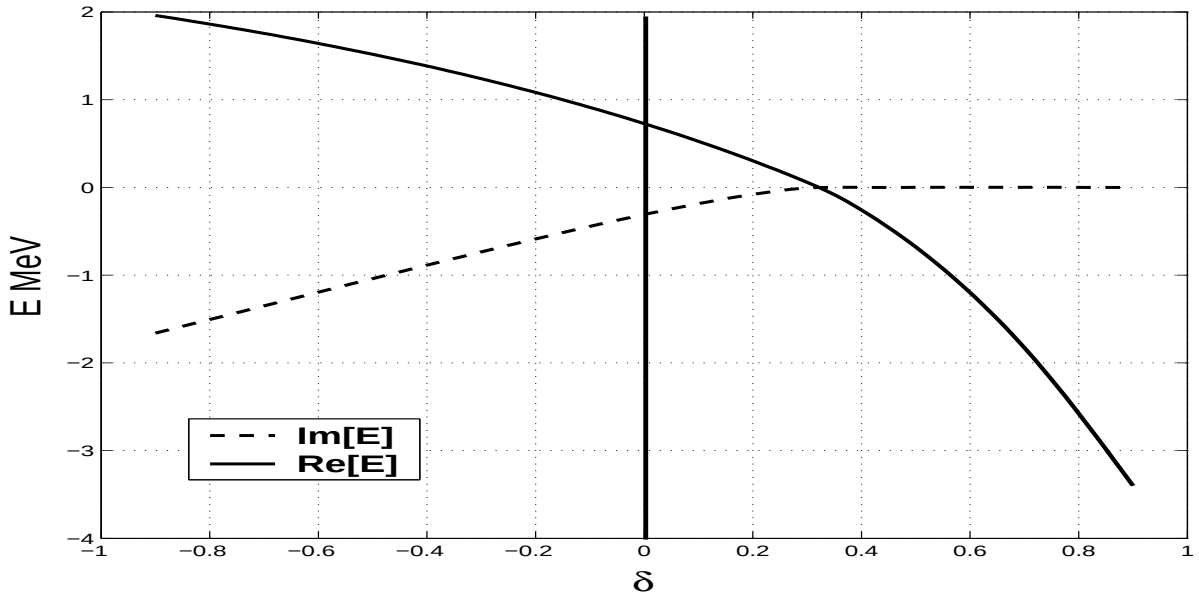

Figure 3.7: Real and imaginary part of the $m^{\pi} = 0^{-}$ state energy in the deformed Gaussian potential as the deformation parameter δ is varied between $-0.9$and 0.9.

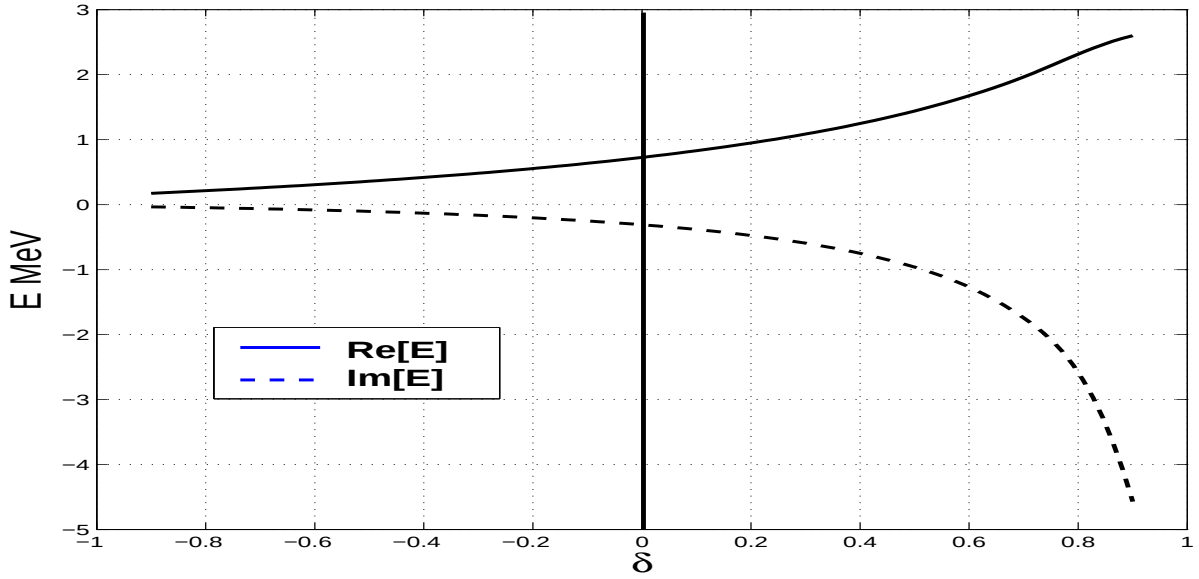

Figure 3.8: Real and imaginary part of the $m^{\pi} = 1^{-}$ state energy in the deformed Gaussian potential as the deformation parameter δ is varied between $-0.9$and 0.9.

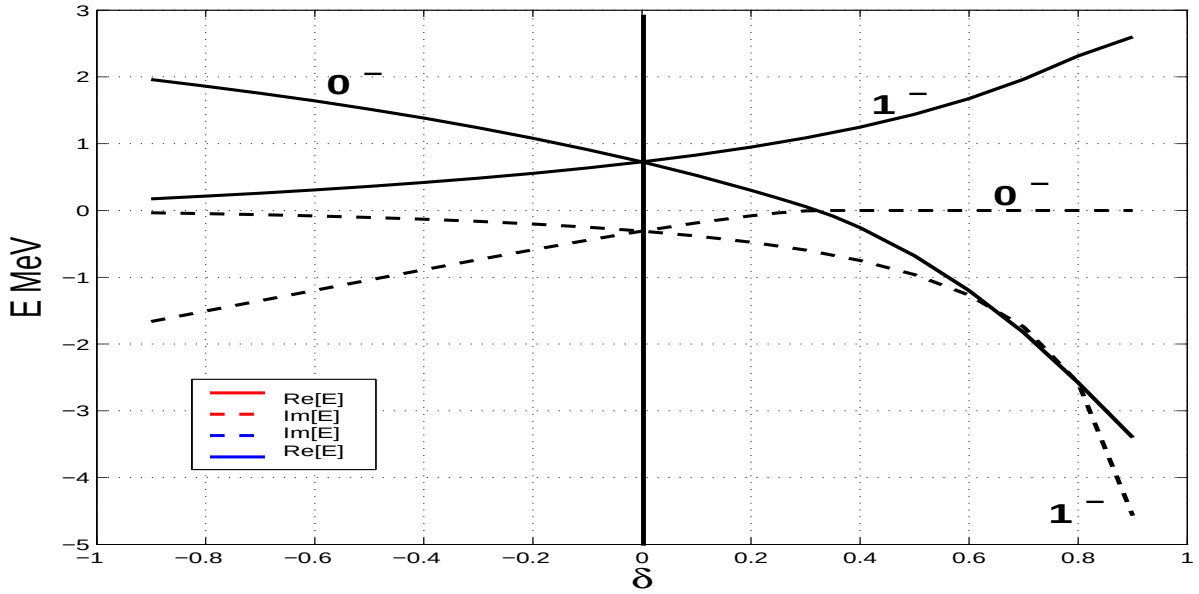

Figure 3.9: Real and imaginary part of the $m^{\pi} = 1^{-}$ state energy in the deformed Gaussian potential as the deformation parameter δ is varied between $-0.9$and 0.9.

3.4 Two-particle resonances and bound states embedded in the continuum in complex potentials

CDM has a number of different applications, in this section scattering from a complex Malfliet-Tjon interaction describing absorbtive and emitting processes is considered. [4] Complex potentials have commonly been used in optical potential models in nuclear and particle physics. Inelastic scattering where the conservation of flux is broken due to the possibility of the particle to be ejected to other exit channels or particles to emerge from them, may be taken into account by a complex absorbing or emitting potentials respectively. Another application of complex potentials, is the nucleon-antinucleon scattering, in which a short range complex annihilation potential may describe how bound- and resonant states are formed such systems.

In letting the interaction strengths be generalized to the complex plane the Schrödinger equation becomes a non-hermitian eigenvalue problem from the very beginning, and the eigenvalues will in general become complex. See Refs. [7, 84] for a more rigorous discussion of complex interactions. Below follows an illustration that CDM gives accurate calculation of the complete energy spectrum for complex interactions. The pole trajectories are studied by varying the absorbtive and emittive strength of the interaction.

In the case of the Malfliet-Tjon interaction two cases are studied. First the attractive strength, $V_A \rightarrow (1+\eta i)V_A$, is scaled by a complex constant $1+\eta i$ keeping the repulsive strength V_R real. Since the attractive strength V_A is a negative quantity, absorbtive scattering takes place for $\eta > 0$ while emittive scattering takes place for $\eta < 0$. Secondly both the attractive and repulsive interaction strengths are scaled, i.e. $V \rightarrow (1+\eta i)V$. Starting with $\nu_A = -5$, so for $\eta = 0$ a resonance at $E = 5.1804 - 3.1555i$ MeV corresponding to a pole at $k = 0.3682 - 0.1033i\,\mathrm{fm}^{-1}$ in the complex k-plane appears (see Paper I) [5]. In figure 3.10 a plot of the pole trajectory for varying η is given, keeping ν_A fixed. An imaginary part is added to the attractive strength V_A while V_R is kept real. From the figure it is seen that when the probability for finding the particle increases ($eta < 0$), the resonance pole approaches the real k-axis, and eventually crosses from the non-physical to the physical energy sheet. In the case of absorbtion ($\eta > 0$) the opposite effect is observed. That the pole becomes "more" physical with a repulsive imaginary part added to the potential, may be understood from the following argument. The resonance is formed inside the potential barrier, with a limited lifetime before it tunnels through the barrier and dies. If more particles are created inside the barrier, the probability of finding a particle inside the barrier should increase with the number of particles added.

In figure 3.11 a plot of the pole trajectory of the resonance at $E = 5.1804 - 3.1555i$ with $\eta = 0$ is given for varying η. Here both attractive and repulsive part are scaled. In scaling both the attractive and repulsive parts of the potential with the same complex con-

[4] See Paper I for a detailed analysis of the structure of the Malfliet-Tjon potential in momentum space, the relevant equations to be solved and the bound, anti-bound and resonant pole distributions as funtion of the interaction strength.

[5] Here $V_A = \nu_A \times \hbar c$, see Paper I for more details.

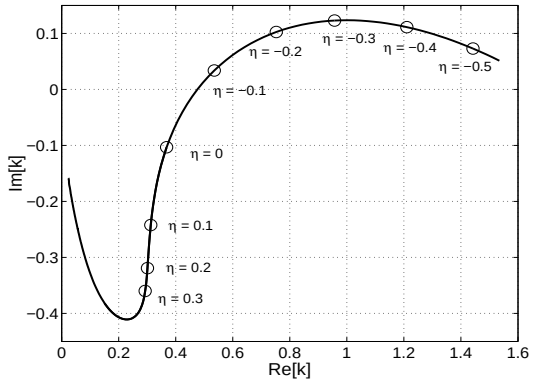

Figure 3.10: Pole trajectory of the $l = 1$ resonance in the $\nu_A = -5$ Malfliet-Tjon interaction, for increasing absorbtion/emission. Here only the attractive strength of the interaction takes complex values,$V_A \to (1 + \eta i)V_A$.

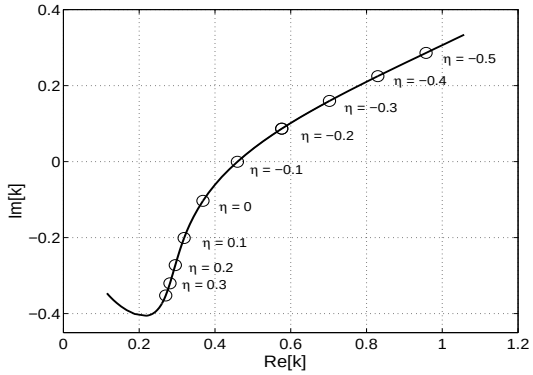

Figure 3.11: Pole trajectory of the $l = 1$ resonance in the $\nu_A = -5$ Malfliet-Tjon interaction, for increasing absorbtion/emission. Here both attractive and repulsive strengths of the interaction takes complex values,$V \to (1 + \eta i)V$.

stant $1 + \eta i$, both absorbtion and emission takes place. However, since the potential is on average more attractive than repulsive, the total effect of letting ηbecome negative will be emission of particles while letting η become positive will result in absorbtion of particles. This is also seen from the figure 3.11, where the pole moves towards the physical sheet for $\eta < 0$, and becomes more "unphysical" for $\eta > 0$. Since absorbtion and emission are competing processes in this case, the dependence of the pole position on increasing/decreasing imaginary part of the potential should be weaker than in the former case where only the attractive part was scaled, i.e. pure absorbtion and emission took place. This is observed from figures. 3.10,3.11. In figure 3.10 the pole has moved onto the physical energy sheet for $\eta = -0.1$ while it is still on the nonphysical sheet in figure 3.11. The same strong and weak dependence on η is observed for the absorbtive process $\eta = 0.1$.

For comparison with the results for the Malfliet-Tjon potential above, the pole trajectory for the $l = 1$ Yamaguchi interaction with $\beta = 2\,\mathrm{fm}^{-1}$ and interaction strength $\lambda = 165\ \mathrm{MeVfm}^{-1}$ is considered as well [6]. This interaction supports a resonance at $E = 0.8736 - 0.1285i$ MeV for $\eta = 0$. Figure 3.12 gives a plot of the pole trajectory of the resonance for varying η. From the figure it is seen that pole behaves in the same

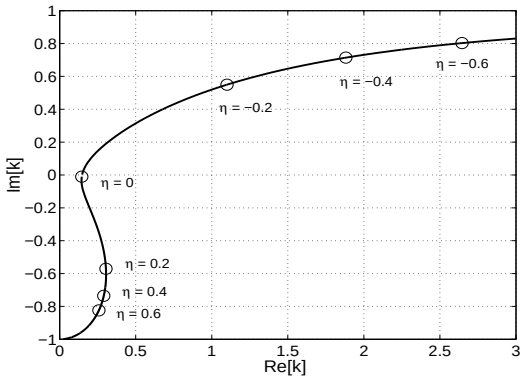

Figure 3.12: Pole trajectory of the resonance at $E = 0.8736 - 0.1285i$ MeV in the Yamaguchi interaction with $\beta = 2\,\mathrm{fm}^{-1}$ and interaction strength $\lambda = 165\ \mathrm{MeVfm}^{-1}$

way with increasing emission and absorbtion as in the Malfliet-Tjon case considered in figures 3.10,3.11.

From the above numerical analysis of the resonance pole trajectory for a complex absorbing or emitting potential, one may make the following conclusion. For increasing emission, i.e. $\eta < 0$, the resonant pole in the third quadrant of the complex k-plane moves towards the real k-axis. Eventually the resonant poles move through the unitarity cut and onto the physical energy sheet (upper half complex k-plane). When the pole crosses the cut, the imaginary part of the resonance energy is zero, that is why poles located on the cut are usually defined as *bound states embedded in the continuum.* Poles which are located on the physical energy sheet may be interpreted as unstable bound states. Poles

[6] See Paper I for details on the $l = 1$ Yamaguchi potential

moving onto the physical energy sheet may therefore give a clear signature in physical observables such as phaseshifts and scattering cross sections. For increasing absorbtion on the other hand, i.e. $\eta > 0$, the resonant pole becomes more and more unphysical in the sense that it moves away from the physical scattering axis. These conclusion apply in all cases considered above, and one may expect these conclusions to hold for other potential shapes.

The illustrations above indicates a general behaviour of decay resonant states when the interaction is scaled by a complex constant. One may ask in a similar fashion in what way the capture resonant states develops as a function of η. Will the symmetry with respect to the imaginary k-axis for capture and decay states prevail ? The answer to this is no. It can be seen by considering the symmetry properties of the scattering matrix in the case of a complex interaction. In particular we have the property, see equations (2.14,2.15)

$$S_l^*(-k^*, \eta^*) = S_l(k, \eta) \tag{3.59}$$

This implies that if the interaction $(1 + i\eta)V$ supports a resonance at k, the complex conjugated interaction $(1 + i\eta)^*V$ supports a resonance at $-k^*$. The number of poles is invariant with respect to η, the poles only get redistributed as η is varied. The symmetry between decay and capture states is therefore broken. As the capture resonance moves away from the real k-axis in the third quadrant of the complex k-plane the capture state moves toward the real k-axis and eventually into the physical energy sheet. It is quite interesting that a capture state which for $\eta = 0$ was considered a non-physical state, may become a physical bound state with a finite lifetime for $\eta > 0$.

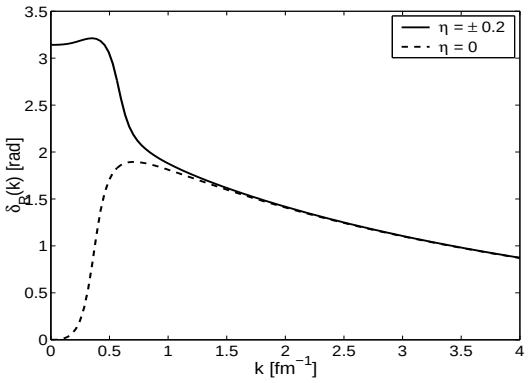

Figure 3.13: Real part of phase shifts for the $l = 1$ Malfliet-Tjon interaction with $\nu_A = -5$. The dashed line gives the phase shifts for $\eta = 0$, while the continuous line give the phase shifts for $\eta \pm 0.2$.

In the case of complex interactions the phase shift is a complex quantity, $\delta = \delta_R + i\delta_I$, the real part δ_R is interpreted as before and describes the elastic scattering while the imaginary part, δ_I, is a measure of the inelastic scattering taking place. Figures 3.13,3.14 gives a plot of the real and imaginary part of the phase shifts for the $l = 1$ Malfliet-Tjon

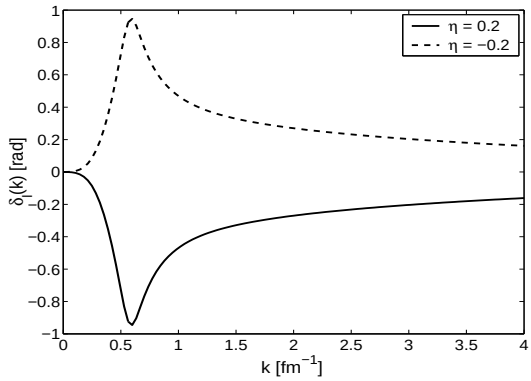

Figure 3.14: Imaginary part of the phase shifts for the $l = 1$ Malfliet-Tjon interaction with $\nu_A = -5$ and $\eta = -0.2$ given by the dashed line and $\eta = 0.2$ by the continuous line.

interaction with $\nu_A = -5$ and $\eta = 0, \pm 0.2$. Here only the attractive strength V_A was scaled, keeping the repulsive part V_R real, see figure 3.10 for details on the pole trajectory. In the case $\eta = -0.2$ the decay state has moved onto the physical energy sheet and become a bound state. In the case $\eta = 0.2$ the capture state has moved into the physical energy sheet and become a bound state, while the decay state has become more unphysical. There is no way to differentiate between the real part of the phase shifts for $\eta = \pm 0.2$. The elastic scattering is the same for both cases, which is expected since the real part of the interaction is the same. The imaginary part of the phase shifts are on the other hand different, and is directly related to the sign of η where either an absorbtion of particles out of the elastic channel or an emission of particles into the elastic channel takes place.

A generalized Levinson theorem may be formulated for the real part of the phase shift [7], $\delta_R(0) - \delta_R(\infty) = n\pi$ where n is the number of poles in the upper half complex k-plane (physical energy sheet). In figure. 3.13 we have for $\eta = \pm 0.2$, $\delta(0) = \pi$ which is in accordance with the generalized Levinson' theorem.

3.5 Two-particle scattering; isolating resonance phenomena by CDM

In this section we will discuss the solution for the full off-shell t-matrix, and hence the full two-body scattering problem, by expanding the two-body Green's function in a complete set of Berggren states. The Berggren representation of the scattering equations gives an analytic continuation in energy, from the upper rim of cut through the cut and into the non-physical energy sheet.

The t-matrix is defined in operator form by

$$t(\omega) = V + V g^{II}(\omega) V, \tag{3.60}$$

or

$$t(\omega) = V + V g_0^{II}(\omega) t(\omega). \tag{3.61}$$

Here ω is the incoming energy, $g^{II}(\omega)$ is the resolvent, commonly known as the Green's operator, and $g_0^{II}(\omega)$ the corresponding free Green's operator. In operator form they are defined by

$$g_0^{II}(\omega) = \frac{1}{\omega - H_0}, \tag{3.62}$$

$$g^{II}(\omega) = \frac{1}{\omega - H}. \tag{3.63}$$

They are related through the Dyson equation

$$g^{II}(\omega) = g_0^{II}(\omega) + g_0^{II}(\omega) V g^{II}(\omega) \tag{3.64}$$

The term H_0 is the kinetic energy operator and H the full two-body Hamiltonian. The physical interpretation of the Green's functions is that g_0^{II} describes the propagation of two noninteracting particles, and g^{II} describes the propagation of two interacting particles in free space.

3.5.1 Berggren representation of the t-matrix

The Berggren representation of the Green's function is obtained by expanding the unit operator using the completeness relation given in equation (3.33). In this case the Green's operator takes the form

$$g^{II}(\omega) = \sum_{n=a,b,c,d} \frac{|\psi_n\rangle\langle\psi_n^*|}{\omega - E_n} + \int_{L^+} dE \frac{|\psi\rangle\langle\psi^*|}{\omega - E}. \tag{3.65}$$

Here n denotes bound, antibound and resonant states. The integration contour L^+ denotes an arbitrary inversion symmetric contour, see e.g. figure 2.4 in SubSec. 2.3 of Chapter 2, and gives the non-resonant distorted continuum contribution to the interacting Green's function. If we neglect the non-resonant continuum contribution to the Green's function we get the *resonant state expansion* of the Green's function. Such expansions have been studied over the last decade for finite range potentials, see e.g. [85, 86, 47]. The Green's function given in equation (3.65) is continuous and analytic in energy across the real axis and into the domain $\mathbf{C}$ of the lower part of the complex energy plane. Equation (3.65) is therefore an analytic continuation in energy of the Green's function defined along the real energy axis.

The Berggren representation of the t-matrix is obtained by inserting the interacting Green's function given by equation (3.65) into equation (3.60), giving

$$t(\omega) = V + \Delta t(\omega) = V + \Delta t^R(\omega) + \Delta t^C(\omega). \tag{3.66}$$

Here $\Delta t^R(\omega)$ is the resonant contribution while $\Delta t^C(\omega)$ is the non-resonant distorted continuum contribution to the t-matrix. By projecting $t(\omega)$ on momentum states, and decomposing into partial waves, the t-matrix elements $t_l(k,k';\omega)$ can be expressed as 1-dimensional integral equations,

$$t_l(k,k',\omega) = V_l(k,k') + \int_{L^+}\int_{L^+} dq\, dq'\, q^2 q'^2 V_l(k,q) g^{II}(q,q';\omega) V_l(q',k'), \tag{3.67}$$

This representation of the t-matrix is valid as long as we do not pass through any singularities of the interaction potential by deforming the real k-axis into the distorted contour L^+.

In numerically solving for equation (3.67), the eigenvalue problem on the discretized contour L^+ given in equation (3.31) has to be solved. Then the interacting Green's function is represented in the discretized complete set of momentum states given in equation (3.33), giving the discretized Green's function,

$$g^{II}(k_i,k_j,\omega) = \sum_n \frac{\psi_{nl}(k_i)\psi_{nl}(k_j)}{\omega - E_{nl}} = \sum_n \left(\sqrt{w_i w_j}k_i k_j\right)^{-1} \frac{\psi_{nl}(i)\psi_{nl}(j)}{\omega - E_{nl}}. \tag{3.68}$$

Inserting this discretized form of the interacting Green's function into equation (3.67) and discretizing the integration over q and q', a discretized version of the t-matrix is obtained. Having obtained $g^{II}(k_i,k_j)$, the full off-shell t-matrix is therefore obtained by the matrix equation

$$t_l(k_i,k_j,\omega) = V_l(k_i,k_j) + \tilde{V}_l^T(i)\tilde{g}^{II}(\omega)\tilde{V}_l(j) \tag{3.69}$$

where $\tilde{V}_l(n)$ is the n'th column of the potential matrix $V_l(k_i,k_j)$ and $\tilde{g}^{II}(\omega)$is the matrix

$$\tilde{g}^{II}(i,j,\omega) = \sqrt{w_i w_j}k_i k_j \sum_n \frac{\psi_{nl}(i)\psi_{nl}(j)}{\omega - E_{nl}}. \tag{3.70}$$

Applying CDM enables us to obtain $t_l(k,k';\omega)$ for both real and complex energies ω. The integral becomes non-singular on the deformed contour for real and positive input energies ω, resulting in numerically stable solutions for physical two-body scattering. Equation (3.67) can also be considered as an analytic continuation of equation (3.67) for complex input energies ω, and stable numerical solutions can be obtained for complex energies above the distorted contour. The Berggren representation of the t-matrix also allows for a separate study of the resonant and continuum contributions. The limitation of this method is due to that most potentials in momentum space have singularities in the complex plane when one argument is real and the other is complex. By applying contour L_1^+, which is based on rotation into the complex plane, in most cases there will be restrictions on both rotation angle (θ) and maximum incoming and outgoing momentum (k,k'), see for example Ref. [25].

Using contour L_2^+ we can avoid these limitations by choosing the integration contour in such a way that the potential singularities always will lie outside the integration contour, and therefore do not give any restriction on rotation angle and maximum incoming and outgoing momentum.

3.5.2 Fredholm representation

The partial wave decomposition of equation (3.61) gives the *Fredholm* representation, commonly known as the Lippmann-Schwinger equation

$$t_l(k,k';\omega) = V_l(k,k') + \frac{2}{\pi}\int_0^\infty \frac{dqq^2 V_l(k,q)t_l(q,k')}{\omega - E(q)}. \tag{3.71}$$

In physical two-body scattering the input energy is real and positive. In this case the *Fredholm* integral equation (3.71) has a singular kernel of Cauchy type. Solving singular integrals can be done by Cauchy's Residue theorem, where we integrate over a closed contour enclosing the poles. There are two ways of doing this, either by letting z lie an infinitesimal distance above the real axis, i.e., $\omega \to z+i\epsilon$, or by letting ω lie on the real axis. In both cases we must choose a suitable contour enclosing the singularity. If we choose the latter position of the singularity, we get a Cauchy *principal-value* integral where we integrate up to - but not through - the singularity, and a second contour integral, where the contour can be chosen as a semicircle around the singularity. Equation (3.71) can thus be given in terms of a principal value part and a second term coming from integration over the semicircle around the pole. The result is

$$t_l(k,k';\omega) = V_l(k,k') + \frac{2}{\pi}\mathcal{P}\int_0^\infty \frac{dqq^2 V_l(k,q)t_l(q,k')}{\omega - E(q)} \; - \; 2i\mu k_0 V_l(k,k_0)t_l(k_0,k';\omega). \tag{3.72}$$

By rewriting the principal value integral using the relation

$$\mathcal{P}\int_0^\infty dk\,\frac{f(k)}{k_0^2-k^2} = \int_0^\infty dk\,\frac{[f(k)-f(k_0)]}{k_0^2-k^2}, \tag{3.73}$$

we obtain an equation suitable for numerical evaluation. Equation (3.72) can be converted into a set of linear equations by approximating the integral by a sum over N Gaussian quadrature points $(k_j; j = 1, ...N)$, each weighted by w_j The full off-shell t-matrix is then obtained by matrix inversion. This method for solving integral equations is known as the Nystrom method. It is numerically effective and stable, except for the rare case when the incoming energy ω coincides with or is very close to one of the integration points.

So far we have only considered physical input energies in equation (3.71), but it has been shown in Ref. [7] that the analytically continued Lippmann-Schwinger equation to complex energies takes the same form as equation (3.72). By solving the full off-shell t-matrix for arbitrary complex input energy, we do not have to alter the set of linear equations obtained for physical energy, the only modification is that the energy is complex.

The Lippmann-Schwinger equation for t-matrix (3.71), can be solved by the contour deformation method as well. Using CDM the integral equation given in equation (3.71) has a compact integral kernel (Schmidt kernel) for positive incoming energies ω, thus the principal value (PV) prescription may be avoided. In the first step we calculate the t-matrix elements $t_l(z,k,\omega)$ where k is on the real axis and z is on a suitable deformed contour L^+. This is obtained by solving the integral equation,

$$t_l(z,k;\omega) = V_l(z,k) + \int_{L^+} \frac{dz'z'^2 V_l(z,z')t_l(z',k)}{\omega - E(z')}. \tag{3.74}$$

Here it is seen that for real input energies ω the integral kernel is non-singular sincel the kinetic energy term $E(z)$ is defined on a deformed contour in the complex k-plane. Having obtained $t_l(z,k;\omega)$ the t-matrix elements $t_l(k,k';\omega)$ is straightforward obtainable by the non-singular integral,

$$t_l(k,k';\omega) = V_l(k,k') + \int_{L^+} \frac{dz z^2 V_l(k,z) t_l(z,k')}{\omega - E(z)}. \tag{3.75}$$

here k and k' are given along the real k-axis, while z is defined along the deformed integration contour L^+. This two-step procedure using CDM offers an alternative approach to the numerical solutions for the t-matrix. Stable solutions will be obtainable as long as the contour does not pass through any singularities of the potential. Below we consider the solution of the t-matrix for the Malfliet-Tjon potential by CDM and compare results with the standard principal value (PV) prescription. First of all, we have to determine the singularity structure of the potential Malfliet-Tjon potential. From equations (3.74,3.67) it is seen that the potential must be defined for one real variable k and one complex variable z given on the contour L^+. So in conclusion, the contour L^+ must be chosen in such a way that the potential admit analytical continuation from the real k-axis to the complex contour L^+.

For an illustration we consider two contours C_1 and C_2. The C_1 contour is just the phase transformation, or complex rotation, $C_1 : |k|exp(-i\theta)$. The C_2 contour consits of a combination of a rotation and a translation in the complex k-plane[7]. If we integrate along contour C_1 there will always be a singularity on the contour given by

$$z = k_{\max} - i\mu, \tag{3.76}$$

where

$$k_{\max} = \mu/\tan(\theta), \tag{3.77}$$

and $\mu = \min[\mu_A, \mu_B]$[8]. For $k, k' > k_{\max}$ the contour C_1 will pass through the singularity of the interaction. However, if the interaction, $V_l(k,k')$, is approximately zero for $k, k' > k_{\max}$, or the t-matrix is wanted only in the low momentum regime ($k, k' \ll k_{\max}$), integrating along contour C_1 can be done as long as

$$\theta < \arctan\left(\mu/k_{\max}\right). \tag{3.78}$$

In this sense we may call $k_{\max}$ the cutoff momentum. This choice may cause numerical unstable solutions for small values of momenta, since the rotated contour may lie very close to the real k-axis where the integral kernel is singular. The same conclusion has already been pointed out by Nuttal in Ref. [74].

Here we see the advantage of integrating along contour C_2. Not only will it be able to reproduce virtual states (see Paper I), but it yields also accurate results for the t-matrix

[7] See Paper I for further details. In this particular study natural units are used, i.e. the momentum k is in units of MeV and the potential is in units of MeV^{-2}. In Paper I conventional units were used.

[8] μ is here considered as the mass of the pions entering the Yukawa potentials; $V(r) = V_0 exp(-\mu r)/r$

for real incoming and outgoing momenta. It will always be possible to choose a contour C_2 lying above the nearest singularity $z = \Re[k] - i\mu$, implying no restriction on rotation angle θ irrespective of cutoff momentum $k_{\max}$. Figure 3.15 gives an illustration.

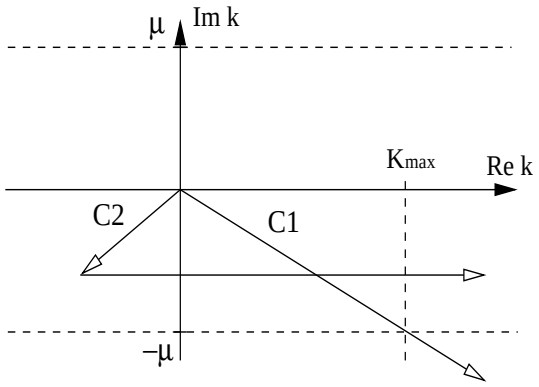

Figure 3.15: Illustration of potential singularities for the Malfliet-Tjon interaction $V_l(k, z)$, where k is real and z complex. Restriction on the integration contours C_1 and C_2 is clearly seen for given cutoff momentum k_{max} ($V_l(k, k') \approx 0$ for $k, k' > k_{\max}$).

Figure 3.16 shows a plot of the calculated t-matrix elements $t_l(k, k; E)$ for incoming energy $E = 100$ MeV for the s-wave Malfliet-Tjon interaction, using the contours C_1 and C_2. In this case we used a rotation angle $\theta = \pi/6$ for both contours, and a translation $b = 300$ MeV for contour C_2. The Malfliet-Tjon interaction has a singularity along contour C_1, given by $k_{\max} = \mu/\tan(\theta) = 529.77$ MeV. In this case the interaction is not sufficiently neglible for $k, k' > k_{\max}$, and using contour C_1 will not give accurate calculation of the t-matrix. This illustrates clearly the advantage of integrating along the contour C_2 instead of C_1, and the importance of choosing a contour which avoids singularities in the potential.

For a comparison of CDM with the standard PV prescription in solving for the t-matrix numerically we consider the the on-shell unitarity for the S-matrix calculated with both methods. Table 3.4 reports calculations done by the principal value prescription and the contour deformation method C_2. The calculations used $N = 50$ integration points for the principal value integration, for the contour deformation method we used 30 points along the rotated line and $N_T = 100, 200$ along the translated line. We observe that we need a higher number of integration points along the translated line of C_2 in order to obtain a comparable accuracy with the PV method.

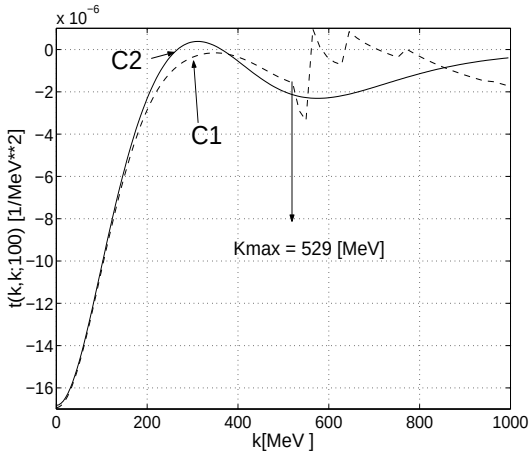

Figure 3.16: Plot of t-matrix elements for the s-wave Malfliet-Tjon interaction using the contour C_1 (dashed line) and the contour C_2 (solid line). The potential singularity along contour C_1 is clearly displayed, and located at $k_{\max} = 529.77$ MeV.

	PV	CDM	
k[MeV]	$N = 50$	$N_T = 100$	$N_T = 200$
10.	1.00000000	1.00000811	1.00000811
110.	1.00000000	0.999999940	1.00000000
210.	1.00000000	0.999999940	1.00000000
310.	1.00000000	0.999999881	1.00000000
410.	1.00000000	0.999999881	1.00000000
510.	1.00000000	0.999999881	1.00000000
610.	1.00000000	0.999999881	1.00000000
710.	1.00000000	0.999999821	1.00000000
810.	1.00000000	0.999999821	1.00000000
910.	1.00000000	0.999999821	1.00000000
1010.	1.00000000	0.999999762	1.00000000
1110.	1.00000000	0.999999702	1.00000000
1210.	1.00000000	0.999999702	1.00000000
1310.	1.00000000	0.999999642	1.00000000
1410.	1.00000000	0.999999523	1.00000000
1510.	1.00000000	0.999999642	1.00000000

Table 3.4: Calculations of S-matrix norm, $|S(k)|$, for the s-wave Malfliet-Tjon potential with parameters $V_A = 7.291$ MeV, $\mu_A = 613.69$ MeV, $V_B = -5$ MeV and $\mu_B = 305.86$ MeV. Column 2 gives results for the principal value prescription (PV), while columns 3,4 give results for the contour deformation method (CDM).

3.6 Application of CDM to resonance-like phenomena in nuclear matter; pair instabilities and the onset of pairing

3.6.1 2p2h spectral structures in a nuclear medium.

In this section we discuss the application of CDM to nucleon-nucleon scattering in infininte nuclear matter. Of particular interest is the formation and decay of two nucleon bound- and resonant states in nuclear matter. In the early 70's Bishop *et. al.* [87, 88] showed that the existence of bound state pairs in a nuclear medium can be directly linked to the singularities of the in-medium t-matrix. The existence of bound pair states in nuclear medium, is closely related to the concept of *cooper* pairs. Cooper pairs are considered as the formation of bound electron pairs in a degenerate electron gas, giving rise the phenomenon of *super conductivity*. Treating holes on equal footing with particles Bishop *et. al.* showed that the pairing effects in nuclear matter where increased when comparing with the standard Bethe-Goldstone approach where only particle propagation is considered, see e.g. Ref. [89]. In Ref. [90] showed that the BCS gap equation is directly related to the 2p2h bound pair states. Two decades later Dickhoff *et. al.* [91, 92, 93] discussed similar properties of composite pair states in nuclear matter, and formally related the BCS gap equation to the 2p2h self-consistent eigenvalue equation for the bound states. There it was suggested that strong pairing effects would be present in nuclear matter at certain densities and total momentum, due to the existence of bound pair states.

It is well known that for a realistic nucleon-nucleon interaction there may appear pairing instabilities in attractive partial waves near the fermi surface. For a continuous single particle spectrum pairing instabilty is interpreted as an instability to form bound 2p2h states in nuclear matter. These pairing instabilities appear as complex poles located around the fermi surface in the effective interaction Γ. In determining the self consistent self energy, one should take the complete energy dependence of the effective interaction into account. In earlier calculations only the non-resonant continuum portions of the effective interaction were taken into account. The inclusion of $K = 0$ 2p2h bound states in the calculation of the self energy, was discussed in Ref. ().

For a continuous single particle spectrum these 2p2h bound pair states appear as complex poles of the effective interaction, located around the Fermi energy $2e_f$. These singularities give rise to serious numerical problems when solving the iterated Feynman - Galitskii integral equation for the effective interaction. In Ref. [93] it was proposed that an introduction of a gap in the single particle spectrum located at the fermi surface would resolve this problem. This suggestion was based on the observation that the 2p2h bound state poles become real poles by introducing a gap in the single particle spectrum at the fermi surface. If there is no gap in the single particle energy spectrum, there is no room for the bound states to appear as real excitations, since the hole-hole continuum extends from $-\infty$ to $2e_f$and the particle-particle continuum extends from $2e_f$ to ∞. So the $2p$ and $2h$poles appear at complex conjugate energies, $E_{2p} = E^*_{2h}$, around the Fermi energy $2e_f$,

this is why the poles of the t-matrix are often called pair-instabilities. By introduction of a mininum gap in the single particle spectrum this instability will disappear and the poles will position themselves on the real energy axis between $2e_f^+$ and $2e_f^-$. Ultimately this gap at the fermi surface would be generated self consistently.

The 2p2h bound states are dependent on both the fermi momentum k_f and the total momentum between the nucleons K. The 2p2h bound states appear only in a specific density region where strong pair correlations are expected, and will eventually dissolve with increasing center of momentum (total momentum) between the nucleons. In this case the complete energy spectrum is exposed without analytic continuation of the eigenvalue problem into the complex k-plane. However, with increasing K_{CM} the 2p2h poles will move towards 2p2h continuum, and one may expect that the 2p2h poles will move into the lower half k-plane (non-physical energy sheet) for a center of momentum K greater that some critical value K_{max}. In close analogy with the free scattering case, these poles may be associated with either virtual or resonant states. In this case CDM may prove to be a reliable and efficient way to calculate these exotic 2p2h states. These 2p2h poles will also appear as singularities in the effective interaction, and may on the same level as the bound state poles cause numerical trouble. One may expect that an introduction of a gap at the fermi surface will not make these complex poles real poles, since they are located on the non-physical energy sheet. From this observation one may conclude that an introduction of a gap at the fermi surface does not completely solve the problem associated with pairing instabilities in the iterated effective interaction Γ.

We start by outlining the formalism for 2p2h bound and scattering problems in infinite nuclear matter, and emphasize the relation between the t-matrix and the two-nucleon eigenvalue equation in nuclear matter. Holes and particles are treated on equal footing, hence allowing for hole-hole and particle-particle propagation. Solving for the effective interaction, Γ, the particle - particle and hole - hole ladder diagrams are summed to infinite order. The influence of the surrounding medium is reflected in the Pauli operator and self energy insertions. The two nucleon system is translational invariant, and center of mass motion can be neglected. The ladder summed effective interaction, $\Gamma(\omega)$, is given in operator form

$$\Gamma(\omega) = V + V g_{II}^{(0)}(\omega)\Gamma(\omega) \tag{3.79}$$

here V is the nucleon-nucleon interaction and $g_{II}^{(0)}(\omega)$ is the non-interacting 2p2h propagator given in terms of a product of two single particle propagators. The effective interaction can also be given in terms of an interacting 2p2h propagator g_{II},

$$\Gamma(\omega) = V + V g_{II}(\omega) V \tag{3.80}$$

$g_{II}(\omega)$ satisfies the Dyson equation

$$g_{II}(\omega) = g_{II}^{(0)}(\omega) + g_{II}^{(0)}(\omega) V g_{II}(\omega) \tag{3.81}$$

From equation (3.80) it is seen that the singularity structure of the effective interaction $\Gamma(\omega)$ is given in terms of the singularties of the interacting 2p2h propagator $g_{II}(\omega)$. By

rewriting equation (3.81) as

$$g_{II}(\omega) = \frac{g_{II}^{(0)}(\omega)}{1 - g_{II}^{(0)}(\omega)V} \tag{3.82}$$

it is seen that finding the poles of $\Gamma(\omega)$ corresponds to solving the characteristic equation

$$\det\left(1 - g_{II}^{(0)}(\omega)V\right) = 0 \tag{3.83}$$

which is associated with the eigenvalue problem

$$(1 - g_{II}^{(0)}(\omega)V)|\Psi\rangle = 0 \tag{3.84}$$

In the following discussion the propagation of particles and holes are considered with respect to an ucorrelated fermi sea, which gives the mean field approximation to the 2p2h propagators. In this picture the propagator $g_{II}^{(0)}$ is known as the Feynman - Galitskii [87] propagator, which in turn gives the Feynman - Galitskii integral equation for the effective interaction $\Gamma(\omega)$. In the lab system the Feynman - Galitskii propagator is given by

$$g_{II}^{FG(0)}(p_1, p_2, \omega) = \frac{Q(p_1, p_2)}{\omega - \epsilon(p_1) - \epsilon(p_2)} \tag{3.85}$$

here $Q = Q_{2p} - Q_{2h}$, the Pauli operator projecting onto the 2p space is given

$$Q_{2p}(p_1, p_2) = \theta(|\mathbf{p}_1| - k_f)\theta(|\mathbf{p}_2| - k_f) \tag{3.86}$$

and the corresponding 2h projector

$$Q_{2h}(p_1, p_2) = \theta(k_f - |\mathbf{p}_1|)\theta(k_f - |\mathbf{p}_2|) \tag{3.87}$$

the Pauli operator is an implicit function of the fermi momentum k_f defining the density of the infinite fermi sea. The eigenvalue equation (3.84) can now be written

$$\left[H_0 + \begin{pmatrix} Q_{2p} & 0 \\ 0 & -Q_{2h} \end{pmatrix} V\right] \begin{pmatrix} \psi_{2p} \\ \psi_{2h} \end{pmatrix} = E \begin{pmatrix} \psi_{2p} \\ \psi_{2h} \end{pmatrix} \tag{3.88}$$

here $H_0(p_1, p_2) = \epsilon(p_1) + \epsilon(p_2)$. The single particle energies ϵ are given by a kinetic energy term and a one body energy dependent self energy term,

$$\epsilon(p) = \frac{p^2}{2M} + \Sigma(p, \epsilon(p)) \tag{3.89}$$

this gives a self consistent equation for the self energy (Σ).

The normalization and completeness relation for the 2p2h states are given

$$\langle\psi_n|\phi_{n'}\rangle = \delta_{n,n'}, \;\; \mathbf{1} = \sum_n |\psi_n\rangle\langle\phi_n|. \tag{3.90}$$

Here the dual states ϕ_{nl} have been introduced. They are solutions of the transposed eigenvalue equation given in equation (3.88), and ϕ_{nl} and ψ_{nl} constitutes a biorthogonal set of states. The discrete sum is over bound states and in addition the sum implies an integration over the 2p2h continuum. Inserting this complete set of 2p2h states into the Feynman - Galitskii propagator equation (3.81) the spectral representation of the 2p2h interacting propagator is obtained,

$$g_{II}^{FG}(\omega) = \frac{\sum_n |\psi_n\rangle\langle\psi_n|}{\omega - E_n} \tag{3.91}$$

As the nucleon-nucleon interaction is given in relative coordinates it is convienient to transform from the nucleon lab system to relative and center of mass coordinates of the two nucleons,

$$\mathbf{k} = \frac{(\mathbf{p_1} - \mathbf{p_2})}{2}, \quad \mathbf{K} = \frac{(\mathbf{p_1} + \mathbf{p_2})}{2} \tag{3.92}$$

Here $\mathbf{k}$ is the relative momentum and $\mathbf{K}$ the center of momentum between the two interacting nucleons. To allow a partial wave decomposition the standard angle averaged Pauli operator $\bar{Q}$ and the angled averaged one body operator $\bar{H}_0$ are introduced.

A partial wave decomposition of the 2p2h eigenvalue equation (3.88) in relative and center of momentum can then be approximated by

$$\bar{H}_0(k,K)\psi_{nl}^{\alpha}(k,K) + \bar{Q}(k,K;k_f)\int_0^{\infty} dk' k'^2 V_l(k,k')\psi_{nl}^{\alpha}(k',K) = E_{nl}^{\alpha}\psi_{nl}^{\alpha}(k,K) \tag{3.93}$$

Here α represents the conserved quantum numbers J, S, T and k_f is the fermi momentum. The normalization integral for the two 2p2h states is

$$\int_0^{\infty} dk\; k^2 \psi_{n'l}^{*}(k,K)\phi_{nl}(k,K) = \delta_{n,n'} \tag{3.94}$$

where the dual 2p2h states $\phi_{nl}(k,K)$ are given in terms of $\psi_{nl}(k,K)$,

$$\phi_{nl}(k,K) = \bar{Q}^{-1}(k,K;k_f)\psi_{nl}(k,K) \tag{3.95}$$

The operator $\bar{H}_0$ is given by

$$\bar{H}_0 = \frac{k^2}{2\mu} + \frac{K^2}{2\mu} + \bar{\Sigma}_1 + \bar{\Sigma}_2, \tag{3.96}$$

The angle averaged Pauli operator,$\bar{Q} = \bar{Q}_{2p} - \bar{Q}_{2h}$, entering equation (3.93) will in this case depend on both fermi momentum, k_f, and the center of momentum K. The hole-hole part, $\bar{Q}_{2h}$ for $K < k_f$ is, see Ref. [94],

$$\bar{Q}_{2h}(k,K;k_f) = \begin{cases} 1 & 0 < k \le k_a \\ \frac{k_f^2 - K^2 - k^2}{2kK} & k_a < k \le \sqrt{k_f^2 - K^2} \\ 0 & \text{otherwise} \end{cases} \tag{3.97}$$

and the particle - particle part, $\bar{Q}_{2p}$, for $K < k_f$ is

$$\bar{Q}_{2p}(k,K;k_f) = \begin{cases} 0 & 0 < k \leq \sqrt{k_f^2 - K^2} \\ \frac{k^2+K^2-k_f^2}{2kK} & \sqrt{k_f^2 - K^2} < k \leq k_b \\ 1 & \text{otherwise} \end{cases} \tag{3.98}$$

here

$$k_a = k_f - K, \;\; k_b = K + k_f \tag{3.99}$$

In the case $K > k_f$, $\bar{Q}_{2h}$ is zero everywhere. The particle - particle part, $\bar{Q}_{2p}$, is given

$$\bar{Q}_{2p}(k,K;k_f) = \begin{cases} 1 & 0 < k \leq k_a \\ \frac{k^2+K^2-k_f^2}{2kK} & k_a < k \leq k_b \\ 1 & \text{otherwise} \end{cases} \tag{3.100}$$

here

$$k_a = K - k_f, \;\; k_b = K + k_f. \tag{3.101}$$

Equation (3.93) represents a non-hermitian eigenvalue problem. The general 2p2h energy spectrum will therefore in general be complex. The energy spectrum will depend on both the single particle energies entering the unpertubed one-body operator $\bar{H}_0$ and the two nucleon interaction $V_l(k,k')$. For a continuous single particle spectrum the 2h continuum extends from $-\infty$ to the fermi energy $E_f = k_f^2/2\mathrm{m}_n$ and the 2p continuum extends from $E_f$to ∞. The analytic structure of the integral kernel is the same as for free scattering except for the angle averaged Pauli operator. If we want to search for pole structures on the non-physical energy sheet, an analytical continuation in energy through the branch cut along the real axis, and onto the non-physical energy sheet has to be performed. The Pauli operator is continuous along the whole real k-axis but presents discontinuous derivatives at k_a and k_b. For real k the Pauli operator is therefore analytic only within the domains $k \in [0,k_a]$, $k \in (k_a,k_b]$ and $k \in (k_b,\infty)$. Summarizing; the Pauli operator is nonsingular in the complex k-plane, and analytic within three domains given by $D_1 = |z| \leq k_a$, $D_2 = k_a < |z| \leq k_b$ and $D_3 = |z| > k_b$. Analytical continuation of equation (3.93) onto the non-physical energy sheet (lower half k-plane) can be carried out within each domain where the integral kernel is analytic. Figure 3.17 gives an illustration of regions in the complex plane where the integral kernel is analytic, singularites in the potential are also shown along with a possible choice of deformed integration contour C. The transformed equation (3.93) will on the distorted contour C take the form

$$\bar{H}_0(k,K)\psi_{nl}^{\alpha}(k,K) + \bar{Q}(k,K;k_f)\int_C dk' k'^2 V_l(k,k')\psi_{nl}^{\alpha}(k',K) = E_{nl}^{\alpha}\psi_{nl}^{\alpha}(k,K) \tag{3.102}$$

here k and k' are both defined on the contour C, giving a closed integral equation. The fermi momentum, k_f, and the center of momentum, K, is kept real, since equation (3.102) is an integral equation in the relative momentum k only. The normalization of the 2p2h states follow the generalized c-product as described for the free scattering case.

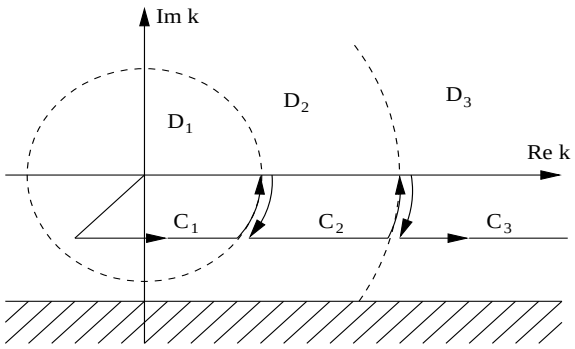

Figure 3.17: D_1, D_2 and D_3 demarcated by dotted circles define the regions in the complex k -plane where the Pauli operator is analytic. The shaded area represents a region in the complex k-plane where singularities in the potential appear. The optimal deformed contour choice for equation (3.93) is given by $C = C_1 + C_2 + C_3$.

3.6.2 Pairing instabilities and resonance-like phenomena for the CD-Bonn interaction.

Here we give a numerical calculation of 2p2h pair states in symmetric nuclear matter using the realistic CD-Bonn [95] nucleon-nucleon interaction. We use a free single particle spectrum with no gap in the calculations. The 2p2h complex pole trajectories of the virtual states in the ${}^1S_0$ channels are considered with increasing fermi momentum (k_f) and center of momentum (K). The 2p2h eigenvalue problem is solved on the contour C consisting of a rotated and a translated part as shown in figure 3.17. The singularity structure of the interaction is the same as for free scattering, the only modification is the angle averaged Pauli operartor entering the integral equation [9]. Figure 3.18 gives the ${}^1S_0$ 2p and 2h complex pair states for $K = 0$ MeV and increasing fermi momentum. Observe that the 2p2h pair states approaches the ${}^1S_0$ virtual states as $k_f \to 0$. For $K = 0$ MeV the 2p2h pair states are located in the upper half complex k-plane. In this case integration along the real k-axis will give the complete energy spectrum, see figure 3.18. It is worth noting that the imaginary part of the 2p2h complex energy fits remarkably well with the pairing gap obtained from the BCS gap equation using a free single particle spectrum, see e.g. Ref. [96]. This serves to illustrates that the BCS gap equation is an approximate solution of the 2p2h eigenvalue problem as pointed out in Ref. [91, 92, 93] Pairing correlations may also appear for $K > 0$. Figure 3.19gives the ${}^1S_0$ 2p complex pole trajectory for increasing center of momentum and fixed fermi momentum. The complex pole move towards the real energy axis and eventually through the branch cut and onto the non-physical energy sheet with increasing center of momentum. Translated to the momentum plane, this implies that the complex pole will move from the upper half k-plane and onto the lower half complex k-plane for a given center of momentum K_{min}. In the case $K > K_{min}$ the complete

[9] See Paper I for a discussion of the singularity structure of the CD-Bonn potential

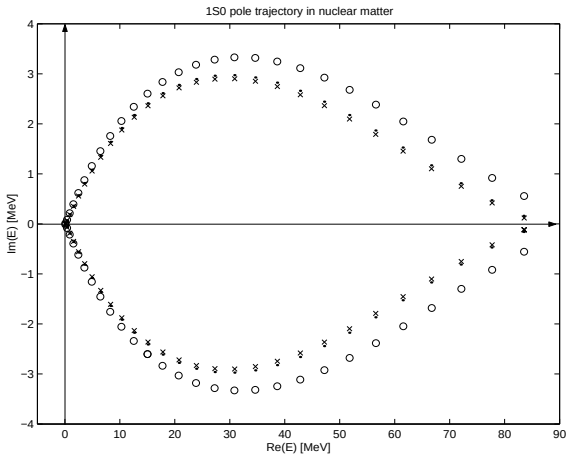

Figure 3.18: ${}^1S_0$ 2p2h pole trajectory in nuclear matter for $K_{CM} = 0$. Crosses: $t_z = -1$ -channel, dots: $t_z = 1$, circles: $t_z = 0$. $k_f \in [0, 280]$ MeV, $\Delta k_f = 10$ MeV.

2p2h energy spectrum is no longer obtainable by integrating along the real k-axis. By a suitable choice of contour CDM provides a method for obtaining the complete 2p2h energy spectrum for any $K > K_{min}$. Figure 3.20 gives a scetch of the ${}^1S_0$ 2p2h pole trajectories in

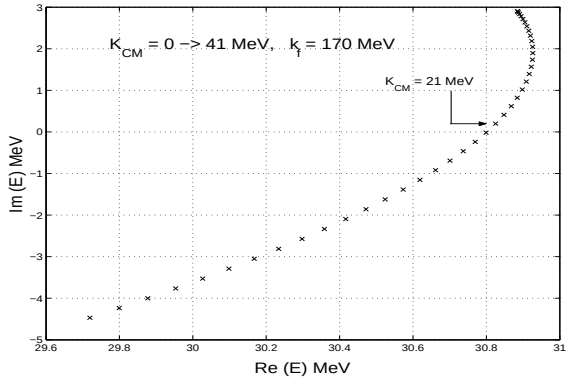

Figure 3.19: Calculated 2p pole trajectory for maximum pairing instability $k_f = 170$ MeV in the ${}^1S_0$ neutron - neutron isospin channel as function of K_{CM}. A rotated + translated contour was used in order to obtain energy spectrum.

nuclear matter. First the center of momentum is held fixed and equal $K = 0$ and the fermi momentum is varied. The 2p and 2h poles will move symmetrically to the imaginary axis in the upper half complex k-plane. Thereafter the fermi momentum is held fixed and the center of momentum is varied $K > 0$. In this case the 2p and 2h poles will move towards the real k-axis and for a given K into the lower half complex k-plane.

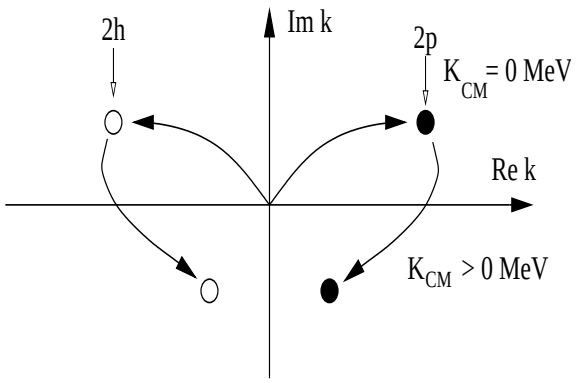

Figure 3.20: Trajectory of 2p2h complex poles (pair instabilities) in nuclear matter for increasing fermi momentum, k_k, and $K_{CM} = 0$ MeV. The figure also give the trajectory for increasing center of momentum K_{CM}, and k_f is held fixed.

3.6.3 Calculation of Γ by CDM for the CD-Bonn nucleon-nucleon interaction.

In this section we will discuss a method for solving the full off-shell vertex function (effective interaction), Γ, in a nuclear medium. This method is based on analytic continuation of the integral equations and expansion of the Green's function on a complete set of Berggren states. This is known as the Lehmann representation of the effective interaction Γ.

For two nucleons in free space the vertex function reduces to the t-matrix, and hence the free full two-body scattering problem. In free space the t-matrix can be interpreted as an effective interaction between two nucleons. In a scattering process the t-matrix includes repeated two body interactions to infinite order, i.e. a summation of all ladder diagrams to infinite order. In analouge to the free scattering case, we will consider only repeated interactions between either hole or particle states in the medium, giving the 2p2h ladder summed vertex function, Γ.

The integral equation (3.79) for the effective interaction may be written in relative and center of momentum coordinates by

$$\Gamma_l(k,k';\omega) = V_l(k,k') + \int_0^\infty dqq^2 V_l(k,q) g_{II}^{FG(0)}(q,\omega)\Gamma_l(q,k';\omega) \tag{3.103}$$

where we introduce the shorthand notation $\Gamma_l(k,k';\omega) = \Gamma_l(k,k',K,k_f;\omega)$. The non-interacting 2p2h propagator is given,

$$g_{II}^{FG(0)}(k,\omega) = \frac{\bar{Q}(k,K;k_f)}{\omega - H_0(k,K)} \tag{3.104}$$

In the case of free scattering $Q = 1$, and equation (3.103) reduces to the Lippmann-Schwinger equation for the t-matrix given in equation (3.71). The spectral representation

of the effective interaction takes the following form in RCM coordinates

$$\Gamma_l(k,k';\omega) = V_l(k,k') + \int_0^\infty dqq^2 \int_0^\infty dq'q'^2 V_l(k,q) g_{II}^{FG}(q,q';\omega) V_l(q',k') \tag{3.105}$$

where the interacting 2p2h propagator is given by equation (3.91). We will consider the solution of Equation (3.105) for the effective interaction by CDM. Using the completeness relation defined on a distorted contour C, shown in figure 3.17, gives the Berggren representation of the effective interaction in a nuclear medium,

$$\Gamma_l(k,k';\omega) = V_l(k,k') + \int_C dzz^2 \int_C dz'z'^2 V_l(k,z) g_{II}^{FG}(z,z';\omega) V_l(z',k') \tag{3.106}$$

here the interacting 2p2h propagator are represented in the 2p2h basis obtained by solving the eigenvalue problem in equation (3.102).

By applying CDM and the spectral representation of the effective interaction, we are able to single out the bound and resonant state contribution from the non-resonant 2p2h continuum contribution to the full effective interaction. The effective interaction may be written in the form,

$$\Gamma(\omega) = V + \Delta\Gamma(\omega) = V + \Delta\Gamma^R(\omega) + \Delta\Gamma^C(\omega),$$

here R denotes the discrete bound and resonant states, C denotes the non-resonant continuum contributions. In this way we may study the resonant, $\Delta\Gamma^R$, and non-resonant contributions, $\Delta\Gamma^C$, to the effective interaction separately. In figure 3.21 the effective interaction Γ for the input energy $\omega = (k^2+K^2)/2m_n$, center of momentum $K = 30$MeV and Fermi momentum $k_f = 170$MeV is given for $^1S_0$ neutron-neutron channel in the CD-Bonn interaction. A sharp peak is observed around the Fermi surface, indicating the existence of bound pair states. In figure 3.22 the non-resonant continuum contribution to the effective interaction is plotted, and it is seen that the peak around the Fermi surface has disappeared. The Discontinuties in the non-resonant contribution is due to the analytic structure of the angle averaged Pauli operator given in equations. (3.97,3.98, 3.100). In figure 3.23 the resonant contribution to the effective interaction is given. The resonant contribution displays a sharp peak around the Fermi surface, while the resonant contributions are neglible moving away from the Fermi surface.

In conclusion, CDM will enable us to obtain $\Gamma_l(k,k',K;\omega)$ for both real and complex input energies ω. The integral becomes non-singular on the deformed contour for real input energies ω, resulting in numerically stable solutions for two-body scattering in both free space and in a uniform medium. In this perspective, CDM offers an alternative approach to the standard PV prescription in solving for the effective interaction, and offers a valuable tool in descrbing different contributions to the effective interaction.

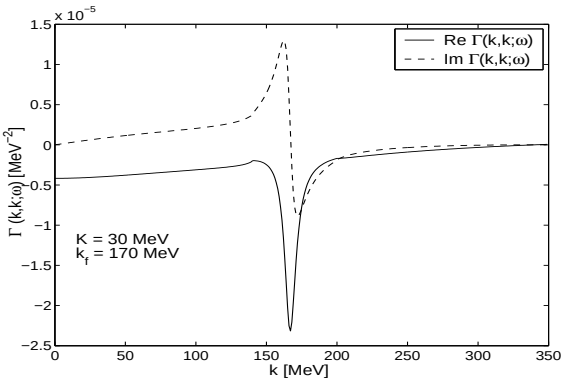

Figure 3.21: Effective interaction $\Gamma(k,k;\omega=(k^2+K^2)/2m_n)$ for $K=30\,\mathrm{MeV}$ and $k_f=170$ MeV for $^1S_0$ neutron-neutron channel in the CD-Bonn interaction. The peak around the fermi surface $k\approx 170$MeV indicates the formation of a pairing instability.

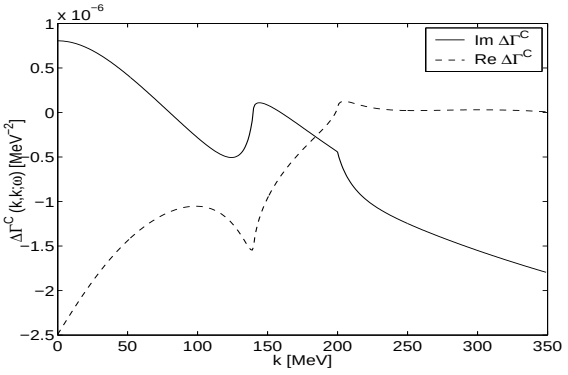

Figure 3.22: Continuum part of effective interaction $\Delta\Gamma(k,k;\omega=(k^2+K^2)/2m_n)$ for $K=30$ MeV and $k_f=170$ MeV for $^1S_0$ neutron-neutron channel in the CD-Bonn interaction. The peak around $k\approx 170$MeV has been washed out.

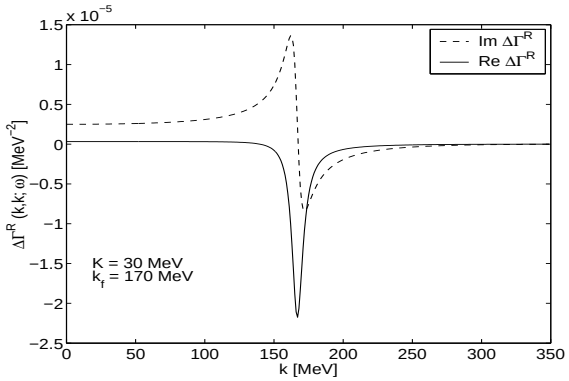

Figure 3.23: Resonant part of effective interaction $\Delta\Gamma(k,k;\omega=(k^2+K^2)/2m_n)$ for $K=30$ MeV and $k_f=170$ MeV for ${}^1S_0$ neutron-neutron channel in the CD-Bonn interaction. The resonant part of Γ has is clearly non-neglible around the fermi surface $k\approx 170$MeV.

Chapter 4

Effective interactions and many-body theory for unstable nuclei

4.1 The Gamow shell model

The standard nuclear shell model often starts with a harmonic oscillator representation for the single particle states. Since the harmonic oscillator potential is an infinite potential, the tail in single particle wave function falls off to rapidly in order to describe realistically single particle motion near the scattering continuum. The harmonic oscillator may therefore be said to work only for deeply bound nucleons. In order for the nuclear shell model to be applicable to nuclei far from the valley of stability, the harmonic oscillator picture of single particle motion has to be abdoned. The proximity of the scattering continuum in loosely bound and unbound nuclei, necessitates a modification and reformulation of the standard nuclear shell model.

From the previous sections, it was shown how a single particle basis consisting of bound, anti-bound and resonant states may be constructed using the Contour Deformation Method in momentum space. Solving the momentum space integral equation on a discretized contour in the complex k-plane a complex symmetric eigenvalue problem for the single particle states where obtained, and from which a complete set of *bi-orthogonal* states follows. Since the basis is discretized on a deformed contour it is possible to assign a unique quantum number to each single particle state. In the case of harmonic oscillator states we have the usual notation for the quantum numbers (n, l, j) where n is nodal number and (lj) the orbital- and total angular momentum of the single particle state. In the general case where bound, anti-bound, resonances and non-resonant continuum states are treated on equal footing, the meaning of the quantum number n has to be redefined and clarified. Since all single particle states have a discrete energy associated with them, it is natural to let n refer to the n'th discrete energy E_n. Defining n is manner, all single particle states have a unique set of quantum number n, l, j. figure 4.1illustrates how N single particle Berggren orbitals for a given (lj) partial wave, obtained by solving the momentum space Schrödinger equation on a N-point discretized contour in the complex k-plane, may be

organized in an ordered way. The non-resonant continuum orbitals are distinguished from the discrete bound- and resonant orbitals. Having constructed a single-particle Berggren

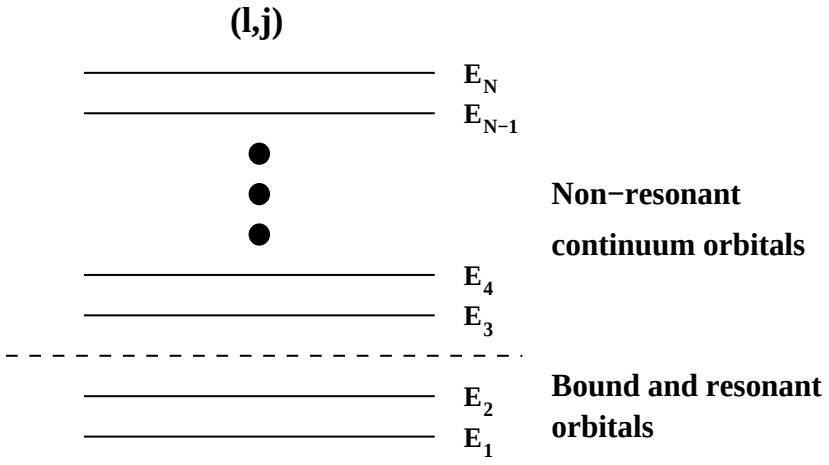

Figure 4.1: Illustration of how the bound, resonant and non-resonant continuum orbitals for a given (lj) single particle configuration may be organized in an ordered way.

basis, a many-body Berggren basis may be constructed in a completely analogous way as when harmonic oscillator states are used. We construct a complete anti-symmetric N-body basis from the Slater determinants consisting of the Berggren orbitals φ_{nljm} i.e.

$$\Phi_{\alpha_1,...,\alpha_n}(1,...,n) = \frac{1}{\sqrt{n!}} \begin{vmatrix} \varphi_{\alpha_1}(1) & \dots & \varphi_{\alpha_1}(n) \\ \vdots & & \vdots \\ \varphi_{\alpha_n}(1) & \dots & \varphi_{\alpha_N}(n) \end{vmatrix}, \tag{4.1}$$

where α_i labels the single particle quantum numbers $(n_i l_i j_i m_i)$. The Slater determinant have eigenvalues $E_i = \varepsilon_{\alpha_1} + ... + \varepsilon_{\alpha_N}$, which is just the sum of all single particle energies. Herethe label i subsumes all the different single particle quantum numbers $\varepsilon_{\alpha_1} + ... + \varepsilon_{\alpha_N}$. We then have at hand a complete set of N many-body Slater determinants, i.e.

$$1 = \sum_i^N |\Phi_i\rangle\langle\Phi_i^*|, \tag{4.2}$$

which the exact many-body wave function may be expanded in. The shell model problem then requires the solution of a complex symmetric $N \times N$ matrix eigenvalue equation,

$$H|\Psi_i\rangle = E_i|\Psi_i\rangle, \tag{4.3}$$

with $i = 1, ..., N$. Representing the shell model states in a complete set of Slater determinants, built from the single particle orbitals with quantum numbers $(nljm)$, is commonly known as the m-scheme representation. The Slater determinants are antisymmetric and

have definite values of the total spin projection $M_J = m_1 + m_2 + ... + m_n$ and total isospin projection $M_T = \tau_1 + \tau_2 + ... + \tau_n$, but they are not states with good quantum number of total spin J and isospin T. In standard large-scale shell model calculations, using the the m-scheme representation, one is typically interested in the the first few low lying energy states. The Lanczos algorithm [97] is an iterative method which has proven to be efficient in solving for a limited set of eigenvalues of large real symmetric matrices.

In the Gamow Shell Model case, the m-scheme and the Lanczos iterartion technique for solving large eigenvalue problem are not optimal approaches. Firstly, the m-scheme representation of the shell model equations does not automatically split the full shell model matrix into smaller sub-martices for different values of the total spin J and isospin T. In standard shell model calculations only bound states appear, but in Gamow Shell Model, not only bound states but a rather large set of continuum states are included for each lj configuration. In a m-scheme represenation, the dimension of the matrix will, in the Gamow Shell Model case, in most cases be too large to handle numerically. On the other hand, one may construct a many-body basis coupled to definite total spin J and T, either by the $j-j$ or the $L-S$ coupling scheme. Thereafter the shell model equations for a given value of spin and isospin may be diagonalized separately. The dimension of each J,T matrix will then be considerably smaller than the full matrix represented in the m-scheme. For Gamow Shell Model calculations the $j-j$ or the $L-S$ coupling scheme seems to be the most suitable representations. Secondly, the Lanczos iteration method aims at calculating a set of eigenvalues lowest in real energy. In Gamow Shell Model calculations there may be a large number of complex continuum states lying below the physical resonances in real energy. In addition it is difficult to predict where the multi-particle resonances will appear after diagonalization. This imply that new methods for solving large complex symmetric eigenvalues has to be developed. Direct diganalization procedures has to be abdoned, since the matrices with increasing number of valence particles soon become too large to store and handle on most modern computers.

Choosing to work Slater determinants coupled to definite spin, the $N-$body anti-symmetric wave function can be constructed viz.,

$$\Psi_\alpha^{JM}(1,...,N) = \sum_i C_i^{JM} \Phi_i^{JM}(1,...,N), \tag{4.4}$$

where the indice i represent the various single-particle orbits. Here $\Phi_i^J(1,...,N)$ is a normalized $N-$body anti-symmetric wave function. The shell model equations we have to solve is then given by

$$H|\Psi_i^J\rangle = E_i^J|\Psi_i^J\rangle, \tag{4.5}$$

In our Gamow Shell Model studies of $^{6-7}$He in Paper II, we worked within the $j-j$ coupling scheme. See Appendix A.2 for the derivation of three-body matrix elements in $j-j$ coupling. Table 4.1 gives the various dimension for the shell model matrices with definite spin and parity J^π for the different $^{5-7}$He isotopes considered in Paper II. It is seen that with a valence space of 24 $p_{1/2}$ and 24 $p_{3/2}$ single particle orbitals, the dimension grows extremely fast with increasing number of valence particles. Even in the case of three

valence particles the dimension is too large for direct diagonalization procedures. This problem of the dimensionality of the Gamow Shell Model equations is what we call the *dimensionality problem*. In order to be able to solve for the eigenvalue spectrum of such

^{5}He		^{6}He		^{7}He	
J^π	N	J^π	N	J^π	N
$1/2^-$	24	0^+	600	$1/2^-$	29648
$3/2^-$	24	1^+	1128	$3/2^-$	38896
		2^+	876	$5/2^-$	27072

Table 4.1: Dimension of the shell model matrices with definite spin and parity J^π for the $^{5-7}$He isotopes.

large complex matrices, effective interaction techniques and matrix perturbation theory generalized for complex symmetric matrices have to be developed and studied. This is the topic of the next sections.

4.2 Lanczos iteration process for many-body resonances.

The Lanczos iteration technique for finding a limited set of eigenvalues and eigenvectors for large real matrices, has over the years been the dominating approach in solving large-scale shell model equations. The method may easily be generalized to apply for complex matrices. This suggest that the method may be a suitable approach for dealing with large complex symmetric matrices which appear in Gamow Shell Model studies. However, we need a reliable prescription for identifying which state is to be associated with the physical multi-particle resonance from the set of eigenvectors obtained from diagonalizing the Lanczos matrix. Below we shall show how such a prescription may be defined. As a test case we consider the bound and resonant spectra of ^{6}He, using a shell model picture with two valence neutrons moving in $p_{3/2}$ Berggren orbitals outside a ^{4}He core. We use 24 single discretization points for the contour in generating the $p_{3/2}$ single particle basis of ^{5}He. See Paper II for further details on the contour, the ^{4}He -n interaction potential and on the residual nucleon-nucleon interaction for the two valence nucleons.

The many-body basis in which we expand the shell model wave function, is constructed from Slater determinants built from the single particle Berggren orbitals in a given valence space, and coupled to total spin Jsince we work in a $j-j$ coupling scheme. corresponding Hamiltonian may be represented in this basis. For the Lanczos iteration scheme to converge rapidly, the choice of a 0th order approximation to the multi-particle resonance should resemble the exact multi-particle resonance as much as possible. Constructing a reasonable starting vector for the Lanczos iteration procedure, is what we have to consider firstly. Having constructed a complete many-body basis from the single particle Berggren orbitals, the many-body space may be partioned into a model space P and an orthogonal

complement space Q by some selection procedure. The shell model Hamiltonian may then subsequently be partioned into two parts according to,

$$H = \begin{pmatrix} PHP & PHQ \\ QHP & QHQ \end{pmatrix} = \begin{pmatrix} H^{PP} & 0 \\ 0 & 0 \end{pmatrix} + \begin{pmatrix} 0 & H^{PQ} \\ H^{QP} & H^{QQ} \end{pmatrix}. \tag{4.6}$$

The model space P should be constructed in such a way that the most important many-body configurations of the many-body resonance wave function are included in this restricted space. Furthermore, the dimension N_P of the model space P should be small enough so that a full diagonalization of H^{PP} is possible. The 0th order lanczos vector $|\text{lanc}_0\rangle$, which is the 0th order approximation to the exact wave function, is then obtained by diagonalizing the $N_P \times N_P$ model space matrix H^{PP}. In choosing the model space P it is natural to assume that the most important configurations are those in which all or several particles are in single particle resonance orbitals. The Q-space consists then of the remaining configurations. In the ^{6}He test case we consider two different model spaces $P = P_1$, P_2. In the first case we let P be given by a single Slater determinant, where both neutrons are in the $p_{3/2}$ single particle resonance orbital, i.e. $P_1 = |RR\rangle$. In this case the 0th order lanczos vector is just the single Slater determninant,

$$|\text{lanc}_0\rangle = |\Phi_i^J\rangle = |RR\rangle. \tag{4.7}$$

In the second choice we construct P from all Slater determinants where at least one neutron is in the $p_{3/2}$ single particle resonance orbital, i.e.

$$P_2 \equiv \{|RR\rangle, |RC\rangle\}, \tag{4.8}$$

and the corresponding model space dimension is $N_{P_2} = 24$. In this case the 0th order Lanczos vector is a linear combination of Slater determinants,

$$|\text{lanc}_0\rangle = \sum_{i=1}^{N_{P_2}} C_{i,j} |\Phi_i^J\rangle. \tag{4.9}$$

Here C is a $N_{P_2} \times N_{P_2}$ orthogonal matrix which diagonalizes H^{PP}. The orthogonal columns j of C have been normalized so that $|\text{lanc}_0\rangle$ is normalized. For each Slater determinant $|\Phi_i\rangle$, $i = 1, ..., N_{P_2}$ a corresponding amplitude $C_{i,j}$ is assigned. As the diagonalization of the model space matrix H^{PP} gives N_{P_2} possible choices for the 0th order Lanczos vector, we have to determine from this set which is the 0th order approximation to the exact two-particle resonance wave function. This may be done by considering each column j of the matrix C, and determine which of these columns have the largest amplitude $C_{i,j}$ for the Slater determinant where all particles are in single particle resonance orbitals.

The Lanczos iteration procedure may be summarized by the following steps,

1. Choose an initial Lanczos vector $|\text{lanc}_0\rangle$ (a linear combination of Slater determinants) as the 0th order approximation to the exact multi-particle resonance wave function. See discussion above, on how to choose this starting vector for Gamow Shell Model applications.

2. The next step involves generating a new vector $|\text{new}_{p+1}\rangle$ by letting the full Hamiltonain H act on the p'th Lanczos vector $|\text{lanc}_p\rangle$, i.e. $|\text{new}_{p+1}\rangle = H|\text{lanc}_p\rangle$. Throughout this process we construct the energy matrix elements of H in this Lanczos basis. The diagonal matrix elements of H are then obtained by

$$\langle \text{lanc}_p|H|\text{lanc}_p\rangle = \langle \text{lanc}_p|\text{new}_{p+1}\rangle. \tag{4.10}$$

3. The new vector $|\text{new}_{p+1}\rangle$ is then orthogonalized to all previously calculated Lanczos vectors by the Gram-Schmidt procedure

$$|\text{new}'_{p+1}\rangle = |\text{new}_{p+1}\rangle - \sum_{q=0}^{p} |\text{lanc}_q\rangle\langle \text{lanc}_q|\text{new}_{p+1}\rangle, \tag{4.11}$$

and normalized

$$|\text{lanc}_{p+1}\rangle = \frac{1}{\sqrt{\langle \text{new}'_{p+1}|\text{new}'_{p+1}\rangle}}|\text{new}'_{p+1}\rangle, \tag{4.12}$$

to give a new normalized Lanczos vector.

4. The off-diagonal matrix elements of H is then obtained by

$$\langle \text{lanc}_{p+1}|H|\text{lanc}_p\rangle = \langle \text{lanc}_{p+1}|\text{new}'_{p+1}\rangle, \tag{4.13}$$

and all other matrix elements are zero.

5. After p iterations we have an energy matrix of tridiagonal form

$$\begin{bmatrix} H_{0,0} & H_{0,1} & 0 & \dots & 0 \\ H_{1,0} & H_{1,1} & H_{1,2} & \dots & 0 \\ 0 & H_{2,1} & H_{2,2} & \dots & 0 \\ \vdots & \vdots & \vdots & \vdots & H_{p-1,p} \\ 0 & 0 & 0 & H_{p,p-1} & H_{p,p} \end{bmatrix} \tag{4.14}$$

as the p'th approximation to the full eigenvalue problem. The number p is a reasonably small number so the matrix can be diagonalized by standard diagonalization routines for sparse matrices of tridiagonal form, to obtain eigenvalues and eigenvectors which are linear combinations of the Lanczos vectors.

6. This process is repeated until a suitable convergence criterion has been reached.

Having determined a converged Lanczos energy matrix, the remaining problem is how to determine which of the states $|\Psi_i(p)\rangle$, $i = 1, ..., p$ gives the p'th approximation to the exact multi-particle resonance. This identification may be done unambigously by determining which state $|\Psi_i(p)\rangle$, $i = 1, ..., p$ has the largest overlap with the initial Lanczos vector $|\text{lanc}_0\rangle$, which is the 0th order approximation to the exact multi-particle resonance.

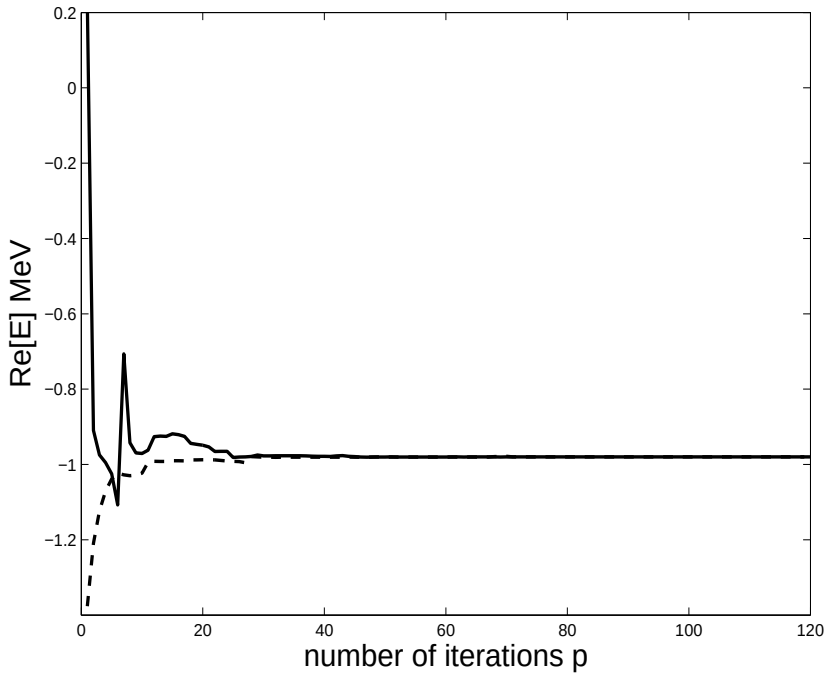

Figure 4.2: Convergence of the real part of the 0^+ ground state energy of ^{6}He.

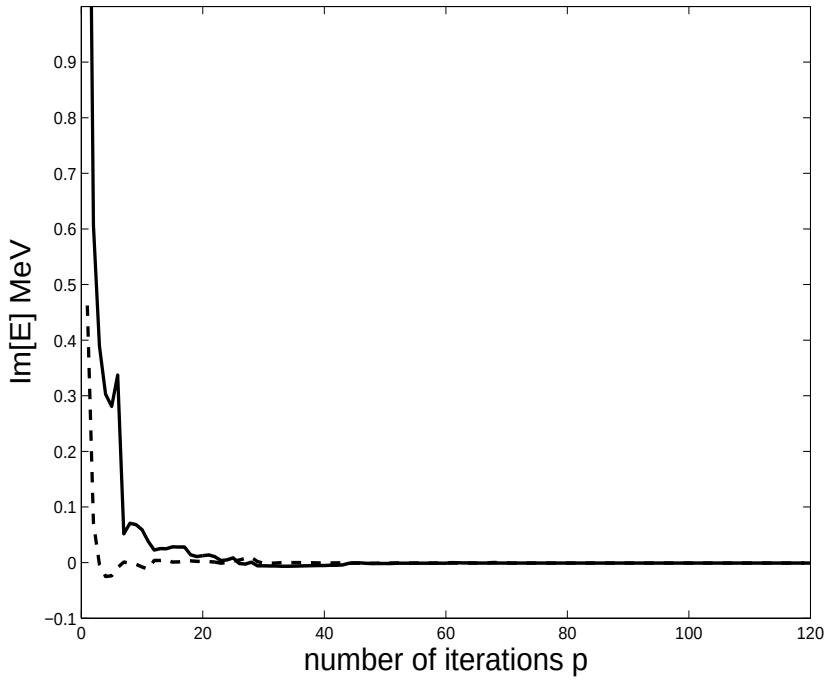

Figure 4.3: Convergence of the imaginary part of the 0^+ ground state energy of ^{6}He.

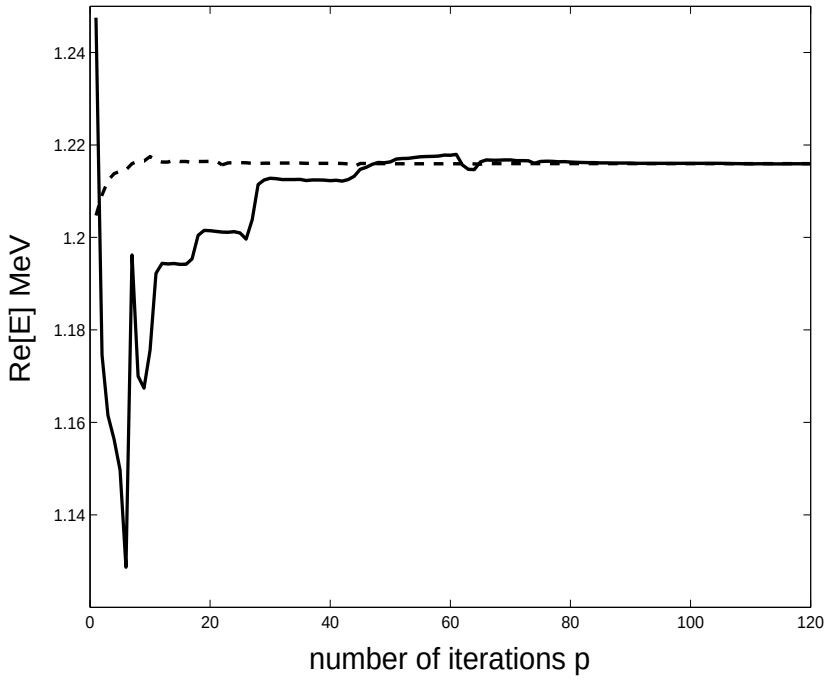

Figure 4.4: Convergence of the real part of the 2^+ resonance energy of ^{6}He.

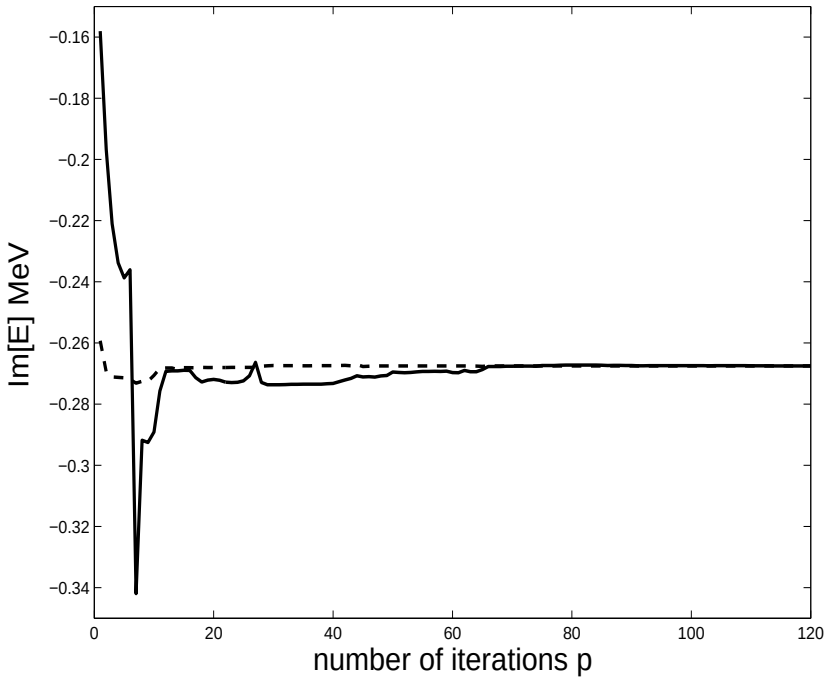

Figure 4.5: Convergence of the imaginary part of the 2^+ resonance energy of ^{6}He.

Figures 4.2 and 4.3 gives the approximate real and imaginary parts of the 0^+ ground state of ^{6}He obtained after p iterations, using the starting vector given in equation (4.7) (solid line) and the starting vector given in equation (4.9) (dashed line). It is seen that both for the real and imaginary parts of the energy, the convergence is faster for the initial Lanczos vector given in equation (4.9) than compared with the convergence using the initial vector in equation (4.7). However, it is interesting to see that both choices converges to the exact ground state energy $E(0^+) = -0.98 + 0.00i$MeV within the number of iterations p considered. Figures 4.4 and 4.5 gives the approximate real and imaginary parts of the 2^+ resonant state of ^{6}He obtained after p iterations, using the starting vector given in equation (4.7) (solid line) and the starting vector given in equation (4.9) (dashed line). Also in this case convergence is faster using equation (4.9) for an initial Lanczos vector. Both choices converges to the exact two-particle resonance energy $E(2^+) = 1.216 - 0.268i$MeV for a reasonable small number of iterations p. This test study of the Lanczos iteration procedure applied to Gamow Shell Model studies, is very promising. Both resonances and bound states are reproduced with a small number of iterations, given a reasonable choice for a 0th order approximation to the two-particle resonance wave function.

4.3 Similarity transformations and effective operators for complex interactions.

The previous section served to introduce and motivate the application of complex scaling and a Berggren basis in studies of weakly bound nuclear systems. However, employing such a momentum space basis soon exceeds feasible dimensionalities in shell-model studies. To circumvent this problem and to be able to define effective interactions of practical use in shell-model calculations, we introduce effective two-body interactions based on similarity transformation methods. These interactions are in turn employed in Gamow shell model calculations. We base our approach on the extensive works of Suzuki, Okamoto, Lee and collaborators, see for example Refs. [98, 99, 100, 101]. This similarity transformation method has been widely used in the construction of a effective two- and three-body interactions for use in the No-Core shell-model approach of Barrett, Navratil, Vary and collaborators, see for example Refs. [36, 37, 38, 39] and references therein. However, since the similarity transformation method has previously only been considered for real interactions, we need to extend its use to Gamow shell model calculations, implying a generalization to complex interactions.

We start with the abstract formulation of the two-body Schrödinger equation,

$$(H_0 + V)\,|\Psi_k\rangle = E_k|\Psi_k\rangle, \tag{4.15}$$

here H_0 includes the single-particle part of the Hamiltonian, kinetic energy and an eventual single-particle potential. The term V is the residual two-body interaction. The Hamiltonian, $H = H_0 + V$, is here a complex symmetric matrix, i.e. $H = H^{\mathrm{T}}$ [1], since the equations are analytically continued to the complex k-plane, and the eigenvalue problem is no longer Hermitian. The eigenvectors form a complete *bi-orthogonal*set, and are normalized according to the *bi-linear* form,

$$\langle\tilde{\Psi}_k|\Psi_{k'}\rangle = \langle\Psi^*_k|\Psi_{k'}\rangle = \delta_{k,k'},$$

Here the left eigenvector $\langle\tilde{\Psi}_k|$ is just the transpose of the right eigenvector $|\Psi_k\rangle$, which follows from the fact the Hamiltonian is complex symmetric (see Appendix A.1 for details). [2] The Hilbert space is now divided in two subspaces, i.e. a model space and a complement space. The operators which project onto the model space and onto its complement space are labeled P and Q, respectively. The projection operators fulfill the relations

$$P^2 = P, \;\; Q^2 = Q, \;\; P^{\mathrm{T}} = P, \tag{4.16}$$

and

$$Q^{\mathrm{T}} = Q, \;\; P + Q = 1, \;\; PQ = 0. \tag{4.17}$$

[1] Here H^{T} means the transpose of H.

[2] In the following we will use the notation for the bi-orthogonal states $\langle\tilde{\Psi}_k| = \langle\Psi^*_k|$ which are the left eigenvectors of a complex symmetric matrix. This is for distinguishing them from the bi-orthogonal states $\langle\tilde{\phi}_k|$ which are left eigenvectors of non-symmetric matrices, which gives $\langle\tilde{\phi}_k| \neq \langle\phi^*_k|$

The projection operators are typically chosen to be the eigenprojectors of the one-body operator H_0, i.e. they are constructed from the basis which diagonalizes H_0,

$$\langle \alpha^* |\, H_0 \, |\alpha' \rangle = \varepsilon_i \delta_{\alpha,\alpha'}, \tag{4.18}$$

from which they have the explicit form,

$$P = \sum_{\alpha_P} |\alpha_P\rangle\langle\alpha_P^*|, \;\; Q = \sum_{\alpha_Q} |\alpha_Q\rangle\langle\alpha_Q^*|, \tag{4.19}$$

From this particular choice it follows,

$$\begin{aligned} [H_0, P] = [H_0, Q] \; &= 0, \\ QH_0P = PH_0Q &= 0. \end{aligned} \tag{4.20}$$

The aim is to construct an effective Hamiltonian within the $P-$space, for which every eigenvalue of the effective Hamiltonian corresponds to one of the exact eigenvalues of full Hamiltonian H. This can be accomplished by a similarity transformation of the full Hamiltonian,

$$\tilde{H} = X^{-1}HX, \;\; |\Phi_k\rangle = X^{-1}|\Psi_k\rangle, \tag{4.21}$$

Representing the Schrödinger equation in the basis of the one-body operator H_0, it can be rewritten in the 2×2 block structure,

$$\begin{pmatrix} P\tilde{H}P & P\tilde{H}Q \\ Q\tilde{H}P & Q\tilde{H}Q \end{pmatrix} \begin{pmatrix} P\Phi_k \\ Q\Phi_k \end{pmatrix} = E_k \begin{pmatrix} P\Phi_k \\ Q\Phi_k \end{pmatrix}. \tag{4.22}$$

which gives the equations,

$$P\tilde{H}P|\Phi_k\rangle + P\tilde{H}Q|\Phi_k\rangle = E_k P|\Phi_k\rangle \tag{4.23}$$

$$Q\tilde{H}P|\Phi_k\rangle + Q\tilde{H}Q|\Phi_k\rangle = E_k Q|\Phi_k\rangle \tag{4.24}$$

Where we have used $P^2 = P$ and $Q^2 = Q$. Solving equation (4.24) for $Q|\Phi_k\rangle$, and inserting into equation (4.24), yields an effective eigenvalue problem in the P-space,

$$\left(P\tilde{H}P + P\tilde{H}Q \frac{1}{E_k - Q\tilde{H}Q} Q\tilde{H}P \right) P|\Phi_k\rangle = E_k P|\Phi_k\rangle \tag{4.25}$$

This effective Hamiltonian depends on the exact eigenvalue E_k of the full problem. However, if a similarity transformation matrix $X$is chosen such that the decoupling equation,

$$Q\tilde{H}P = Q(X^{-1}HX)P = 0, \tag{4.26}$$

is satisfied, then we end up with an effective Hamiltonian in the P-space which is energy independent, i.e.

$$\left(P\tilde{H}P \right) P|\Phi_k\rangle = E_k P|\Phi_k\rangle \tag{4.27}$$

There are infinitely many different transformations Xwhich decouple the P- and Q-spaces, see e.g. Refs. [102, 103]. Here we choose the Lee-Suzuki (LS) similarity transformation, see Ref. [98]. The LS transformation is the simplest transformation, and given by,

$$\begin{aligned} X &= \exp(\omega) && (4.28)\\ \Rightarrow \tilde{H}_{LS} &= \exp(-\omega) H \exp(\omega), \;\; |\Phi_k\rangle = \exp(-\omega)|\Psi_k\rangle, && (4.29) \end{aligned}$$

here ω has the property,

$$\omega = Q\omega P, \tag{4.30}$$

where it is seen that ω acts as a mapping between the P and Qspaces. From equation (4.30) it follows that $\omega^2 = \omega^3 = ... = 0$ and the transformation operators X and X^{-1} simplify to

$$X = \exp(\omega) = 1 + \omega, \;\; X^{-1} = \exp(-\omega) = 1 - \omega, \tag{4.31}$$

for which it immediately follows for the effective Hamiltonian and interaction in the P-space,

$$\begin{aligned} P\tilde{H}_{LS}P &= PH(P+\omega), \\ PV_{LS}P &= PH(P+\omega) - PH_0P = PVP + PV\omega = PVP + PVQ\omega, \end{aligned} \tag{4.32}$$

Where we have used the identity $Q\omega = Q\omega P = \omega$. [3] The decoupling equation (4.26) becomes,

$$QHP + QHQ\omega - \omega PHP - \omega PHQ\omega = 0. \tag{4.34}$$

The P-space Schrödinger equation (4.27) now becomes,

$$P(H_0 + V_{LS})P|\phi_k\rangle = E_k|\phi_k\rangle \tag{4.35}$$

where $|\phi_k\rangle = P|\Phi_k\rangle$. The true eigen state Ψ_k of the original Schrödinger equation (4.15) is related to the P-space eigen state ϕ_k of equation (4.35) in the following way,

$$|\Psi_k\rangle = XP|\Phi_k\rangle = \exp(\omega)P|\Phi_k\rangle = (P+\omega)|\phi_k\rangle. \tag{4.36}$$

Here it is seen that $\omega|\phi_k\rangle$ is the Q-space component of the true eigen state $|\Psi_k\rangle$. The eigenvalue problem for the P-space eigen states in equation (4.35), is of a non-symmetric type. This means that the left and right eigenvectors form a complete bi-orthogonal set. Solving for the left eigenvectors $\langle\tilde{\phi}_k|$ of equation (4.35) which are *bi-orthogonal* to the right eigenvectors (see Appendix A.1 for details) $|\phi_k\rangle$, we get

$$\langle\tilde{\phi}_k|\phi_{k'}\rangle = \delta_{k,k'}, \tag{4.37}$$

[3] In Ref. [103] Okamoto *et. al.* classified all energy independent effective interactions in the time independent approach, and formally showed that they may be written as

$$\tilde{H}(m,n) = (P + \omega^\dagger\omega)^{-m} H (P+\omega)(P+\omega^\dagger\omega)^n. \tag{4.33}$$

Where m, n are integers of half-integers. For $m = n = 0$ the non-Hermitian Lee-Suzuki effective interaction in equation (4.32), which is the simplest transformation, is obtained.

Using the orthogonality of the true eigenvectors in equation (4.15) we may derive a relationship between the left and right eigenvectors,

$$\langle \Psi_k^* | \Psi_{k'} \rangle = \langle \phi_k^* | (P + \omega^{\mathrm{T}} \omega) | \phi_{k'} \rangle = \delta_{k,k'}, \tag{4.38}$$

from which the following properties follow,

$$\langle \tilde{\phi}_k | = \langle \phi_k^* | (P + \omega^{\mathrm{T}} \omega), \tag{4.39}$$

and

$$(P + \omega^{\mathrm{T}} \omega) = (P + \omega^{\mathrm{T}} \omega)^{\mathrm{T}}. \tag{4.40}$$

Given the left and right eigenvectors of the LS effective Hamiltonian, the formal solution to ω is given by,

$$\omega = \sum_{k=1}^{d} Q | \Psi_k \rangle \langle \tilde{\phi}_k | P, \tag{4.41}$$

here $d = N_P$ is the dimension of the P-space. The solution to ω is ambiguous in the sense that how to choose the N_P exact eigen states $|\Psi_k\rangle$ is not unique. The effective interaction will depend on the choice of eigenvectors, and this is why the LS effective interaction is often called a *state-dependent* interaction. With the solution to ω, the N_P eigenvalues of the P-space equation will correspond exactly with the N_P arbitrary chosen eigenvalues of the original Schrödinger equation (4.15). Representing ω in the basis which diagonalizes H_0 (see equation (4.18)) and defines the projection operators P and Q gives,

$$\langle \alpha_Q^* | \, \omega \, | \alpha_P \rangle = \sum_{k=1}^{d} \langle \alpha_Q^* | \Psi_k \rangle \langle \tilde{\phi}_k | \alpha_P \rangle. \tag{4.42}$$

The bra states $\langle \tilde{\phi}_k |$ may be obtained from the true eigenstate $|\Psi_k\rangle$. Using the property that the matrix of left eigenvectors is the inverse of the matrix of right eigenvectors for a general matrix (see Appendix A.1), we get for the matrix of bra states,

$$[\langle \tilde{\phi}_k | \alpha_P \rangle] = [\langle \alpha_P^* | \phi_k \rangle]^{-1} = [\langle \alpha_P^* | \Psi_k \rangle]^{-1}. \tag{4.43}$$

here [...] refer to the full $N_P \times N_P$ matrix. Then ω in the represenation of H_0 is given by the matrix equation,

$$[\langle \alpha_Q^* | \, \omega \, | \alpha_P \rangle] = [\langle \alpha_Q^* | \Psi_k \rangle][\langle \alpha_P^* | \Psi_k \rangle]^{-1}. \tag{4.44}$$

It is seen that a solution for ω is obtainable provided the matrix $[\langle \alpha_Q^* | \Psi_k \rangle]$ is non-singular. In numerical implementations it is therefore preferable to choose those N_P exact eigen states Ψ_k which have the largest overlap with the $P-$space, $O_n = \sum_{\alpha_P} |\langle \Psi_n^* | \alpha_P \rangle|^2$. The matrix elements of the LS non-Hermitian Hamiltonian in equation (4.32) in the represenation of H_0 (see equation (4.18)) are given as,

$$\langle \alpha_P^* | \tilde{H}_{LS} | \alpha_P' \rangle = \sum_{k=1}^{d} \left[\langle \alpha_P^* | \Psi_k \rangle E_k \langle \Psi_k^* | \alpha_P' \rangle + \sum_{\alpha_Q} \langle \alpha_P^* | \Psi_k \rangle \; E_k \; \langle \Psi_k^* | \alpha_Q \rangle \langle \alpha_Q^* | \omega | \alpha_P' \rangle \right]. \tag{4.45}$$

Here E_k are the exact eigenvalues obtained by diagonalizing the full Hamiltonian given in equation (4.15). When diagonalizing the LS effective Hamiltonian, the E_k, $k = 1, ..., d$ exact eigenvalues are obtained. The LS effective interaction becomes in the represenation of H_0,

$$\langle \alpha_P^* | V_{LS} | \alpha_P' \rangle = \langle \alpha_P^* | \tilde{H}_{LS} | \alpha_P' \rangle - \varepsilon_{\alpha_P} \delta_{\alpha_P, \alpha_P'} \tag{4.46}$$

The LS effective Hamiltonian is non-Hermitian and non-symmetric. It would be preferable to obtain a complex symmetric effective interaction, in order to take advantage of the anti-symmetrization of the two-particle basis. This may be accomplished by a Z-transformation of the P-space states,

$$|\nu_k\rangle = Z|\phi_k\rangle, \tag{4.47}$$

which gives the following property

$$\langle \tilde{\nu}_k | \nu_{k'} \rangle = \langle \nu_k^* | \nu_{k'} \rangle = \delta_{k,k'}. \tag{4.48}$$

Using again the orthogonality of the true eigenstates $|\Psi_k\rangle$, we get

$$\langle \Psi_k^* | \Psi_{k'} \rangle = \langle \phi_k^* | (P + \omega^{\mathrm{T}} \omega) | \phi_{k'} \rangle = \langle \nu_k^* | (Z^{-1})^{\mathrm{T}} (P + \omega^{\mathrm{T}} \omega)(Z^{-1}) | \nu_{k'} \rangle = \delta_{k,k'}, \tag{4.49}$$

which gives the following condition for the Z-transformation in order for equation (4.48) to be fulfilled,

$$Z^{\mathrm{T}} Z = P + \omega^{\mathrm{T}} \omega. \tag{4.50}$$

Having obtained a solution for Z which obeys equation (4.50), the complex symmetric (CS) effective interaction is given by,

$$V_{CS} = Z(H_0 + V_{LS})Z^{-1} - PH_0P. \tag{4.51}$$

That the Z-transformed LS effective Hamiltonian is complex symmetric follows from the orthogonality in equation (4.48), where the left eigenvector is the transpose of the right eigenvector, which is the case for symmetric matrices only (see Appendix A.1). Refs. [102, 103] derived and discussed several such Z-transformations for which a Hermitian effective interaction is obtained. One such Z-transformation is,

$$Z = P(1 + \omega^{\mathrm{T}} \omega)^{1/2} P. \tag{4.52}$$

From equation (4.40) it follows that $Z = Z^{\mathrm{T}}$ for this particular choice, and it is easily seen that equation (4.50) is fulfilled. This choice of Z leads to an effective interaction of the Okubo form [104],

$$V_{okb} = P(1 + \omega^{\mathrm{T}} \omega)^{1/2} P(H_0 + V_{LS}) P(1 + \omega^{\mathrm{T}} \omega)^{-1/2} P - PH_0P. \tag{4.53}$$

The matrix element of the Okubo effective interaction in the representation of H_0 becomes,

$$\langle \alpha_P^* | V_{okb} | \alpha_P' \rangle = \sum_{\gamma_P} \sum_{\gamma_P'} \langle \alpha_P^* | (P + \omega^{\mathrm{T}} \omega)^{1/2} | \gamma_P \rangle \langle \gamma_P^* | H_{LS} | \gamma_P' \rangle \langle \gamma_P'^* | (P + \omega^{\mathrm{T}} \omega)^{-1/2} | \alpha_P' \rangle - \varepsilon_{\alpha_P} \delta_{\alpha_P, \alpha_P'} \tag{4.54}$$

To determine V_{okb}, one has to find the square root of the matrix $A = \left[\langle\alpha^*|(P+\omega^{\mathrm{T}}\omega)|\alpha'_P\rangle\right]$. In the case of A being real and positive definite the method based on eigenvector decomposition gives generally a stable solution. Using the eigenvector decomposition, with X representing an orthogonal matrix with the eigenvectors of A and D a diagonal matrix composed of the eigenvalues, we have the following

$$A = XDX^T, X^TX = XX^T = 1, D = (D)^{1/2}(D)^{1/2}, \tag{4.55}$$

which gives,

$$A = \left(XD^{1/2}X^T\right)\left(XD^{1/2}X^T\right), \tag{4.56}$$

the square root of the matrix A is then given by,

$$A^{1/2} = XD^{1/2}X^T. \tag{4.57}$$

For a complex matrix A the procedure based on eigenvector decomposition is generally numerically unstable [105]. An approach suitable for complex matrices is based on properties of the matrix sign function. It can be shown that the square root of the matrix is related to the matrix sign function, see Ref. [105] for more details. In the case of A being complex and having all eigenvalues in the open right half complex plane, iterations based on the matrix sign function are generally more stable

$$\mathrm{sign}\left(\begin{bmatrix} 0 & A \\ I & 0 \end{bmatrix}\right) = \begin{bmatrix} 0 & A^{1/2} \\ A^{-1/2} & 0 \end{bmatrix}. \tag{4.58}$$

One stable iteration scheme for the matrix sign was derived by Denman and Beavers [106], as a special case of a method for solving the algebraic Riccati equation

$$Y_0 = A, \;\; Z_0 = I, \tag{4.59}$$

$$Y_{k+1} = \frac{1}{2}(Y_k + Z_k^{-1}), \tag{4.60}$$

$$Z_{k+1} = \frac{1}{2}(Z_k + Y_k^{-1}), \;\; k = 0, 1, 2, ..., \tag{4.61}$$

and provided A has no non-positive eigenvalues this iteration scheme exhibits a quadratic convergence rate with

$$Y_k \rightarrow A^{1/2}, \quad Z_k \rightarrow A^{-1/2} \;\; \text{as} \;\; k \rightarrow \infty. \tag{4.62}$$

4.4 Non-Hermitian Many-Body perturbation theory

The former section dealt with the problem of constructing an energy independent effective two-body interaction using similarity transformation methods, generalized to complex interactions. Having constructed an effective interaction in the two-particle model space, this interaction is then the basic ingredient in the many-body problem. However, dealing

with many particles moving in large valence space, the dimensionlality may still be of an order not suitable of a practical solution. The single particle resonances have many of the same characteristics as bound states on deformed contours in the complex$k$-plane, they are discrete square integrable states with a set of definite quantum number. Based on this it is reasonable to assume that in the many-body problem, many-body perturbation theory orginally developed for bound states, may be generalized to apply for many-body resonances.

The focus in this section will be on the non-Hermitian multi-reference perturbation theory method (MRPTM), which in the Hermitian case has recently been revived in quantum chemistry, see for example Refs. [107, 108, 109]. The MRPTM differs from standard many-body perturbation techniques, in that a set of reference states are constructed by diagonalizing N-body model-space Hamiltonian exactly. Having constructed a more suitable basis which decouples the P-space, this basis serves as starting points for a perturbation expansion. It can be shown that this expansion converges much faster than the single-reference perturbation theory, since many higher order terms are already incorporated into the zeroth order term. The chosen N-body model-space P should be of such kind that the coupling of P with the complement space Q is weak, for the perturbation expansion to converge.

For clarity we first outline the standard Many-Body perturbation theory where only single references appear. Thereafter we outline the multi-reference theory for non-Hermitian interactions, and show that even at the first order, MRPTM sums a class of diagrams to infinite order in appearing in the standard Rayleigh-Schrödinger perturbation expansion.

4.4.1 Single-Reference perturbation theory.

Here we outline the standard many-body perturbation theory, applicable to the case of many-body resonances. Starting with the N-body schrödinger equation,

$$H\Psi = E\Psi \tag{4.63}$$

where the Hamiltonian is split into an unperturbed part H_0 for which we can obtain exact solutions, and a perturbation V, i.e.

$$H = H_0 + V \tag{4.64}$$

where

$$H_0 = \sum_i (T_i + U_i), \;\; V = \sum_{i<j} V_{i,j} - \sum_i U_i. \tag{4.65}$$

The exact solution of H_0 are given by,

$$H_0\Phi_i = \varepsilon_i\Phi_i, \tag{4.66}$$

where the N-body unperturbed energy ε_i is given by the sum of N single particle energies obtained by solving the one-body Hamiltonian, $T + U$, and Φ_i is a Slater determinant

composed of N-particles occupying the relevant single-particle orbitals. Having obtained a complete set of many-body Slater determinants, we may define a model space P and complement space Q which project into orthogonal parts of the full space,

$$P = \sum_{i=1}^{N_P} |\Phi_i\rangle\langle\Phi_i^*|, \;\; Q = \sum_{i=N_P+1}^{N} |\Phi_i\rangle\langle\Phi_i^*|. \tag{4.67}$$

Here N_P is the dimension of the model space and N is the dimension of the full space. They satisfy the usual equations given in equations (4.16) and (4.17). There are many ways of constructing the many-body P- and Q-spaces. The most usual is to construct them from the single particle model space. So that P is the space constructed from all single particles occupying orbits in the single particle model space p, and Q is the remaining orthogonal space. The exact N-body wave function may then be expanded in this basis,

$$\Psi = \sum_{i=1}^{N_P} C_i\Phi_i + \sum_{i=N_P+1}^{N} C_i\Phi_i = P\Psi + Q\Psi,$$

and the full Schrödinger equation may be written in the 2×2 block structure given in equation (4.22). An effective eigenvalue problem in the P-space may then be otained (see former section),

$$\left(PHP + PHQG(E_k)QHP\right) P|\Psi_k\rangle = E_k P|\Psi_k\rangle \tag{4.68}$$

where we have introduced the complete interacting Green's function in the Q-space,

$$G(E) = \frac{Q}{E - QHQ} = \frac{Q}{E - H_0 - QVQ} \tag{4.69}$$

Using the operator identity $(AB)^{-1} = B^{-1}A^{-1}$ the interacting Green's function $G(E)$ may be written in the form, neglecting the dependence on E,

$$G = \frac{Q}{1 - G_0QVQ}G_0 = G_0\frac{Q}{1 - QVQG_0}, \tag{4.70}$$

where the non-interacting Green's function G_0 in the Q-space is given by,

$$G_0 = \frac{Q}{E - H_0}. \tag{4.71}$$

By using $(1-x)^{-1} = 1 + x + x^2 + x^3 + ...$ we may write

$$\frac{1}{1 - QVQG_0} = 1 + QVQG_0 + (QVQG_0)(QVQG_0) + (QVQG_0)(QVQG_0)(QVQG_0) + ..., \tag{4.72}$$

which gives for the interacting Q-space Green's function

$$G = G_0(1 + QVQG_0 + (QVQG_0)(QVQG_0) + (QVQG_0)(QVQG_0)(QVQG_0) + ...), \tag{4.73}$$

which is just the iterated integral equation for $G(E)$,

$$G = G_0 + G_0 QVQG. \tag{4.74}$$

Inserting the iterated Q-space Green's function into the equation for the effective Hamiltonian given in equation (4.68), we get the iterated effective interaction,

$$V_{\text{eff}} = PVP + PVQ\frac{1}{E - H_0}QVP + PVQ\frac{1}{E - H_0}QVQ\frac{1}{E - H_0}QVP + ... \tag{4.75}$$

where we have used the fact the operator Q commutes with H_0, since P and Q are built from the basis which diagonalizes H_0. The effective interaction given in equation (4.75) still depends on the exact energy, which is to be determined. This problem may be removed by invoking a Taylor expansion in E around the unperturbed energies ε_a of the effective interaction, see Refs. [110, 111] for details. In particular it may be shown that only linked diagrams contribute in the expansion, giving the Goldstone linked-cluster expansion Ref. [112]. Due to the cancellation of certain diagrams at each order in the perturbation expansion, it is possible to do partial infinite summations of the effective interaction. One such example of infinite partial summation is the the ladder equation for the effective interaction,

$$V_{\text{eff}} = V + V\frac{Q}{\varepsilon_a - H_0}V_{\text{eff}}. \tag{4.76}$$

Our focus in this subsection is on the single-reference Rayleigh-Schrödinger perturbation expansion for the energy. Single-reference means that only a single model space state is considered, which gives the projection operators

$$P = |\Phi_a\rangle\langle\Phi_a^*|, \;\; Q = \sum_{i\neq a}^{N} |\Phi_i\rangle\langle\Phi_i^*| \tag{4.77}$$

A perturbative treatment of a single model space state, may only be expected to give convergent results as long as the coupling with the Q-space is weak. In Gamow Shell Model applications, it is natural to choose the many-body configuration where all particles are in resonant orbitals as the reference state, $|\Phi_a\rangle = |RRR...\rangle$, and then add perturbations to this state by taking into account all kinds excitations to non-resonant continuum states. However, as shown in Paper II the coupling with configurations where one or two particles are in non-resonant continuum orbits may not be considered weak in most cases. By projecting the secular equation for the P-space state onto the single model space state Φ_a gives the standard Brillouin-Wigner perturbation expansion for the energy,

$$\begin{aligned} E = \varepsilon_a + \langle\Phi_a^*|PVP + PVQ\frac{1}{E - H_0}QVP + \\ PVQ\frac{1}{E - H_0}QVQ\frac{1}{E - H_0}QVP + ...|\Phi_a\rangle. \end{aligned} \tag{4.78}$$

In the Brillouin-Wigner perturbation expansion the exact energy in which we wish to determine appears from second order and to infinity in the energy denominators $E - H_0$.

Equation (4.78) may be rewritten in such a way that only unperturbed energies appear in the denominators, giving the Rayleigh-Schrödinger perturbation expansion. Writing the energy denominator in the form,

$$E - H_0 = \Delta E + \varepsilon_a - H_0$$

where ΔE is the energy shift we wish to determine, we obtain the following expression,

$$\frac{1}{E - H_0} = \frac{1}{\varepsilon_a - H_0}\left(1 + \frac{\Delta E}{\varepsilon_a - H_0}\right)^{-1} = \frac{1}{a}\left(1 - \frac{\Delta E}{a} + \left(\frac{\Delta E}{a}\right)^2 - + ...\right), \tag{4.79}$$

where we have defined $a = \varepsilon_a - H_0$. Inserting equation (4.79) into equation (4.78) we get the following equation for the energy shift ΔE,

$$\begin{aligned}\Delta E = \langle \Phi_a^* | PVP + PVQ\frac{1}{a}\left(1 - \frac{\Delta E}{a} + \left(\frac{\Delta E}{a}\right)^2 - + ...\right) QVP + \\ PVQ\frac{1}{a}\left(1 - \frac{\Delta E}{a} + \left(\frac{\Delta E}{a}\right)^2 - + ...\right) QVQ \times \\ \frac{1}{a}\left(1 - \frac{\Delta E}{a} + \left(\frac{\Delta E}{a}\right)^2 - + ...\right) QVP + ... | \Phi_a \rangle.\end{aligned} \tag{4.80}$$

Inserting the expression for ΔE back into itself we get order by order correction to the energy by sorting the different powers in V. It may be shown [113] that the n'th term in the Rayleigh-Schrödinger perturbation expansion for the energy is given by the expansion,

$$E_n = \langle V S_{n-1} \rangle - \sum_{m=1}^{n-1} E_m \langle S_{n-m} \rangle, \tag{4.81}$$

where

$$S_n = \frac{Q}{a} V S_{n-1} - \frac{Q}{a} \sum_{m=1}^{n-1} E_m S_{n-m}, \;\; S_0 = 1. \tag{4.82}$$

Here we have introduced the notation $\langle V \rangle = \langle \Phi_a^* | V | \Phi_a \rangle$. By further introducing the quantity $\mathcal{U} = V - \langle V \rangle$, the perturbation expansion up through fifth order may easily shown to be,

$$\begin{aligned} E_0 &= \varepsilon_a = \langle H_0 \rangle, \\ E_1 &= \langle V \rangle, \\ E_2 &= \left\langle V \frac{Q}{a} V \right\rangle, \\ E_3 &= \left\langle V \frac{Q}{a} \mathcal{U} \frac{Q}{a} V \right\rangle, \end{aligned} \tag{4.83}$$

$$
\begin{aligned}
E_4 &= \left\langle V\frac{Q}{a}\left[u\frac{Q}{a}u - \left\langle u\frac{Q}{a}u\right\rangle\right]\frac{Q}{a}V\right\rangle, \\
E_5 &= \left\langle V\frac{Q}{a}\left[u\frac{Q}{a}u\frac{Q}{a}u - \left\langle u\frac{Q}{a}u\frac{Q}{a}u\right\rangle - u\frac{Q}{a}\left\langle u\frac{Q}{a}u\right\rangle - \left\langle u\frac{Q}{a}u\right\rangle\frac{Q}{a}u\right]\frac{Q}{a}V\right\rangle.
\end{aligned}
$$

Here all matrix elements of the form,

$$\left\langle \frac{Q}{a} \text{ or } \frac{Q}{a}\right\rangle = 0. \tag{4.84}$$

Since the model space state Φ_a is orthogonal to all states in the complement space Q. The exact energy may then be written as a Taylor series in the pertubation λ, which for $lambda = 1$ gives the desired result,

$$E = \sum_{n=0}^{\infty} E_n\lambda^n = E_0 + E_1\lambda + E_2\lambda^2 + ... \tag{4.85}$$

A more general and effective approximation which generally gives a more rapid convergence to the exact energy is the Padé approximation [7]. The Pade approximant $E^{[N,M]}$ to the exact energy E is given by the rational fractional expression,

$$E^{[N,M]}(\lambda) = \frac{P_N(\lambda)}{Q_M(\lambda)}, \tag{4.86}$$

where P_n and Q_M are polynomials of degrees N and M respectively. The polynomials P_N and Q_M may be obtained from the coefficients E_i of the Taylor expansion of the exact energy in equation (4.85) by the following formulas,

$$P_N(\lambda) = \begin{vmatrix} E_{N-M+1} & E_{N-M+2} & \dots & E_{N+1} \\ \vdots & \vdots & \vdots & \vdots \\ E_N & E_{N+1} & \dots & E_{N+M} \\ \sum_{j=M}^{N} E_{j-M}\lambda^j & \sum_{j=M-1}^{N} E_{j-M+1}\lambda^j & \dots & \dots \sum_{j=0}^{N} E_j\lambda^j \end{vmatrix} \tag{4.87}$$

and

$$Q_M(\lambda) = \begin{vmatrix} E_{N-M+1} & E_{N-M+2} & \dots & E_{N+1} \\ \vdots & \vdots & \vdots & \vdots \\ E_N & E_{N+1} & \dots & E_{N+M} \\ \lambda^M & \lambda^{M-1} & \dots & 1 \end{vmatrix} \tag{4.88}$$

The first few Pade approximants take the following form,

$$
\begin{aligned}
E^{[0,0]} &= E_0 \\
E^{[1,1]} &= \frac{E_0E_1 + (E_1^2 - E_0E_2)\lambda}{E_1 - E_2\lambda} \\
E^{[2,1]} &= \frac{E_0E_2 + (E_1E_2 - E_0E_3)\lambda + (E_2^2 - E_1E_3)\lambda^2}{E_2 - E_3\lambda}
\end{aligned}
$$

$$
\begin{aligned}
E^{[1,2]} &= \frac{(E_0^2E_2 - E_0E_1^2) + (2E_0E_1E_2 - E_0^2E_3 - E_1^3)\lambda}{(E_0E_2 - E_1^2) + (E_1E_2 - E_0E_3)\lambda + (E_1E_3 - E_2^2)\lambda^2} \\
E_{[2,2]} &= \big[(E_0E_1E_3 - E_0E_2^2) + (E_1^2E_3 + E_0E_2E_3 - E_0E_2E_3 - E_0E_1E_4 - E_1E_2^2)\lambda \\
&+ (E_1E_2E_3 + E_0E_2E_4 + E_1E_2E_3 - E_1^2E_4 - E_2^3 - E_0E_3^2)\lambda^2\big] / \\
&\quad (E_1E_3 - E_2^2) + (E_2E_3 - E_1E_4)\lambda + (E_2E_4 - E_3^2)\lambda^2
\end{aligned}
\tag{4.89}
$$

In order to clarify the use of single-reference perturbation theory in Gamow Shell Model calculations, we consider the convergence of the Pade approximant $E^{[2,1]}$ versus the standard energy expansion up through third order in energy, to the 0^+ ground state of ^{6}He as the residual nucleon-nucleon interaction is gradually turned on. ^{6}He is here modeled by an inert ^{4}He core with two valence nucleons moving in 24 lj orbits $p_{3/2}$, where one is a single particle resonant orbit and the remaining 23 orbits are in the non-resonant continuum. See Paper II for further details on the single particle potential and the residual nucleon-nucleon interaction. The two-particle single model space state is then the configuration where both particles are in resonant orbits, $|RR\rangle$, and the complement space is then all configurations of the type $|RC\rangle, |CC\rangle$, where C labels a non-resonant continuum orbit. Figure 4.6 gives

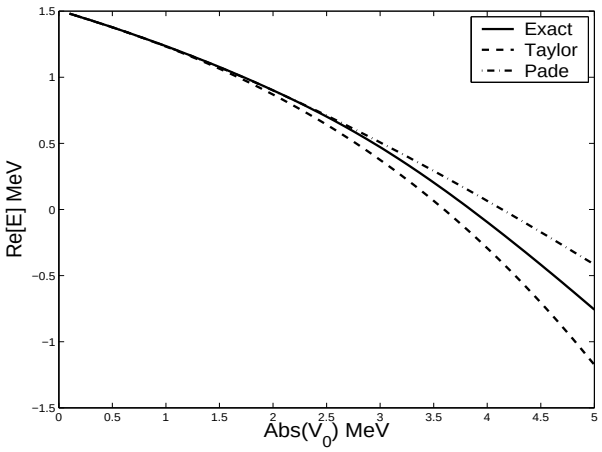

Figure 4.6: Plot of real part of 0^+ energy in ^{6}He, for increasing interaction strength V_0. Solid line gives the exact energy, the dashed line gives the series expansion of the energy up through third order and the dashed-dotted line gives the $E^{[2,1]}$ Pade approximation to the energy.

the real part of the 0^+ energy, while figure 4.7 gives the corresponding imaginary part of the energy, as the interaction strength is gradually turned on. In both cases it is seen that the Pade approximant $E^{[2,1]}$ gives a better fit to the exact energy, than the Taylor expansion up through third order. In both cases the single-reference perturbation theory fails to give satisfactory result for the energy when the interaction strength is that of Paper II, i.e. $V_0 = -5.315$MeV. It is also seen that single-reference perturbation theory gives convergent results in this specific case only for interaction strengths less than 1MeV. One

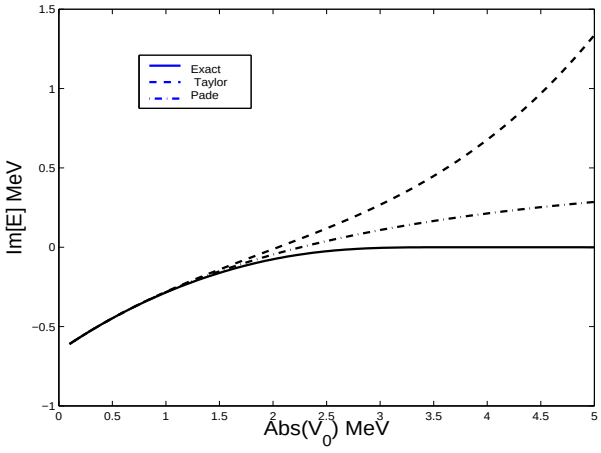

Figure 4.7: Plot of imaginary part of 0^+ energy in ^{6}He, for increasing interaction strength V_0. Solid line gives the exact energy, the dashed line gives the series expansion of the energy up through third order and the dashed-dotted line gives the $E^{[2,1]}$ Pade approximation to the energy.

may therefore conclude that single-reference perturbation theory, is not suitable in Gamow Shell Model calculations, since the coupling with the complement space is too strong, for being treated perturbatively.

4.4.2 Multi-reference perturbation theory.

In this section we outline the non-Hermitian multi-reference perturbation theory. We proceed in similar manner as in the previous section, and construct a N-body model space P and a complement (orthogonal) space Q according to equation (4.67). The choice of P should be dictacted by some intuition on which single particle configurations play the dominant part in the fully correlated many-body wave function. Having constructed P and Q the many-body wave function and the corresponding Hamiltonian may be represented in this basis. The Hamiltonian may subsequently be partioned into two parts according to,

$$\begin{pmatrix} PHP & PHQ \\ QHP & QHQ \end{pmatrix} = \begin{pmatrix} H^{PP} & 0 \\ 0 & H^{QQ} \end{pmatrix} + \begin{pmatrix} 0 & H^{PQ} \\ H^{QP} & \tilde{H}^{QQ} \end{pmatrix} = H_0 + H_1. \tag{4.90}$$

Here D^{QQ} is the diagonal part and $\tilde{H}^{QQ}$ the off-diagonal part of QHQ respectively. Written in this form, it is seen that H^0 defines the unperturbed part while H^1 gives the perturbations to H^0. Provided H^0 is non-singular, the model space block PHP may be decoupled by constructing a complex orthogonal matrix $\mathbf{C}$ which diagonalizes H^0, i.e. $\mathbf{C}H^0\mathbf{C}^T = Diag(E_1^0, E_2^0, ..., E_N^0)$. Since H^0 is a block diagonal matrix, the matrix $\mathbf{C}$ is

given in the form

$$\mathbf{C} = \begin{bmatrix} \chi & \mathbf{0} \\ \mathbf{0} & \mathbf{1} \end{bmatrix} \tag{4.91}$$

A more convienient many-body basis which decouples (diagonalizes) the reference space is then given by

$$\Upsilon_i = \sum_{j=1}^{N} C_{i,j}\Phi_j = \begin{cases} \sum_{j=1}^{N_P} \chi_{i,j}\Phi_j, & i = 1, N_P \\ \Phi_i, & i = N_P + 1, N \end{cases} \tag{4.92}$$

and they are solutions of the eigenvalue problem,

$$H_0|\Upsilon_i\rangle = \tilde{\varepsilon}_i|\Upsilon_i\rangle. \tag{4.93}$$

We assume here that the states $|\Upsilon_i\rangle$ are normalized to unity. The complex orthogonal matrix χ which span the reference space P, defines our new set of reference states. The states Υ_i, $i = 1, ..., N_P$ span the same space as the original P-space states Φ_i, but they have been reoriented in space so that they diagonalize PHP. As a measure of how well the zeroth order wave function $\Upsilon^J_{i=\mathrm{res}}$ resembles the exact wave function, one can calculate the complex variance σ_c^2 see Refs. [14, 114],

$$\begin{aligned} \sigma_c^2 &= \langle \Upsilon_i^{J*}| \left(H - E_i^0\right)^2 |\Upsilon_i^J\rangle \\ &= \chi_i^T H^{PQ} H^{QP} \chi_i, \end{aligned} \tag{4.94}$$

where $i = \mathrm{res}$ and χ_i labels the i'th column of the $N_P \times N_P$ matrix χ. In Ref. [114] it was proved that the complex variance σ_c provides an upper bound to the exact resonance energy,

$$\left|E_{\mathrm{res}}^{\mathrm{exact}} - E_{\mathrm{res}}^0\right| \leq |\sigma_c| \tag{4.95}$$

Having constructed a new many-body anti-symmetric basis, we develop a perturbation expansion in terms of these eigenvectors of the reference space. Derivation of the Rayleigh - Schrödinger perturbation expansion for the exact energy and wave function follows in exactly the same manner as in previous section. We wish to study how a single reference state Υ_i changes order by order in the Rayleigh-Schrödinger perturbation expansion by adding the perturbation matrix H^1. So the P-space is a single state and the orthogonal complement is the remaining states

$$\tilde{P} = |\Upsilon_a\rangle\langle\Upsilon_a^*|, \;\; \tilde{Q} = \sum_{i\neq a} |\Upsilon_i\rangle\langle\Upsilon_i^*|. \tag{4.96}$$

Consider the 1'st order correction to the energy for any state Υ_p in the model space, i.e.

$$E_1(p) = \langle\Upsilon_p^*|H_1|\Upsilon_p\rangle = \begin{pmatrix} \chi_p^{\mathrm{T}} & 0 \end{pmatrix} \begin{pmatrix} 0 & H^{PQ} \\ H^{QP} & H^{QQ} \end{pmatrix} \begin{pmatrix} \chi_p \\ 0 \end{pmatrix} = 0, \tag{4.97}$$

which gives zero contribution. This is an extremely nice feature, since all expansion terms where 1'st order matrix elements E_1 appear in a product with more complicated terms

give zero contribution. The 1'st order correction to the energy may be said to have been incorporated into the zeroth order energy $\tilde{\varepsilon}_i$. The second order correction to an unperturbed energy $\tilde{\varepsilon}_p$ becomes

$$E_2(p) = \sum_{a\neq p}^{N} \frac{\langle \Upsilon_p^*|H_1|\Upsilon_a\rangle\langle\Upsilon_a^*|H_1|\Upsilon_p\rangle}{\tilde{\varepsilon}_p - \tilde{\varepsilon}_a} \tag{4.98}$$

from the structure of the perturbation matrix H^1 is easily seen that the sum over Q-space states is restricted to $a > N_P$ by taken into the account $\langle\Upsilon_i^*|H_1|\Upsilon_j\rangle = 0,\ \ i,j \leq N_P$. This illustrates that many excitations from the P- into the Q-space have already been taken into account in the zeroth order wave function. The second order energy term then becomes,

$$\begin{aligned} E_2(p) &= \sum_{a>N_P}^{N} \frac{\langle \Upsilon_p^*|H_1|\Upsilon_a\rangle\langle\Upsilon_a^*|H_1|\Upsilon_p\rangle}{\tilde{\varepsilon}_p - \tilde{\varepsilon}_a} = \sum_{i,j\leq N_P}\sum_{a>N_P} \frac{\chi_{p,i}\langle\Phi_i^*|H_1|\Phi_a\rangle\langle\Phi_a^*|H_1|\Phi_j\rangle\chi_{j,p}}{\tilde{\varepsilon}_p - \tilde{\varepsilon}_a} \\ &= \sum_{i,j\leq N_P}\sum_{a>N_P} \frac{\chi_{p,i}H_{i,a}^{PQ}H_{a,j}^{QP}\chi_{j,p}}{\tilde{\varepsilon}_p - D_{a,a}^{QQ}}. \end{aligned} \tag{4.99}$$

and the third order term becomes

$$E_3(p) = \sum_{\substack{a,b>N_P \\ a\neq b}}^{N} \frac{\langle \Upsilon_p^*|H_1|\Upsilon_a\rangle\langle\Upsilon_b^*|H_1|\Upsilon_p\rangle}{(\tilde{\varepsilon}_p - \tilde{\varepsilon}_a)(\tilde{\varepsilon}_p - \tilde{\varepsilon}_b)} = \sum_{i,j\leq N_P}\sum_{\substack{a,b>N_P \\ a\neq b}} \frac{\chi_{p,i}H_{i,a}^{PQ}\tilde{H}_{a,b}^{QQ}H_{b,j}^{QP}\chi_{j,p}}{(\tilde{\varepsilon}_p - D_{a,a}^{QQ})(\tilde{\varepsilon}_p - D_{b,b}^{QQ})}. \tag{4.100}$$

Higher order terms may easily calculated from the Rayleigh-Schrödinger perturbation expansion given in equation(4.84). Summarizing we get through fourth order,

$$\begin{aligned} E_0(p) &= \langle\Upsilon_p^*|H^0|\Upsilon_p\rangle = \tilde{\varepsilon}_p, \\ E_1(p) &= \langle\Upsilon_p^*|H^1|\Upsilon_p\rangle = 0, \\ E_2(p) &= \langle\Upsilon_p^*|H^1\frac{Q}{\tilde{\varepsilon}_p - H^0}H^1|\Upsilon_p\rangle, \\ E_3(p) &= \langle\Upsilon_p^*|H^1\frac{Q}{\tilde{\varepsilon}_p - H^0}H^1\frac{Q}{\tilde{\varepsilon}_p - H^0}H^1|\Upsilon_p\rangle, \\ E_4(p) &= \langle\Upsilon_p^*|H^1\frac{Q}{\tilde{\varepsilon}_p - H^0}H^1\frac{Q}{\tilde{\varepsilon}_p - H^0}H^1\frac{Q}{\tilde{\varepsilon}_p - H^0}H^1|\Upsilon_p\rangle \\ &- E_2(p)\langle\Upsilon_p^*|H^1\frac{Q}{(\tilde{\varepsilon}_p - H^0)^2}H^1|\Upsilon_p\rangle. \end{aligned} \tag{4.101}$$

Where $Q = \sum_{i>N_P}|\Upsilon_i\rangle\langle\Upsilon_i^*|$.

The above perturbation series is a theory which treats one-state-at-a-time, this theory differs from the standard multi-reference perturbation theory which diagonalizes an effective Hamiltonian and solves for all states in the model space simultaneously. The above perturbation theory sets no restrictions on the choice of many-body reference space, and can in principle be chosen by any suitable selection criterion. The theory also allows for

a freely variation of the reference space size, so that it is possible to achieve satisfactory convergent results at a given order in the perturbation series. If the coupling between the reference states is turned off, the perturbation series reduces to the standard single-reference Rayleigh-Schrödinger perturbation theory discussed in the previous section.

In the application of the above multi-reference perturbation theory method to Gamow Shell Model calculations, a reference space which takes into account most of the correlations has to be chosen. Further the size of the P-space should be small enough to allow for a direct diagonalization in order to obtain the reference states $\Upsilon_i, i = 1, ..., N_P$. The most important configuration in a many-body resonance may be expected to be the pure resonance pole configuration $|RRR...\rangle$. We wish then to generate correlations on this unperturbed many-body resonance state, in order to obtain the fully correlated many-body resonance. The correlations are generated by virtual excitations of one or several particles occupying the single particle resonant orbitals to non-resonant continuum orbitals, induced by the residual nucleon-nucleon interaction. A viable starting point for Gamow Shell Model applications, would be to construct a reference space P conisisting of a set of low lying many-body unperturbed states where at least one particle is in a single particle resonance orbital. The orthogonal complement space Q consits then of the remaining states. In Paper II where the above perturbation theory where applied to the unbound nucleus ^{7}He, the three-particle model space, and corresponding complement space, where defined by

$$P \equiv \left\{ \begin{array}{c} |RRR\rangle, |RRC\rangle, |RCC\rangle, \\ \mathrm{Re}(e_a + e_b + e_c) < E_{\mathrm{cut}}, \\ \mathrm{Im}(e_a + e_b + e_c) > -E_{\mathrm{cut}} \end{array} \right\} \quad Q = 1 - P, \tag{4.102}$$

here the P space is given by configurations where at most two particles move in continuum orbits. In addition, P is further defined by a rectangular cutoff in the complex energy plane. This cutoff in energy is motivated by an assumption that three-particle configurations high in energy play a minor role on the formation of low-lying resonances. Figure 4.8 gives a plot of the $J^\pi = 3/2^-$ unperturbed (non-interacting) three-particle spectrum of ^{7}He used in Paper II. At most two particles move in complex continuum orbits, and three different cut-offs in energies and corresponding model spaces are shown. Note that only $p_{3/2}$ single particle orbitals are taken into account. Having constructed a suitable model space P, a full diagonalization is performed. We wish to study the effect of adding the perturbation H^1 to the new many-body resonance wave function. Since the above theory is one-state-at-a-time theory, the zeroth order resonance $\Upsilon(i = res)$ has to be identified from the zeroth order energy spectrum. This identification may may be done by determining which state Υ_i, $i = 1, ..., N_P$ has the largest overlap with the pure pole configuration $|\Phi_{\mathrm{res}}\rangle = |RRR...\rangle$,

$$\mathrm{Max}\left\{ \left| \langle \tilde{\Phi}(\mathrm{res}) | \Upsilon_i \rangle \right| \right\}_{i=1}^{N_P} = \mathrm{Max}\left\{ |\chi_{i,j=\mathrm{res}}| \right\}_{i=1}^{N_P} \tag{4.103}$$

To make sure the "correct" physical state is picked out, the complex energy trajectories as the interaction is gradually turned on may be studied.

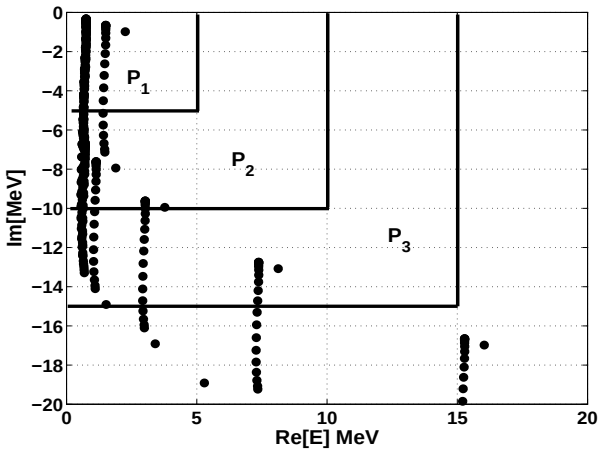

Figure 4.8: Three choices of the model space used in the multi-configuration perturbation method. The three-particle model space states are constructed such that at most two particles move in the non-resonant continuum.

4.5 Effective interaction scheme for Gamow shell model calculations

In the previous sections it was shown that the Lee-Suzuki similarity transformation and the multi-reference perturbation method may be used in the Gamow shell model in order to account for the most important correlations of for example a multi-particle resonance. Although the dimensionality of the problem derived either from the similarity transformation method or the multi-reference perturbation method was significantly reduced compared to the full problem, the dimensionality may still be a severe problem when dealing with more than three particles in a big valence space.

The drawback of the multi-reference perturbation method is that one has to store extremely large matrices H^{QQ} if one wishes to go beyond second order in perturbation theory. In the similarity transformation method one does not have to deal with H^{QQ}, as couplings with the Q-space states have been dealt with, in practical calculations at least at the two-body level. Going to systems with larger degrees of freedom, the P-space may nevertheless, at the converged level, be too large for our brute force diagonalization approach.

The aim of this section is to propose an effective interaction and perturbation theory scheme for the Gamow shell model. This approach combines the similarity transformation method and the multi-reference perturbation method, so that hopefully multi-particle resonances where several particles move in large valence spaces, may be calculated without a diagonalization in the full space. Our algorithm is as follows

1. Choose an optimal set of n_{sp} single-particle orbits, which in turn defines two-body P_{2p} and many-body spaces. In our case these single-particle orbits are defined by

selected states in ^{5}He.

2. Construct a two-particle effective interaction by the Lee-Suzuki similarity transformation method within the two-particle model space P_{2p}. Such diagonalizations can be done for very large spaces, see for example Refs. [36, 37, 38, 39].

3. The next step is to divide the multi-particle model space P in two smaller spaces P' and Q', where $P = P' + Q'$ and $N_P = N_{P'} + N_{Q'}$. The choice of P' should be dictated by our knowledge of the physical system. As an example, one may consider those single-particle configurations within the $P-$space that play the dominant role in the formation of the multi-particle resonance. The number $N_P = N_{P'} + N_{Q'}$ represents the total number of many-body configurations within the $P-$space.

4. Now that we have divided the P-space in two sub-spaces P' and Q', we use for example the multi-reference perturbation method to account for excitations from the $P'-$ space to the $Q'-$ space to obtain energy corrections to a specific order. Increase the size of the $P'-$space until convergence is obtained. In the case $N_{P'} = N_P$ and $N_{Q'} = N_P - N_{P'} = 0$ the multi-reference perturbation expansion terminates at zeroth order, and corresponds to a full diagonalization within the $P-$space. Another option is to use for example the coupled cluster method as exposed in Refs. [44, 45].

5. Start from top again with a larger set of single-particle orbits, and continue until a convergence criterion is reached.

We illustrate these various choices of model spaces in the following two figures. figure 4.9 defines our model space for the Lee-Suzuki similarity transformation at the two-body level. This corresponds to steps one and two in the above algorithm. The set of single-particle orbits defines the last single-particle orbit in the model space n_{sp}. Note that we could have chosen a model space defined by a cut in energy, as done by the No-Core collaboration, see for example Refs. [36, 37, 38, 39]. These examples serve just to illustrate the algorithm. Figure 4.10 demonstrates again a possible division of the three- and many particle space into the full model space P and a smaller space P'. Again, this figure serves only the purpose of illustrating the method. In our actual calculations we define the smaller space P' via an energy cut in the real and imaginary eigenvalues and selected many-body configurations.

In summary, defining a set of single-particle orbits in order to construct the two-body and many-body model spaces, we obtain first an effective two-body interaction in the space P_{2p} by performing the Lee-Suzuki [98, 99, 100, 101] transformation. This interaction and the pertinent single-particle orbits are then used to define a large many-body space. It is therefore of interest to see if we can reduce this dimensionality through the definition of smaller spaces and perturbative corrections.

4.6 Inclusion of realistic nucleon-nucleon interactions in Gamow shell model calculations

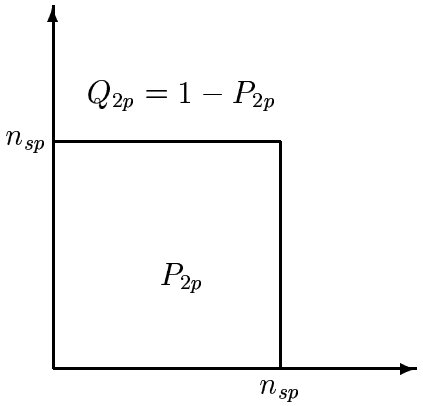

Figure 4.9: Possible definition of the two-body exclusion operator $Q_{2p} = 1 - P_{2p}$ used to compute the Lee-Suzuki similarity transformation and its effective interaction at the two-body level. The border of the model space is defined by the last single-particle orbit n_{sp}.

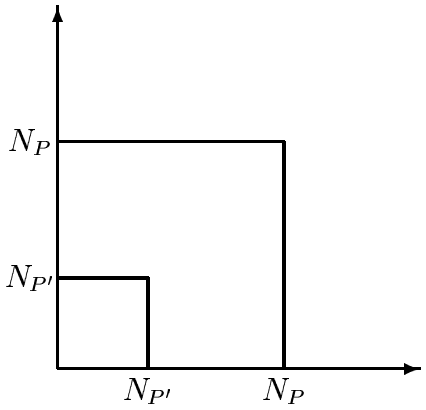

Figure 4.10: Possible definition of many-body space N_P and reduced space N'_P.

Chapter 5

Paper1

5.1 Introduction to Paper I

Paper I discusses how the momentum space Schrödinger equation may be analytically continued to the second energy sheet. The method of anlytical continuation is based on deforming (distoting) the integration contour, and this method is commonly known as the Contour Deformation Method (CDM). The rules for analytical continuation of integral equations are discussed, and as an example the Schrödinger equation for the Malfliet-Tjon potential, which is a nucleon-nucleon potential consisting of Yukawa terms, is analytically continued to the second Riemann sheet. It is found, by choosing a suitable deformed contour (rotation+translation), that the analytical structure of the Malfliet-Tjon potential allows for a continuation into the third quadrant of the complex k-plane, and consequently the Contour Deformation Method allows for a study of virtual states as well as decaying resonances. Further, CDM is an alternative approach to the full solution of the off-shell scattering amplitude. In the case of potentials consisting of Yukawa terms, choosing a rotated+translated contour which avoid the singularities of the potential, allows for a complete solution of the t-matrix in a large momentum range. Not only does CDM give us information of the complete pole structure of the scattering matrix but also the scattering amplitude is obtainable by expanding the Green's function in a complete set of Berggren states. Expanding the Green's function in a complete set of states, consisting of bound, resonant and non-resonant continuum states allows for a separate study of the resonant contributions to the scattering amplitude. Disentangling the resonant behaviour of the scattering amplitude from the smooth continuum backrground is gives interesting insights, since the most interesting process taking place in the continuum is the production of resonance phenomena. Finally CDM is applied to the CD-Bonn interaction, which is a realisitic nucleon-nucleon potential, and virtual states in the isospin triplet channel $^1S_0$ are solved for.

5.2 *The contour deformation method in momentum space, applied to subatomic physics*

G. Hagen, J. S. Vaagen and M. Hjorth-Jensen

J. Phys. A: Math. Gen., **37**, 8991 (2004).

Chapter 6

Paper2

6.1 Introduction to Paper 2

Paper II deals with the recently developed Gamow Shell Model. Constructing a single particle Berggren basis in momentum space, generated from the Sack-Biedenharn and Breit (SBB) potential for ^{5}He, a complete anti-symmetric two- and three particle basis is constructed. Limiting the discussion to $p_{1/2}$ and $p_{3/2}$ single particle motion, the energy spectrum of ^{6}He and ^{7}He is solved for, using a phenomenological nucleon-nucleon interaction of a Gaussian type. In using CDM in constructing the single particle basis, it is shown that convergence of the energy spectrum of ^{6}He with increasing number of non-resonant continuum orbitals is rather fast. However the dimension of the many-body space for nuclei with a larger number of valence particles increases extemely fast, and direct diagonalization methods are no longer possible. This paper deals primarily with this *dimensionality* problem. It is shown how the Lee-Suzuki similarity transformation method may be generalized to complex interactions. Constructing a two-body effective interaction in a reduced space, which exactly reproduce a limited set of eigen values of the full Hamiltonian, is used in the calculation of the resonant energy spectrum of ^{7}He. It is shown that the convergence using the similarity transformed interaction is appreciably faster than compared with the bare interaction as the model space is increased. Further, we discuss how a Multi-Reference-Perturbation-Theory-Method (MRPTM), which differs from standard MRPTM in that it is a one-state-at-a-time perturbation theory, may be applied to Gamow-Shell-Model calculations. It is shown that to second order, MRPTM gives satisfactory converged results for ^{7}He, and reducing the dimension of the full problem to $8-10\%$. Finally an effective interaction scheme for the Gamow-Shell-Model is discussed, which combines the Lee-Suzuki similarity transformation method with the one-state-at-a-time MRPTM. And converged results for the resonant spectrum of ^{7}He is shown using a model space consisting of both $p_{1/2}$ and $p_{3/2}$ single particle orbitals. The dimension is in the most severe case, of the state $J^\pi = 3/2^-$, reduced from ≈ 40000 to ≈ 1600. This is a promising result, and which may allow for Gamow-Shell-Model studies of nuclei consisting of a larger number of valence particles moving in a large valence space.

6.2 *Effective Interaction Techniques for the Gamow Shell Model*

G. Hagen, M. Hjorth-Jensen and J. S. Vaagen

Accepted in Phys. Rev. C

Chapter 7

Summary and perspectives

The main purpose of this thesis has been to study and develop methods suitable for study of resonance phenomena in nuclear and subatomic physics. Our emphasis has been on the momentum space formulation of the Schrödinger equation. It has been shown, starting with the integral formulation of the Schrödinger equation, that an efficient way of obtaining a complete set of states including bound-, anti-bound and resonant states is through the Contour Deformation Method. The strength of the Contour Deformation Method has been illustrated by studying a wide range of different cases in subatomic physics where resonance phenomena appear. These applications ranges from the case of a single particle moving in a spherically symmetric field to the case of strong deformations of the field. Further, it has been studied how resonances may be solved for in complex potentials which models absorbtive and emittive processes, using the Contour Deformation Method. The results obtained in these specific applications, strongly favour the Contour Deformation Method in comparison with other methods such as complex coordinate scaling and analytic continuation in the coupling strength. The most appealing feature of CDM is that, not only does it give accurate results for resonances and anti-bound states, but in addition it provides us with a complete set of states which may be used in many different eigenfunction expansions. The only limitation of CDM is that the analytic structure of the potential has to be known, since the choice of contour has to be dictated by the singularity structure of the potential. The revival and study of CDM applied to nuclear physics, may be considered the main issue of the first part of this thesis, and is also the topic of Paper I.

In the second part of this thesis, the focus is directed towards the issue of how resonance phenomena may be understood in nuclei, where several valence particles are present. The newly developed Gamow Shell Model is a promising approach in the study of loosely bound and unbound nuclei along the drip lines. The main ingredient in the Gamow Shell Model is the construction of a complete set of many-body Slater determinants built up from a single particle Berggren basis. It has been shown in this work that a viable starting point in Gamow Shell Model studies is to obtain a single particle basis by the Contour Deformation Method in momentum space. The results displayed in Paper II, indicate rapid convergence for many-body resonances using a single particle basis in momentum space.

The challenge for present and future Gamow Shell Model calculations is how to deal

with the extreme growth of the number of Slater determinants in the many-body expansion basis. This topic was the main issue of the second part of the thesis. The basic idea was to modify standard effective interaction theory and many-body perturbation theory, so that that their range of applicability encompass the complex interactions and matrices which follows from the generalization of the standard Shell Model to the complex energy plane. Further, the extreme dimension of the Shell Model Hamiltonian matrix requires development of large-scale matrix diagonalization routines which can handle both real and complex matrices. In this thesis it was shown how the Lanczos iteration method may be generalized to complex energy matrices. It was further shown, that by choosing a reasonable initial Lanczos vector for the 0th order multi-particle resonance, the multi-particle resonance may be unambigously picked out from the set of states obtained from diagonalization at each iteration, by identifying the state which has the largest overlap with the 0th order Lanczos vector.

Another important result was the generalization of the Lee-Suzuki similarity transformation to include complex interactions. The emphasis was on the derivation of effective interactions for for loosely bound or unbound nuclei which has a strong coupling with the continuum. We demonstrated by a numerical study in Paper II, that the construction of an effective two-body interaction based on the Lee-Suzuki similarity transformation method, leads to a drastic reduction of the Gamow shell-model dimensionality for more than two particles. Furthermore it was shown in Paper II that the one-state-at-a-time Multi-Reference-Perturbation-Theory combined with the construction of an effective two-body interaction, reduces drastically the dimension of Shell Model space. This result is very promising when extending the Gamow shell model to applications in structure calculations of heavier dripline nuclei, with a larger number of valence particles moving in a large valence space.

With further progress in computational power one may hope that *ab intio* calculations of light and medium size nuclei within the Berggren representation may become possible in the near future. Coupled-Cluster techniques has proven to be a promising method for calculations of medium size nuclei. Very recently [44, 45, 46], converged Coupled-Cluster results for the ground- and first excited state of ^{16}O where reported, using modern nucleon-nucleon interactions derived from effective field-theory. A promising way of approach would be to generalize the Coupled-Cluster method to complex interactions, and at the first stage see how resonant structures are formed in light nuclei starting from an *ab initio* approach. As this thesis only deals with a phenomenological residual nucleon-nucleon interaction, the next step is to include a realistic and microscopically derived effective nucleon-nucleon interaction in Gamow Shell Model calculations. Constructing a single particle Berggren basis by solving the Hartree-Fock equation self-consistently with an effective nucleon-nucleon interaction constructed from the G-matrix approach or with the recently developed low-momentum nucleon-nucleon interaction ($V_{\mathrm{low-k}}$), and then calculating matrix elements of the effective interaction in this basis is a future challenge for the Gamow Shell Model. How single particle resonances are formed from the underlying nucleon-nucleon interaction is a very interesting study in itself, and work along these lines are in progress using a renormalized nucleon-nucleon interaction of the $V_{\mathrm{low-k}}$ type, generalized to the complex

k-plane.

Bibliography

[1] I. Tanihata, H. Hamagaki, O. Hashimoto, Y. Shida, and N. Yoshikawa. Measurements of interaction cross sections and nuclear radii in the light p-shell region. *Phys. Rev. Lett.*, 55:2676, 1985. pages 3

[2] V. Zhukov, B.V. Danilin, D.V. Fedorov, J.M. Bang, I.J. Thompson, and J.S. Vaagen. Bound state properties of borromean halo nuclei: ^{6}he and ^{11}li. *Phys. Rep.*, 231:151, 1993. pages 4

[3] B. Jonson. Light dripline nuclei. *Phys. Rep.*, 389:1, 2004. pages 5

[4] G. A. Gamow. unknown. *Zs. f. Physik*, 51:204, 1928. pages 6

[5] G. Breit and E. P. Wigner. Capture of slow neutrons. *Phys. Rev.*, 49:519, 1936. pages 6

[6] R. G. Newton. *Scattering Theory of Waves and Particles.* Springer-Verlag, New York, 1982. pages 7, 15, 16, 17, 24, 38, 39

[7] V. I. Kukulin, V. M. Krasnopol'sky, and J. Horáček. *Theory of Resonances.* Kluwer Academic publishers, Amsterdam, 1989. pages 7, 38, 52, 56, 59, 94

[8] A. G. Sitenko. *Lectures in scattering theory.* Pergamon Press Ltd. Oxford, 1971. pages 7, 15, 16, 18

[9] Y. B. Zel'dovich. *JETP (Sov. Phys.)*, 39:776, 1960. pages 7, 8, 21

[10] J. Aguilar and J. M. Combes. Class of analytic perturbations for one-body schrödinger hamiltonians. *Commun. Math. Phys.*, 22:265, 1971. pages 7

[11] E. Balslev and J. M. Combes. Spectral properties of many-body schrödinger operators with dilatation-analytic interactions. *Commun. Math. Phys.*, 22:280, 1971. pages 7

[12] N. Moiseyev and C.T. Corcoran. Autoionizing states of H_2 and using the complex scaling method. *Phys. Rev. A*, 20:814, 1979. pages 7

[13] N. Moiseyev. Resonance states by the generalized complex variational method. *Mol. Phys.*, 47:582, 1982. pages 7

[14] N. Moiseyev. Quantum theory of resonances: Calculating energies, widths and cross-sections by complex scaling. *Phys. Rep.*, 302:211, 1998. pages 7, 24, 39, 97

[15] A. Csoto. Three-body resonances by complex scaling. *Phys. Rev. C*, 49:2244, 1994. pages 7

[16] T. Myo, K. Kato, S. Aoyama, and K. Ikeda. Analysis of ^{6}he coulomb breakup in the complex scaling method. *Phys. Rev. C*, 63:054313, 1998. pages 7

[17] E. Garrido, D. V. Fedorov, and A. S. Jensen. Dipole excited states in ^{11}li with complex scaling. *Nucl. Phys. A*, 708:277, 2002. pages 7

[18] I. Raskinyte. Resonances in few-body systems. *PhD Thesis University of Bergen 2002, unpublished*, 2002. pages 7

[19] S. A. Rakityansky, S. A. Sofianos, and K. Amos. A method for calculating the jost function for analytic potentials. *Il Nuovo Cimento*, 111B, N.3:363, 1996. pages 7

[20] S. A. Sofianos and S. A. Rakityansky. Exact method for locating potential resonances and regge trajectories. *J. Phys. A: Math. Gen.*, 30:3725, 1997. pages 7

[21] S. Aoyama. Theoretical prediction for the ground state of 10he with the method of analytic continuation in the coupling constant. *Phys. Rev. Lett.*, 89:052501, 2002. pages 7

[22] G. Hagen, J. S. Vaagen, and M. Hjorth-Jensen. The contour deformation method in momentum space, applied to subatomic physics. *J. Phys. A: Math. Gen.*, 37:8991, 2004. pages 8, 12

[23] I. R. Afnan. Resonances in few-body systems. *Aust. J. Phys.*, 44:201, 1991. pages 8

[24] D. Brayshaw. Off- and on-shell analyticity of three-particle scattering amplitudes. *Phys. Rev.*, 176:1855, 1968. pages 8

[25] J. Nuttall and H. L. Cohen. Method of complex coordinates for three-body calculations above the breakup threshold. *Phys. Rev.*, 188:1542, 1969. pages 8, 37, 58

[26] A. T. Stelbovics. On the application of contour rotation to three-body amplitudes. *Nucl. Phys. A*, 288:461, 1978. pages 8

[27] W. Glöckle. S-matrix pole trajectory in a three-neutron model. *Phys. Rev. C*, 18:18, 1978. pages 8

[28] T. Berggren. On the use of resonant states in eigenfunction expansions of scattering and reaction amplitudes. *Nucl. Phys. A*, 109:265, 1968. pages 8, 25, 29

[29] B.S. Pudlinger, V.R. Pandharipande, J. Carlson, and R. Wiringa. Quantum monte carlo calculations of A <= 6 nuclei. *Phys. Rev. Lett.*, 74:4396, 1995. pages 9

[30] B. S. Pudlinger, V. R. Pandharipande, J. Carlson, Steven C. Pieper, and R. B. Wiringa. Quantum monte carlo calculations of nuclei with A < 7. *Phys. Rev. C*, 56:1720, 1997. pages 9

[31] R. B. Wiringa, Steven C. Pieper, J. Carlson, and V. R. Pandharipande. Quantum monte carlo calculations of A = 8 nuclei. *Phys. Rev. C*, 62:014001, 2000. pages 9

[32] Steven C. Pieper and R. B. Wiringa. Quantum monte carlo calculations of light nuclei. *Ann. Rev. Nucl. Part. Sci.*, 51:53, 2001. pages 9

[33] Steven C. Pieper, V. R. Pandharipande, R. B. Wiringa, and J. Carlson. Realistic models of pion-exchange three-nucleon interactions. *Phys. Rev. C*, 64:014001, 2001. pages 9

[34] Steven C. Pieper, K. Varga, and R. B. Wiringa. Quantum monte carlo calculations of A = 9, 10 nuclei. *Phys. Rev. C*, 66:044310, 2002. pages 9

[35] Steven C. Pieper, R. B. Wiringa, and J. Carlson. Quantum monte carlo calculations of excited states in A = 6 − −8 nuclei. *nucl-th/0409012*, 2004. pages 9

[36] P. Navrátil and B. R. Barrett. Shell-model calculations for the three-nucleon system. *Phys. Rev. C*, 57:562, 1998. pages 9, 84, 101

[37] P. Navrátil, J. P. Vary, and B. R. Barrett. Properties of ^{12}c in the ab initio nuclear shell model. *Phys. Rev. Lett.*, 84:5728, 2000. pages 9, 84, 101

[38] P. Navrátil, J. P. Vary, and B. R. Barrett. Large-basis ab initio no-core shell model and its application to ^{12}c. *Phys. Rev. C*, 62:054311, 2000. pages 9, 84, 101

[39] P. Navrátil, G. P. Kamuntavicius, and B. R. Barrett. Few-nucleon systems in a translationally invariant harmonic oscillator basis. *Phys. Rev. C*, 61:044001, 2000. pages 9, 84, 101

[40] F. Coester. Bound states of a many-particle system. *Nuclear Phys.*, 7:421, 1958. pages 10

[41] F. Coester and H. Kümmel. Short-range correlations in nuclear wave functions. *Nuclear Phys.*, 17:477, 1960. pages 10

[42] P. Piecuch, P. D. Fan, K. Jedziniak, and K. Kowalski. Exactness of two-body cluster expansions in many-body quantum theory. *Phys. Rev. Lett.*, 90:113001, 2003. pages 10

[43] K. Kowalski and P. Piecuch. Extension of the method of moments of coupled-cluster equations to excited states: The triples and quadruples corrections to the eomccsd energies. *J. Chem. Phys.*, 116:7411, 2002. pages 10

[44] D. J. Dean and M. Hjorth-Jensen. Coupled-cluster approach to nuclear physics. *Phys. Rev. C*, 69:054320, 2004. pages 10, 101, 108

[45] K. Kowalski, D. J. Dean, M. Hjorth-Jensen, T. Papenbrock, and P. Piecuch. Coupled cluster calculations of ground and excited states of nuclei. *Phys. Rev. Lett.*, 92:132501, 2004. pages 10, 101, 108

[46] M. Wloch, D. J. Dean, J. R. Gour, M. Hjorth-Jensen, K. Kowalski, T. Papenbrock, and P. Piecuch. Ab initio couplec-cluster study of ^{16}o. *nucl-th/0501067*, 2005. pages 10, 108

[47] P. Lind. Completeness relations and resonant state expansions. *Phys. Rev. C*, 47:1903, 1993. pages 10, 25, 26, 27, 57

[48] R. J. Liotta, E. Maglione, N. Sandulescu, and T. Vertse. A representation to describe nuclear processes in the continuum. *Phys. Lett. B*, 367:1, 1996. pages 10, 12

[49] H. Feshbach. A unified of nuclear reactions. *Ann. Phys.*, 5:357, 1958. pages 11

[50] H. Feshbach. A unified of nuclear reactions.II. *Ann. Phys.*, 19:287, 1962. pages 11

[51] U. Fano. Effects of configuration interaction on intensities and phase shifts. *Phys. Rev.*, 124:1866, 1961. pages 11

[52] K. Bennaceur, F. Nowacki, J. Okolowicz, and M. Ploszajczak. Study of the ^{7}be$(p,\gamma)^{8}$b and 7li$(n,\gamma)^{8}$li capture reactions using the shell model embedded in the continuum. *Nucl. Phys. A*, 651:289, 1999. pages 11

[53] K. Bennaceur, F. Nowacki, J. Okolowicz, and M. Ploszajczak. Analysis of the ^{16}o$(p,\gamma)^{17}$f capture reaction using the shell model embedded in the continuum. *Nucl. Phys. A*, 671:203, 2000. pages 11

[54] J. Okolowicz, M. PImageoszajczak, and I. Rotter. Dynamics of quantum systems embedded in a continuum. *Phys. Rep.*, 374:271, 2003. pages 11

[55] A. Volya and V. Zelevinsky. Non-hermitian effective hamiltonian and continuum shell model. *Phys. Rev. C*, 67:054322, 2003. pages 11

[56] N. Michel, W. Nazarewicz, and M. Płoszajczak. Proton-neutron coupling in the gamow shell model: the lithium chain. *nucl-th/0407110*, 2004. pages 12

[57] N. Michel, W. Nazarewicz, M. Płoszajczak, and J. Rotureau. Gamow shell-model description of weakly bound and unbound nuclear states. *nucl-th/0401036*, 2004. pages 12

[58] J. Dobaczewski, W. Nazarewicz N. Michel, M. Płoszajczak, and M. V. Stoitsov. Structure of exotic nuclei. *nucl-th/0401034*, 2004. pages 12

[59] R. IdBetan, R. J. Liotta, N. Sandulescu, , and T. Vertse. Shell model in the complex energy plane and two-particle resonances. *Phys. Rev. C*, 67:014322, 2003. pages 12

[60] N. Michel, W. Nazarewicz, M. Ploszajczak, and K. Bennaceur. Gamow shell model description of neutron-rich nuclei. *Phys. Rev. Lett.*, 89:042502, 2002. pages 12

[61] N. Michel, W. Nazarewicz, M. Ploszajczak, and J. Okołowicz. Gamow shell model description of weakly bound nuclei and unbound nuclear states. *Phys. Rev. C*, 67:054311, 2003. pages 12

[62] R. IdBetan, R. J. Liotta, N. Sandulescu, and T. Vertse. Two-particle resonant states in a many-body mean field. *Phys. Rev. Lett.*, 89:042501, 2002. pages 12

[63] R. IdBetan, R. J. Liotta, N. Sandulescu, and T. Vertse. A shell model representation with antibound states. *Phys. Lett. B*, 584:48, 2004. pages 12, 13

[64] G. H. Hardy. *Divergent Series.* Clarendon Press, 2nd edition, 1956. pages 21

[65] M. L. Boas. *Mathematical Methods in the Physical Sciences.* John Wiley and Sons, Inc, 2nd edition, 1983. pages 21

[66] B. Gyarmati and T. Vertse. On the normalization of gamow functions. *Nucl. Phys. A*, 160:523, 1971. pages 22

[67] B. Gyarmati, F. Krisztinkovics, and T. Vertse. On the expectation value in gamow state. *Phys. Lett. B*, 41:110, 1972. pages 29

[68] T. Berggren. On the interpretation of complex cross sections for production of resonant final states. *Phys. Lett. B*, 73:389, 1978. pages 29

[69] T. Berggren. Expectation value of an operator in a resonant state. *Phys. Lett. B*, 373:1, 1996. pages 29

[70] L. C. Biedenharn and H. Van Dam. *Quantum theory of angular momentum : a collection of reprints and original papers.* New York : Academic Press, 1965. pages 35

[71] I. S. Gradshteyn and I. M. Ryzhik. *Table of Integrals Series and Products.* Academic Press Inc., 4th edition, 1963. pages 35, 39

[72] M. Abramowitz and I. A. Stegun. *Handbook of mathematical functions.* Dover Publications, Inc., New York, 1972. pages 35, 45

[73] G. Tiktopoulos. Euclidean approach to the bethe-salpeter equation for scattering. *Phys. Rev.*, 136:275, 1964. pages 37

[74] J. Nuttall. Analytic continuation of the off-energy shell scattering amplitude. *J. Math. Phys.*, 8:873, 1966. pages 37, 60

[75] J. Nuttall. Contour distortions in relativistic three-particle scattering functions. *Phys. Rev.*, 160:1459, 1967. pages 37

[76] G. C. Wick. Properties of bethe-salpeter wave functions. *Phys. Rev.*, 96:1124, 1954. pages 37

[77] T. Berggren. On the treatment of resonant final states in direct reactions. *Nucl. Phys. A*, 169:353, 1971. pages 39

[78] I. Bar-On and V. Ryaboy. Fast diagonalization of large and dense complex symmetric matrices, with applications to quantum reaciton dynamics. *Scientific Computing*, 44:1412, 1997. pages 39

[79] I. Bar-On and M. Paprzycki. An efficient algorithm for finding eigenvalues of complex symmetric matrices. *Computer Assisted Mechanics and Engineering Sciences*, 5:85, 1998. pages 39

[80] I. Bar-On and M. Paprzycki. High performance solution of the complex symmetric eigenproblem. *Numerical Algorithms*, 18:195, 1998. pages 39

[81] L.S. Ferreira, E. Maglione, and R. J. Liotta. Nucleon resonances in deformed nuclei. *Phys. Rev. Lett.*, 78:1640, 1997. pages 42

[82] K. Hagino and Nguyen Van Giai. Structure of positive energy states in a deformed mean-field potential. *Nucl. Phys. A*, 735:55, 2004. pages 42

[83] D. A. Varshalovich, A. N. Moskalev, and V. K. Khersonskii. *Quantum theory of angular momentum: irreducible tensors, spherical harmonics, vector coupling coefficients, 3nj symbols.* Singapore : World Scientific, 1989. pages 44

[84] L. P. Kok and H. van. Haeringen. On the theory of complex potential scattering. *Ann. of Phys.*, 131:426, 1981. pages 52

[85] T. Vertse, P. Curutchet, R. J. Liotta, and J. Bang. On the role of anti-bound states in the rpa description of the giant monopole resonance. *Acta Physica Hungaria*, 65:305, 1989. pages 57

[86] T. Vertse, R. J. Liotta, and E. Maglione. Exact and approximate calculation of giant resonances. *Nucl. Phys. A*, 584:13, 1995. pages 57

[87] R.F. Bishop, M. R. Strayer, and J. M. Irvine. Singularities in the galitskii-feynmann t matrix. *Phys. Rev. A*, 10:2423, 1974. pages 63, 65

[88] R.F. Bishop, H. B. Ghassib, and M. R. Strayer. Composite pairs and effective two-body scattering in a many-body medium. *Phys. Rev. A*, 13:1570, 1976. pages 63

[89] M. I. Haftel and F. Tabakin. Nuclear saturation and smoothness of nucleon-nucleon potentials. *Nucl. Phys. A*, 158:1, 1970. pages 63

[90] A. Goldberg and R. D. Puff. Bose condensation of fermion composites. *Phys. Rev. Lett.*, 30:869, 1973. pages 63

[91] W. H. Dickhoff. Connection between brueckner ladders and pairing correlations. *Phys. Lett. B*, 210:15, 1988. pages 63, 68

[92] W. H. Dickhoff, C. C. Gearhart, B. E. Vonderfecht, A. Polls, and A. Ramos. A new state of nuclear matter. *Recent Progress in Many-Body Theories*, 2:141, 1990. pages 63, 68

[93] B. E. Vonderfecht, C.C. Gearhart, and W. H. Dickhoff. Bound pair states in nuclear matter. *Phys. Lett. B*, 253:1, 1991. pages 63, 68

[94] A. Ramos, A. Polls, and W. H. Dickhoff. Single-particle properties and short-range correlations in nuclear matter. *Nucl. Phys. A*, 503:1, 1989. pages 66

[95] R. Machleidt. The high-precision, charge-dependent bonn nucleon-nucleon potential (cd-bonn). *Phys. Rev. C*, 63:024001, 2001. pages 68

[96] D.J. Dean and M. Hjorth-Jensen. Pairing in nuclear systems: from neutron stars to finite nuclei. *Rev. Mod. Phys.*, 75:607, 2003. pages 68

[97] R. R. Whitehead, A. Watt, B. J. Cole, and I. Morrison. *Adv. Nucl. Phys.*, 9:123, 1977. pages 77

[98] K. Suzuki and S. Y. Lee. Convergent theory for effective interaction in nuclei. *Progr. Theor. Phys.*, 64:2091, 1980. pages 84, 86, 101

[99] K. Suzuki. Construction of hermitian effective interaction in nuclei — general relation between hermitian and non-hermitian forms —. *Progr. Theor. Phys.*, 68:246, 1982. pages 84, 101

[100] K. Suzuki and R. Okamoto. Effective operators in time-independent approach. *Progr. Theor. Phys.*, 93:905, 1995. pages 84, 101

[101] S. Fujii, E. Epelbaum, H. Kamada, R. Okamoto, K. Suzuki, and W. Glöckle. Low-momentum nucleon-nucleon interaction and its application to few-nucleon systems. *Phys. Rev. C*, 70:024003, 2004. pages 84, 101

[102] Jason D. Holt, T.T.S. Kuo, and G.E. Brown. Family of hermitian low-momentum nucleon interactions with phase shift equivalence. *Phys. Rev. C*, 69:034329, 2004. pages 86, 88

[103] R. Okamoto, S. Fujii, and K. Suzuki. Formal relation among various hermitian and non-hermitian effective interactions. *Int. J. Mod. Phys. E*, 14:1, 2005. pages 86, 88

[104] S. Okubo. unknown. *Prog. Theor. Phys.*, 12:603, 1954. pages 88

[105] N. J. Higham. Stable iterations for the matrix square root. *Num. Algorithms*, 15:227, 1997. pages 89

[106] E. D. Denman and A. N. Beavers. The matrix sign function and computations in systems. *Appl. Math. Comput.*, 2:63, 1976. pages 89

[107] C. Buth, R. Santra, and L. S. Cederbaum. Non-hermitian rayleigh-schrdinger perturbation theory. *Phys. Rev. A*, 69:032505, 2004. pages 90

[108] F. Chen, E. R. Davidson, and S. Iwata. New time-independent perturbation theory for the multireference problem. *Int. J. Quantum Chem.*, 86:256, 2002. pages 90

[109] R. Santra and L. S. Cederbaum. Non-hermitian electronic theory and applications to clusters. *Phys. Rep.*, 368:1, 2002. pages 90

[110] M. Hjorth-Jensen, Thomas T. S. Kuo, and Eivind Osnes. Realistic effective interactions for nuclear systems. *Phys. Rep.*, 261:125, 1995. pages 92

[111] P. J. Ellis and E. Osnes. An introductory guide to effective operators in nuclei. *Rev. Mod. Phys*, 49:777, 1977. pages 92

[112] B. H. Brandow. Linked-cluster expansions for the nuclear many-body problem. *Rev. Mod. Phys.*, 39:771, 1967. pages 92

[113] K. A. Brueckner. Many-body problem for strongly interacting particles. ii. linked cluster expansion. *Phys. Rev.*, 100:36, 1955. pages 93

[114] E. R. Davidson, E. Engdahl, and N. Moiseyev. New bounds to resonance eigenvalues. *Phys. Rev. A*, 33:2436, 1986. pages 97

Appendix A

A.1 Left and right eigenvectors and bi-orthogonal sets.

Given the eigenvalue equation,

$$A^{\mathrm{T}} y = \lambda y, \tag{A.1}$$

where the $n \times n$ matrix A^{T} is of general form. The eigenvalues λ are determined by the characteristic equation,

$$\det(A^{\mathrm{T}} - \lambda I) = \det(A - \lambda I) = 0, \tag{A.2}$$

which shows that the eigenvalues of A^{T} are the same as those of A. Consider the eigenvalue equation for the i'th eigenvector,

$$A^{\mathrm{T}} y_i = \lambda_i y_i, \tag{A.3}$$

then the transpose of this equation gives,

$$y_i^{\mathrm{T}} A = \lambda_i y_i^{\mathrm{T}}, \tag{A.4}$$

here y_i^{T} is the left eigenvector of A corresponding to the eigenvalue λ_i. The eigenvalue equation for A is

$$A x_j = \lambda_j x_j, \tag{A.5}$$

where it is seen that x_j is the right eigenvector of the matrix A corresponding to the eigenvalue λ_j. Now multiply Eq. (A.4) with x_j from the right and Eq. (A.5) with y_i^{T} from the left, and subtract to obtain,

$$\begin{aligned} \lambda_j y_i^{\mathrm{T}} x_j &= \lambda_i y_i^{\mathrm{T}} x_j, & \text{(A.6)} \\ \Rightarrow\ (\lambda_j - \lambda_i) y_i^{\mathrm{T}} x_j &= 0, & \text{(A.7)} \\ \Rightarrow\ y_i^{\mathrm{T}} x_j &= 0 \text{ if} \lambda_i \neq \lambda_j, & \text{(A.8)} \end{aligned}$$

where it is customary to say that the left y_i^{T} and right x_j eigenvectors of a matrix A are *bi-orthogonal* to each other. If all n eigenvalues of the matrix $A$are distinct, then $y_i^{\mathrm{T}} x_j = 0$ for $i, j = 1, 2, ..., n$, $i \neq j$, but $y_i^{\mathrm{T}} x_i \neq 0$. This implies that the right and left eigenvectors can be scaled so they form a complete set of *bi-orthogonal* vectors.

$$Y^{\mathrm{T}} X = \sum_{i,j=1}^{n} y_i^{\mathrm{T}} x_i = \sum_{i,j=1}^{n} \delta_{i,j} = 1. \tag{A.9}$$

Here Y^{T} is a matrix whose rows are $y_i^{\mathrm{T}}, i = 1, ..., n$and $X$is a matrix whose columns are $x_i, i = 1, ..., n$. This shows explicitly that Y^{T} is the inverse of X. It is clear that this works for any matrix which has a complete set of linearly independent eigenvectors (a nondefective matrix) regardless of whether the eigenvalues are distinct. As we have seen before, we can write in this case

$$X^{-1}AX = \mathrm{diag}\,[\lambda_i].$$

Indeed, if we can find any matrix Z such that $Z^{-1}AZ$ is diagonal, then the columns of Z are the right eigenvectors of A, and the rows of Z^{-1} are the left eigenvectors of A, while the diagonal entries of $Z^{-1}AZ$ are the eigenvalues of A. Defective matrices have an incomplete set of eigenvectors, and the theory requires their reduction to Jordan normal form.

In the special case of A being a complex symmetric matrix, which is often the case in physical applications, then the left eigenvectors are just the transpose of the right eigenvectors. In this case it is sufficient to solve the right eigenvalue equation, and a complete set of *bi-orthogonal* vectors are obtained directly.

A.2 Three-body matrix elements in $j-j$ coupling

Throughout this section the anti-symmetric three-, two-body wave functions are written as $\bar{\Psi}$ and $\bar{\Phi}$ respectively, while the non-anti-symmetrized functions are without the bar. The single-particle wave functions are given by ϕ. The anti-symmetric three-body wave function may be written

$$\bar{\Psi}^{JM}_{(ab)c}(123) = \frac{1}{\sqrt{3}}\left\{\Psi^{JM}_{(ab)c}(123) - \Psi^{JM}_{(ab)c}(132) + \Psi^{JM}_{(ab)c}(231)\right\} \tag{A.10}$$

here $(ab)c$ labels all relevant single particle quantum numbers $a = n_a, l_a, j_a$, and the coupling rule $(j_a \otimes j_b)_{J_{ab}} \otimes j_c$ is indicated. The wave function in Eq. A.10 is anti-symmetric only in case where at least two of the orbits abc are different. In the case $a = b = c$ one has to make use of coefficients of fractional parentage to make the three-body wave function anti-symmetric. The non anti-symmetrized wave functions $\Psi^{JM}_{(ab)c}(123)$ are given by

$$\Psi^{JM}_{(ab)c}(123) = \Psi\left(\bar{\Phi}^{J_{ab}}_{ab}(12)\phi_c(3); JM\right) \tag{A.11}$$

Here $\bar{\Phi}^{J_{ab}}_{ab}(12)$ is an anti-symmetric two-particle wave function.

$$\bar{\Phi}^{J_{ab}}_{ab}(12) = \frac{1}{\sqrt{2(1+\delta_{ab})}} \sum_{m_a, m_b} \langle j_a m_a, j_b m_b | J_{ab} M_{ab}\rangle \left(\phi_a(1)\phi_b(2) - \phi_a(2)\phi_b(1)\right) \tag{A.12}$$

In the following derivation the total spin and projection JM will be suppressed for notational economy.

Consider a matrix element of the three-body wave function in Eq. A.10 with a general interaction consisting of only two-body terms $V = V_{12} + V_{13} + V_{23}$.

$$\langle \bar{\Psi}_{(ab)c}(123)|V|\bar{\Psi}_{(de)f}(123)\rangle = \tag{A.13}$$

$$\frac{1}{\sqrt{3}}\langle \Psi_{(ab)c}(123) - \Psi_{(ab)c}(132) + \Psi_{(ab)c}(231)|V|\bar{\Psi}_{(de)f}(123)\rangle \tag{A.14}$$

from the anti-symmetry follows

$$\begin{aligned}\langle \Psi_{(ab)c}(123)|V|\bar{\Psi}_{(de)f}(123)\rangle &= \langle -\Psi_{(ab)c}(131)|V|\bar{\Psi}_{(de)f}(123)\rangle &\text{(A.15)}\\ &= \langle \Psi_{(ab)c}(231)|V|\bar{\Psi}_{(de)f}(123)\rangle &\text{(A.16)}\end{aligned}$$

and henceforth

$$\langle \bar{\Psi}_{(ab)c}(123)|V|\bar{\Psi}_{(de)f}(123)\rangle = \sqrt{3}\langle \Psi_{(ab)c}(123)|V|\bar{\Psi}_{(de)f}(123)\rangle = \tag{A.17}$$

$$\langle \Psi_{(ab)c}(123)|V_{12}|\Psi_{(de)f}(123) - \Psi_{(de)f}(132) + \Psi_{(de)f}(231)\rangle + \tag{A.18}$$

$$2\langle \Psi_{(ab)c}(123)|V_{23}|\Psi_{(de)f}(123) - \Psi_{(de)f}(132) + \Psi_{(de)f}(231)\rangle \tag{A.19}$$

Starting with the matrix element of V_{12}, one has

$$\langle \Psi_{(ab)c}(123)|V_{12}|\Psi_{(de)f}(123) - \Psi_{(de)f}(132) + \Psi_{(de)f}(231)\rangle = V_{12}^1 + V_{12}^2 + V_{12}^3 \tag{A.20}$$

where

$$V_{12}^1 = \langle ab|V_{12}|de\rangle_{J_{ab}}^{AS}\,\delta_{c,f}\,\delta_{J_{ab},J_{de}} \tag{A.21}$$

and

$$V_{12}^2 + V_{12}^3 = \langle \Psi_{(ab)c}(123)|V_{12}|\,-\big(\Psi_{(de)f}(132) - \Psi_{(de)f}(231)\big)\rangle \tag{A.22}$$

recoupling $1,3 \to 1,2$ in $\Psi_{(de)f}(132)$ and $2,3 \to 2,1$ in $\Psi_{(de)f}(231)$ one may show by angular momentum algebra that

$$-\big(\Psi_{(de)f}(132) - \Psi_{(de)f}(231)\big) = \tag{A.23}$$

$$\left(\frac{1+\delta_{d,f}}{1+\delta_{d,e}}\right)^{1/2}\sum_{J_{df}}(-1)^{j_d+J_{df}-J_{de}-J}U(j_e\ j_d\ J\ j_f;J_{de}\ J_{df})\Psi_{(df)e}(123) \tag{A.24}$$

$$-\left(\frac{1+\delta_{e,f}}{1+\delta_{d,e}}\right)^{1/2}\sum_{J_{ef}}(-1)^{j_d+J_{ef}-J}U(j_d\ j_e\ J\ j_f;J_{de}\ J_{ef})\Psi_{(ef)d}(123) \tag{A.25}$$

here $U(j_a\ j_b\ J\ j_c;J_{ab}\ J_{bc})$ are the normalized Racah coefficients. It follows that the terms V_{12}^2 and V_{12}^3 are given by

$$V_{12}^2 = \left(\frac{1+\delta_{d,f}}{1+\delta_{d,e}}\right)^{1/2}\sum_{J_{df}}(-1)^{j_d+J_{df}-J_{de}-J}U(j_e\ j_d\ J\ j_f;J_{de}\ J_{df})\times$$

$$\langle ab|V_{12}|df\rangle_{J_{ab}}^{AS}\,\delta_{c,e}\delta_{J_{ab},J_{df}} \tag{A.26}$$

$$V_{12}^3 = -\left(\frac{1+\delta_{e,f}}{1+\delta_{d,e}}\right)^{1/2}\sum_{J_{ef}}(-1)^{j_d+J_{ef}-J}U(j_d\ j_e\ J\ j_f;J_{de}\ J_{df})\times \langle ab|V_{12}|ef\rangle^{AS}_{J_{ab}}\ \delta_{c,d}\delta_{J_{ab},J_{ef}} \tag{A.27}$$

Calculating the matrix element of V_{23} one first recouple $1,2\rightarrow 2,3$ in the $\langle$bra$|$.

$$\Psi_{(ab)c}(123) = \left(\frac{1}{2(1+\delta_{a,b})}\right)\times \tag{A.28}$$

$$\left\{\sum_{J_{bc}}(-1)^{j_a+J_{bc}-J}U(j_aj_bJj_c;J_{ab}J_{bc})\Psi\left(\Phi^{J_{bc}}_{bc}(23)\phi_a(1)\right)+ \tag{A.29}$$

$$\sum_{J_{ac}}(-1)^{j_a-J_{ab}+J_{ac}-J}U(j_bj_aJj_c;J_{ab}J_{ac})\Psi\left(\Phi^{J_{ac}}_{ac}(23)\phi_b(1)\right)\right\} \tag{A.30}$$

here $\Phi^{J_{bc}}_{bc}$ and $\Phi^{J_{ac}}_{ac}$ are non anti-symmetric two-body wave functions. Anti-symmetric two-body matrix elements may be expressed in terms non anti-symmetric matrix elements by

$$\langle\bar{\Phi}_{ab}(12)|V_{12}|\bar{\Phi}_{cd}(12)\rangle = \left(\frac{2}{(1+\delta_{ab})}\right)^{1/2}\langle\Phi_{ab}(12)|V_{12}|\bar{\Phi}_{cd}(12)\rangle \tag{A.31}$$

Evaluating the matrix element of V_{23} one has to evaluate the following matrix elements

$$\langle\Psi_{(bc)a}(231)|V_{23}|\Psi_{(de)f}(123)-\Psi_{(de)f}(132)+\Psi_{(de)f}(231)\rangle \tag{A.32}$$

and

$$\langle\Psi_{(ac)b}(231)|V_{23}|\Psi_{(de)f}(123)-\Psi_{(de)f}(132)+\Psi_{(de)f}(231)\rangle \tag{A.33}$$

which are evaluated in the same manner as the evaluation of V_{12} in Eq. A.20. After some angular momentum recoupling algebra in the $|$ket$\rangle$, one ends up with the final expressions

$$\begin{aligned}
\langle\bar{\Psi}_{(ab)c}(123)|V|\bar{\Psi}_{(de)f}(123)\rangle &= \langle ab|V_{12}|de\rangle^{AS}_{J_{ab}}\ \delta_{c,f}\ \delta_{J_{ab},J_{de}}+\\
\left(\frac{1+\delta_{d,f}}{1+\delta_{d,e}}\right)^{1/2}&(-1)^{j_d-J_{de}+J_{ab}-J}U(j_ej_dJj_f;J_{de}J_{ab})\langle ab|v|df\rangle^{AS}_{J_{ab}}\ \delta_{c,e}-\\
\left(\frac{1+\delta_{e,f}}{1+\delta_{d,e}}\right)^{1/2}&(-1)^{j_d+J_{ab}-J}U(j_dj_eJj_f;J_{de}J_{ab})\langle ab|v|ef\rangle^{AS}_{J_{ab}}\ \delta_{c,d}+\\
\left(\frac{1+\delta_{b,c}}{1+\delta_{a,b}}\right)^{1/2}&(-1)^{j_a+J_{de}-J}U(j_aj_bJj_c;J_{ab}J_{de})\langle bc|v|de\rangle^{AS}_{J_{de}}\delta_{a,f}+\\
&\left(\frac{1+\delta_{b,c}}{1+\delta_{a,b}}\right)^{1/2}\sum_{J_{bc}}(-1)^{j_a+j_d-2J}U(j_aj_bJj_c;J_{ab}J_{bc})\times\\
&\left\{\left(\frac{1+\delta_{d,f}}{1+\delta_{d,e}}\right)^{1/2}(-1)^{J_{de}}U(j_ej_dJj_f;J_{de}J_{bc})\langle bc|v|df\rangle^{AS}_{J_{bc}}\delta_{a,e}+\right.
\end{aligned}$$

$$\left(\frac{1+\delta_{e,f}}{1+\delta_{d,e}}\right)^{1/2} U(j_d j_e J j_f; J_{de} J_{bc}) \langle bc|v|ef\rangle^{AS}_{J_{bc}} \delta_{a,d} \Bigg\} +$$

$$\left(\frac{1+\delta_{a,c}}{1+\delta_{a,b}}\right)^{1/2} (-1)^{j_a - J_{ab} + J_{de} - J} U(j_b j_a J j_c; J_{ab} J_{de}) \langle ac|v|de\rangle^{AS}_{J_{de}} \delta_{b,f} +$$

$$\left(\frac{1+\delta_{a,c}}{1+\delta_{a,b}}\right)^{1/2} \sum_{J_{ac}} (-1)^{j_a + j_d - J_{ab} - 2J} U(j_b j_a J j_c; J_{ab} J_{ac}) \times$$

$$\Bigg\{ \left(\frac{1+\delta_{d,f}}{1+\delta_{d,e}}\right)^{1/2} (-1)^{J_{de}} U(j_e j_d J j_f; J_{de} J_{ac}) \langle ac|v|df\rangle^{AS}_{J_{ac}} \delta_{b,e} +$$

$$\left(\frac{1+\delta_{e,f}}{1+\delta_{d,e}}\right)^{1/2} U(j_d j_e J j_f; J_{de} J_{ac}) \langle ac|v|ef\rangle^{AS}_{J_{ac}} \delta_{b,d} \Bigg\} \tag{A.34}$$

In the case $a = b = d = e \neq c = f$ and $J_{ab} = J_{aa}, J_{de} = J'_{aa}$ are even, Eq. A.34 simplifies to

$$\langle \bar{\Psi}_{(aa)c}(123)|V|\bar{\Psi}_{(aa)c}(123)\rangle = \langle aa|v|aa\rangle^{AS}_{J_{aa}} \, \delta_{J_{aa},J'_{aa}} +$$

$$2\sum_{J_{ac}} (2J_{ac}+1)\sqrt{(2J_{aa}+1)(2J'_{aa}+1)} \left\{ \begin{array}{ccc} j_a & j_a & J_{aa} \\ j_c & J & J_{ac} \end{array} \right\} \left\{ \begin{array}{ccc} j_a & j_a & J'_{aa} \\ j_c & J & J_{ac} \end{array} \right\} \langle ac|v|ac\rangle_{J_{ac}}$$

where the normalized Racah coefficients are expressed in terms of $6-j$ symbols. Next consider the case where all the single particle orbits in the ket are equivalent, i.e. $d = e = f$, in this case one has to make a coefficients of fractional parentage expansion to make the three-body wave function totally anti-symmetric in the $j-j$ coupling scheme;

$$\bar{\Psi}_{ddd}(123) = \sum_K \langle j_d^2 K, j_d | \} \, j_d^3 J\rangle \Psi_{(dd)d}(123) \tag{A.35}$$

In this way the wave function is expressed in terms of anti-symmetric two-particle wave functions, and one may proceed in the same manner as for the case considered above. After some angular momentum recouplings, one ends up with the final expression for the matrix element,

$$\langle \bar{\Psi}_{(ab)c}(123)|V|\bar{\Psi}_{(dd)d}(123)\rangle = \sqrt{3}\, \langle j_d^2 J_{ab}, j_d | \} \, j_d^3 J\rangle \langle ab|v|dd\rangle^{AS}_{J_{ab}} \delta_{c,d} +$$

$$\sqrt{3}(-1)^{j_a + j_d - 2J} \sum_K \langle j_d^2 K, j_d | \} \, j_d^3 J\rangle \times$$

$$\Bigg\{ \left(\frac{1+\delta_{b,c}}{1+\delta_{a,b}}\right)^{1/2} \sum_{J_{bc}} U(j_a j_b J j_c; J_{ab} J_{bc}) U(j_d j_d J j_d; K J_{bc}) \langle bc|v|dd\rangle_{J_{bc}} \delta_{a,d} +$$

$$\left(\frac{1+\delta_{a,c}}{1+\delta_{a,b}}\right)^{1/2} \sum_{J_{ac}} (-1)^{J_{ab}} U(j_b j_a J j_c; J_{ab} J_{ac}) U(j_d j_d J j_d; K J_{ac}) \langle ac|v|dd\rangle_{J_{bc}} \delta_{b,d} \Bigg\} \tag{A.36}$$